THE UNIVERSITY of ADELAIDE

Infrared Spectroscopy of Astrophysically Relevant Molecules

Masters of Philosophy Thesis

School of Physical Sciences (Chemistry)

Hayley Bunn

April 2017

Hayley Bunn

Supervisors: Prof. Gregory F Metha & Dr. Paul L Raston

Declaration

I certify that this work contains no material which has been accepted for the award of any other degree or diploma in my name, in any university or other tertiary institution and, to the best of my knowledge and belief, contains no material previously published or written by another person, except where due reference has been made in the text.

In addition, I certify that no part of this work will, in the future, be used in a submission in my name, for any other degree or diploma in any university or other tertiary institution without the prior approval of the University of Adelaide and where applicable, any partner institution responsible for the joint-award of this degree.

I give consent to this copy of my thesis when deposited in the University Library, being made available for loan and photocopying, subject to the provisions of the Copyright Act 1968.

I acknowledge that copyright of published works contained within this thesis resides with the copyright holder(s) of those works.

I also give permission for the digital version of my thesis to be made available on the web, via the University's digital research repository, the Library Search and also through web search engines, unless permission has been granted by the University to restrict access for a period of time.

I acknowledge the support I have received for my research through the provision of an Australian Government Research Training Program Scholarship.

Hayley Bunn 27/03/17

Acknowledgements

Firstly I would like to give my deepest appreciation to Dr Paul Raston, for all his help and guidance in the past few years and particularly for taking me on even after moving to the other side of the world. Thanks for putting up with me spamming your inbox with a million emails only to come to a conclusion myself, and supporting me when I couldn't. If not for your relaxed nature and encouragement to take on new and difficult challenges I would not have learnt and achieved anywhere near as much. I would also like to thank Prof. Greg Metha for looking after me in Adelaide, making sure I was always on track and for being available for assistance. Thanks to everyone else in the Metha group for providing a fun and comfortable environment, and particularly Jason Alvino and Alex Gentlemen (now at University of Oxford) for helping with calculations. All experiments reported in this thesis were undertaken at the Terahertz & Far-Infrared Beamline at the Australian Synchrotron, Victoria, Australia. A big thank you to the beamline staff Dom Appadoo and Ruth Plathe, as well as Courtney Ennis (now at La Trobe University), for assistance in experiments and beamline operation as well as stimulating and helpful discussions and for being available even at odd hours of the evening/morning. A special thanks to Rohan, Aidan, Junda, Irene, Sophia and Alex, for taking time out of your own work and rearranging sleeping habits to help out with synchrotron trips, if not for this I wouldn't have had any results.

Of course I would also like to acknowledge and thank my family for being so patient, putting up with my long working hours, lifting my spirits during stressful periods and generally always being there to help, even when they don't understand a word I say. Thank you to the rest of my friends for also being patient, keeping me entertained (not to mention sane) and not falling off the edge of the Earth even though we were all so busy. Good luck for the rest of your work/study.

Abstract

This thesis involves use of the Terahertz & Far-Infrared Beamline facility at the Australian Synchrotron to record spectra and try to resolve the rotational fine structure of species having astrophysical relevance. The primordial nature of hydrogen makes understanding its interaction with other species interesting in terms of the origin and evolution of interstellar media and planetary systems. The interaction of molecular hydrogen with rare gas atoms constituted some of the first spectroscopic experiments on van der Waals complexes, and part of this thesis involves extending this body of work to the far-infrared spectra of H_2/D_2–Xe. The high polarisability of Xe makes the complex an "easy" spectroscopic target, and attempts at collecting high resolution spectra of the H_2/D_2–Xe complexes were successful. From rare gas species the field evolved into the interaction of H_2 with other homonuclear diatomics such as N_2 and O_2, and this thesis expands on a previous far-infrared study on H_2–O_2 by providing and analysing the mid-infrared spectra of H_2–O_2 and the far-infrared spectra of D_2–O_2. Spectroscopic signatures of interstellar molecules provide the foundation for experimental studies into astronomically relevant systems such as vinyl alcohol, which was observed towards Sagittarius B2(N) in 2001. The second and major component of this thesis involves the analysis of the torsional bands of vinyl alcohol. The fundamental and first two hot bands of *syn*-vinyl alcohol are observed, along with the first infrared observation of the *anti* rotamer, including the fundamental and first hot band. High resolution far-infrared spectroscopy is used, with the assistance of computational calculations and a spectral analysis program, to refine the ground state, and provide accurate excited state, rotational and centrifugal distortion constants as well as the determination of relative rotamer abundance. Far-infrared spectra of monodeuterated vinyl alcohol, CH_2CHOD, is also presented, similarly showing the OD torsional fundamental and first two hot bands of *syn* rotamer, and the fundamental and first hot band of the *anti* rotamer.

Contents

1. Introduction

This thesis focuses on the ro-vibrational spectroscopy of gaseous species that are unstable (vinyl alcohol) and weakly absorbing (van der Waals species such as H_2–O_2). The rotational analysis of gaseous species provides an excellent source of reference data for the detection of molecules in planetary atmospheres and the interstellar medium (ISM). The ISM is the collection of matter, predominately gas and dust, within a galaxy that fills the space between stars. The ISM is a very heterogeneous environment with densities and temperatures varying substantially, and therefore chemical composition within them is anything but consistent or uniform. Yet even in regions of very low temperature and density the ISM is still chemically rich and very little is known about the formation and evolution of these regions of space. We do, however, know that the astrochemical evolution of the ISM is strongly dependent on molecular composition, which in turn, is dependent upon the physical conditions of the ISM such as temperature, radiation and pressure. Rotational analysis of particular species and their isomers can provide insight into these conditions as well as chemical compositions and abundances. This information can then provide important clues about the formation of such molecules in the ISM and allows for a further understanding into the evolution of cold molecular clouds, hot cores and star forming regions [1].

I. VAN DER WAALS COMPLEXES

Hydrogen is the most abundant element (and molecule in the form of H_2) in the universe followed by helium, oxygen and carbon. Interaction of species with hydrogen is extremely important in understanding the chemical and physical development of the universe including cold ISM, hot core (regions of protostars with warm temperatures, i.e. ~200 K and relatively dense gas) and star forming regions, as well as planetary bodies and their atmospheres. Being a homonuclear diatomic molecule, molecular hydrogen does not possess a dipole moment, which is most commonly used in detecting gaseous species. However, it can be observed via quadrupolar transitions [2] or Collision Induced Absorption (CIA). A CIA essentially results from a dipole moment induced by a collision that interacts with radiation. Due to the short lifetime of the collision it is observed as a broad feature [3]. Molecular hydrogen has been extensively observed in the ISM and also in various planetary atmospheres, where the first collision-induced first overtone band (a vibrational transition with a change in vibrational quantum number of 2 or more, e.g. $\nu = 2–0$) was observed by Welsh *et al.* in 1951 [4]. During a later study into the CIA of H_2, Watanabe and Welsh observed the first IR spectrum of the molecular hydrogen dimer, $(H_2)_2$ [5]. Within such a complex they observed not only broad CIA features, but also sharper transitions owing to the longer lifetime resulting from the *end-over-end* rotation of the complex. The far-IR spectra that shows the $l = 2–1$ *end-over-end* transition (also showing a broad feature due to the CIA), where l is the rotational quantum number of the complex, was later observed by the Voyager spacecraft in Jupiter (~350 and 590 cm^{-1}) and Saturn (~350 cm^{-1}) [6-8]. McKellar then extended the work on $(H_2)_2$ to high resolution with the inclusion of deuterium [9].

Molecular hydrogen has two nuclear spin isomers; *ortho* has symmetric nuclear spin states, and *para* has antisymmetric spin states. Since the overall wavefunction must be antisymmetric, the *ortho* nuclear spin isomer exists in antisymmetric rotational states (j_H = odd) and the *para* nuclear spin isomers exists in symmetric rotational states (j_H = even). The nuclear spin degeneracy for *ortho* hydrogen is 3 and for *para* hydrogen is 1. This is what determines their relative abundance at room temperature (i.e. 3:1). The next most abundant, stable, isotope of hydrogen is deuterium (^{2}H or D). Molecular deuterium also has two nuclear spin isomers, however, they must have an overall symmetric wavefunction. Therefore the *ortho* nuclear spin isomer exists in symmetric rotational states (j_D = even) and the *para* nuclear spin isomers exists in antisymmetric rotational states (j_D = odd). The nuclear spin degeneracy is 2 for *ortho* and 1 for *para*, thereby resulting in a relative abundance of 2:1 at room temperature. Upon cooling hydrogen, the relative abundance of the nuclear spin isomers is preserved as nuclear spin conversion is strongly forbidden, unless a paramagnetic molecule like O_2 is present [3].

Not long after the discovery of $(H_2)_2$, the first infrared (IR) spectrum for the H_2–Ar complex was reported where rotational structure corresponding to *end-over-end* rotation of the complex was superimposed on two CIA bands located around 4500 and 4700 cm^{-1} [10]. Investigations into H_2–Ar were then extended to include the hydrogen isotopologues, D_2 and HD [11]. In addition to spectroscopic investigations, the complex has been the subject of many theoretical investigations. The accuracy to which the H_2–Ar potential is known from spectroscopic studies provides a stringent test for the accuracy of *ab initio* calculations. Studies to this day have also included van der Waals complexes of H_2 with He, Ne, Kr and Xe [12-16].

The intensity of a transition in these complexes depends on the population of the states and the induced dipole moment, which is generally orientated along the internuclear axis. For complexes of H_2 with rare gases, H_2–Rg, the strength of the induced dipole moment is proportional to the polarisability of the Rg, which increases with size. Therefore, the low polarisability and small reduced mass means the H_2–Ne complex has very few bound states (up to l = 3) and a small induced dipole moment, making it an especially weak absorber [15]. Additionally, the H_2–Ne complex requires much lower temperatures making the experiment more energy expensive. Thus, the current spectroscopic database on H_2–Ne is rather limited. However, even with these limitations there is published work presenting highly resolved spectra of the complex [13]. Even more troublesome than H_2–Ne is the H_2–He complex, which has only one bound rotational state and therefore only broad CIA has been observed [16]. Similar to H_2–Ar, the H_2–Kr complex has undergone extensive investigation with the best and most detailed spectra of H_2/D_2–Kr published in 2005 [14]. It is important to emphasise that the van der Waals complexes composed of H_2 and a rare gas atoms are rather weakly bound, particularly for H_2-Ne and H_2-He, where the binding energy of H_2-He has been theoretically suggested to be as low as 0.03 cm^{-1} [12].

The H_2–Xe complex forms part of this thesis and will be discussed in Chapter 3. In brief, the H_2/D_2–Xe spectra have been reported and are well resolved, however they show significant blending of peaks that are otherwise predicted to be split, predominantly resulting from the

anisotropic nature of the complex [15]. Resolving these lines will assist in improving the potential energy surface (PES) of the complex. Chapter 3 shows the spectra of H_2–Xe and its deuterated equivalent, D_2–Xe, in the far-IR region using similar temperatures to those used previously in the mid-IR [15]. Lower pressures are required to reduce the effect of pressure broadening, therefore assisting in resolving the blended peaks. However, the far-IR spectroscopy required higher pressures, due to an order of magnitude shorter pathlengths used here in comparison to the previously reported mid-IR investigation, and so resolving blended peaks in this region is problematic.

Following the detection and analysis of H_2–Rg species, the field evolved to include van der Waals species containing a second homonuclear diatomic molecule such as H_2–O_2 (see Fig. 1). Although considered the third most abundant molecule in the universe, molecular oxygen wasn't observed in the ISM until 2007 by its millimetre wave, magnetic dipole transition [17]. In order to verify the currently accepted abundance of oxygen in the ISM, further spectroscopic data are necessary, particularly involving interaction with other abundant molecules such as H_2. This is also important as the modelling of planetary atmospheres and the ISM requires accurate transition frequencies [18]. Furthermore, the study into low temperature, weak van der Waals complexes composed of homonuclear diatomic molecules are important in understanding reactions in the ISM, where the estimation of abundances requires information on collisional rates and the PES of the complex [19]. In particular, collisions between H_2 and O_2 can result in ro-vibrational energy transfer [19], which is astronomically important as such collisions compete with radiative processes within interstellar regions.

A similar system, H_2–N_2, has also been previously observed spectroscopically in both the mid- and far-IR regions [20]. There is evidence that the H_2–N_2 complex has been observed in the far-IR spectrum collected by the Voyager spacecraft from Titan (one of Saturn's satellites), making it of astrophysical importance [20-22]. The detection of this species and the large predicted abundance of O_2 in the ISM and in other planetary atmospheres suggests the likely existence of H_2–O_2. However, it is unlikely to be directly observed due to the weak induced dipole moment of the complex [3] (not to mention if it were largely abundant this would provide a rather unstable, explosive atmosphere). Following on from the recently published far-IR work [3], Chapter 3 also focuses on the H_2–O_2 complex, presenting spectra in the mid-IR for H_2–O_2 and far-IR for D_2–O_2, with both showing evidence of rotational structure. In comparison with the H_2–Rg complexes, where diatomic H_2 is interacting with a single atom, the H_2–O_2 spectra have broader peaks due to the diatomic nature of O_2 and its ability to rotate and change orientation relative to hydrogen. The van der Waals complexes formed with H_2, like those presented in this thesis (H_2–Rg and H_2–O_2), are classified as a linear diatomic molecule (*pseudo*-diatomic), where a linear molecule is defined in terms of moments of inertia, $I_B=I_C$, $I_A=0$.

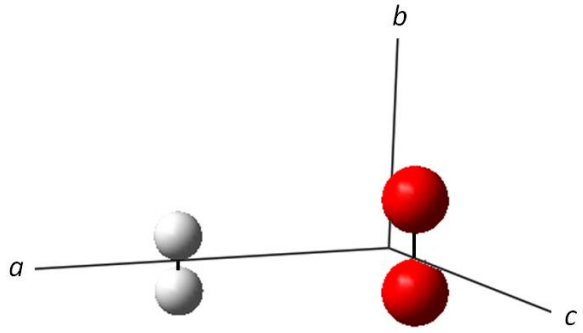

Figure 1. Approximate average, (C_{2v} parallel stacked) geometry of H_2–O_2 showing the alignment of the molecule to the standard *a*, *b* and *c* axes.

II. VINYL ALCOHOL

Vinyl alcohol, CH_2CHOH, is the simplest enol and well known for its astrochemical and biological relevance, and more recently its atmospheric relevance. Enols are well known for their unstable and short lived nature, tautomerising to the more stable keto form, in this case acetaldehyde, CH_3CHO. The high energy barrier associated with keto-enol tautomerisations has lead to the assumption that the higher energy enol forms are not present under terrestrial conditions. Atmospheric models for the production of organic acids have fallen short of the observed abundances. The inclusion of enol contributions accounts for this discrepancy, however it has been previously disregarded because of the energy barrier [23]. A recent study, however, shows that this conversion can become more efficient when catalysed via photochemical processes or by inorganic acid catalysts, suggesting their possible existence under atmospheric conditions [23-25]. This lead to a study in 2014, where it was proposed that vinyl alcohol may actually exist in the troposphere and act as an intermediate in the combustion and oxidation of hydrocarbons, and in the formation of organic acids [26]. A spectroscopic analysis of vinyl alcohol could assist in atmospheric identification, which would provide insight into its contribution in the formation of these organic acids.

According to the Cologne Database for Molecular Spectroscopy (CDMS), as of November 2016 near 200 molecules have been detected with up to 13 atoms, as well as C_{60} and C_{70}, in the ISM and circumstellar shells. Although predicted by Saito in 1976, vinyl alcohol wasn't reported in the ISM until 2001, when Turner and Apponi observed its millimetre wave transitions towards the dense molecular cloud Sagittarius (Sgr) B2(N) [27]. Unofficially nicknamed the "Large Molecular Heimet", this molecular cloud is well known for its significant proportion of "complex" ($\geq$ 6 atoms) organic molecules with some other recent identifications attributable to methyl formate [28], amino acetonitrile [29] and glycolaldehyde [30]. The more thermodynamically stable isomer of vinyl alcohol, acetaldehyde, and kinetically stable cyclic isomer, ethylene oxide, are both well known to exist in the ISM [31, 32]. Acetaldehyde is important astrobiologically owing to its discovery as a precursor to the amino acid intermediate acrolein [33]. The discovery of ethylene oxide has lead scientists to believe that other cyclic structures are also present in the ISM, such as furan, important in the formation of the sugars

ribose and deoxyribose that make up RNA and DNA, respectively [34]. Larger organic species, however, are much more difficult to detect due to the weak transitions caused by large partition functions and low abundance.

Vinyl alcohol is a planar, polyatomic molecule, with C_s symmetry and 3 unique moments of inertia $I_A<I_B<I_C$ (see Fig. 2) that characterise it as an asymmetric top. It has 15 fundamental modes (i.e. 3N-6, where N = 7), 11 of these are symmetric (*a*') and 4 asymmetric (*a*''). Until now only 10 out of 15 vibrational modes of gas phase vinyl alcohol have been observed. In comparison to diatomic or *pseudo*-diatomic molecules like the van der Waals complexes introduced above, polyatomic molecules such as vinyl alcohol are much more rotationally and vibrationally complex, making for an interesting and more complex analysis. Vinyl alcohol also exists as two rotamers, known as *syn* and *anti*, corresponding to a torsional CCOH dihedral angle of 0° and 180°, respectively. The detection of vinyl alcohol dates back to 1973 in NMR studies [35] and yet the presence of the *anti* conformer was not confirmed until 1985 [36].

The most detailed analysis, so far, for *syn*-vinyl alcohol has been on the ν_{13} mode, which shows perturbations resulting from Coriolis interactions between ν_{13} and $2\,\nu_{15}$. A Coriolis perturbation is a vibrational-rotational interaction where the rotation of a molecule introduces a Coriolis force resulting in the coupling of vibrations, and often results in the splitting and/or shifting of energy levels [37]. A Coriolis perturbation generally occurs between two states of opposite symmetry, however this is not always the case e.g. see [38], and is most noticeable in a spectrum when the interaction occurs between two vibrational states typically within 100 cm^{-1} of each other. Previous observations of vinyl alcohol in the IR have also shown the presence of perturbations resulting from Fermi resonances i.e. between ν_9 and $\nu_{14} + \nu_{15}$ combination band [39]. Fermi interactions result from an interaction between two nearby states with the same symmetry and very similar energy, which results in shifting of energies and intensities of the interacting modes.

This thesis, starting in Chapter 4, presents the first observation of the ν_{15} OH torsional mode of both *syn*- and *anti*-vinyl alcohol, including highly resolved rotational structure. In addition to the fundamental transitions, detailed spectra of the corresponding hot band(s) are observed for both the *syn* and *anti* rotamers, where a hot band originates from an already excited vibrational state. Chapter 4 also includes detailed results from CCSD(T) calculations, providing accurate vibrational frequencies and energy barriers between the two rotamers. Chapters 5 and 6 present details on the high resolution analysis of *syn* and *anti*-vinyl alcohol respectively, providing accurate rotational and centrifugal distortion constants up to the sextic level. The first far-IR detection of monodeuterated vinyl alcohol, CH_2CHOD, is presented in Chapter 7, providing estimated column densities and giving insight into the possibility of its detection in the ISM. Chapter 8 summarises the work presented in Chapters 3–7 and provides thoughts into possible future research.

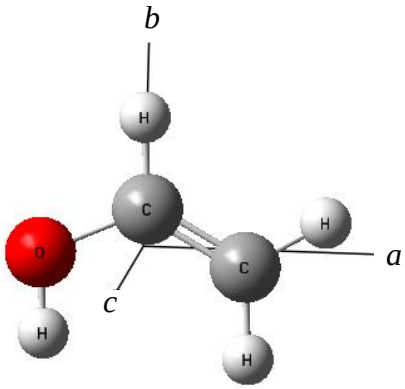

Figure 2. CCSD(T) optimised structure of *syn*-vinyl alcohol showing the alignment of the molecules to the standard *a*, *b* and *c* axes.

REFERENCES

[1] E. F. Dishoeck, Faraday Discuss. **168**, 9 (2014).

[2] H. M. James, A. S. Coolidge, ApJ **87**, 438 (1938).

[3] H. Bunn, T. Bennett, A. Karaylian, P. L. Raston, ApJ **799**, 65 (2015).

[4] H. L. Welsh, M. F. Crawford, J. C. F. MacDonald, D. A. Chrisholm, Phys. Rev. **83**, 1264 (1951).

[5] A. Watanabe, H. L. Welsh, Phys. Rev. Lett. **13**, 26 (1964).

[6] A. R. W. McKellar, Can. J. Phys. **62**, 760 (1984).

[7] R. S. L. Frommhold, G. Birnbaum, ApJ **283**, 79 (1984).

[8] A. R. W. McKellar, ApJ **326**, 75 (1988).

[9] A. R. W. McKellar, J. Schaefer, J. Chem. Phys. **95**, 3081 (1991).

[10] A. Kudian, H. L. Welsh, A. Watanabe, J. Chem. Phys. **43**, 3397 (1965).

[11] A. R. W. McKellar, J. Chem. Phys. **105**, 2628 (1996).

[12] B. W. Bakr, D. G. A. Smith, K. Patkowski, J. Chem. Phys. **139**, 144305 (2013).

[13] A. R. W. McKellar, Can. J. Phys. **87**, (2009).

[14] A. R. W. McKellar, J. Chem. Phys. **122**, 084320 (2005).

[15] A. R. W. McKellar, Can. J. Phys. **91**, 957 (2013).

[16] P. Barletta, Eur. Phys. J. D **53**, 33 (2009).

[17] B. Larsson, R. Liseau, L. Pagani, P. Bergman, P. Bernath, N. Biver, J. H. Black, R. S. Booth, V. Buat, J. Crovisier, C. L. Curry, M. Dahlgren, P. J. Encrenaz, E. Falgarone, P. A. Feldman, M. Fich, H. G. Florén, M. Fredrixon, U. Frisk, G. F. Gahm, M. Gerin, M. Hagström, J. Harju, T. Hasegawa, Å. Hjalmarson, L. E. B. Johansson, K. Justtanont, A. Klotz, E. Kyrölä, S. Kwok, A. Lecacheux, T. Liljeström, E. J. Llewellyn, S. Lundin, G. Mégie, G. F. Mitchell, D. Murtagh, L. H. Nordh, L.-Å. Nyman, M. Olberg, A. O. H. Olofsson, G. Olofsson, H. Olofsson, G. Persson, R. Plume, H. Rickman, I. Ristorcelli, G. Rydbeck, A. A. Sandqvist, F. V. Schéele, G. Serra, S. Torchinsky, N. F. Tothill, K. Volk, T. Wiklind, C. D. Wilson, A. Winnberg, and G. Witt, A&A **466**, 99 (2007).

[18] P. Maréchal, Y. P. Viala, J. J. Benayoun, A&A **324**, 221 (1997).

[19] Y. Kalugina, O. D. Alpizar, T. Stoeklin, F. Lique, Phys. Chem. Chem. Phys. **14**, 16458 (2012).

[20] A. R. W. McKellar, J. Chem. Phys. **93**, 18 (1990).

[21] A. Borysow, L. Frommhold, ApJ **303**, 495 (1986).

[22] G. Bachet, D. Gautier,, A. Coustenis, C. R. Acad. Sci. Paris **307**, 133 (1988).

[23] A. E. Clubb, M. J. T. Jordon, S. H. Kable, D. L. Osborn, J. Phys. Chem. Lett. **3**, 3522 (2012).

[24] D.U. Andrews, B.R. Heazlewood, A.T. Maccarone, T. Conroy, R.J. Payne, M.J.T. Jordan, S.H. Kable, Sci. **337**, 1203 (2012).

[25] G. d. Silva, Angew. Chem. Int. Ed. **49**, 7523 (2010).

[26] S. So, U. Wille, G. da Silva, ES&T **48**, 6694 (2014).

[27] B. E. Turner, A. J. Apponi, ApJ **561**, 207 (2001).

[28] J. L. Neill, M. T. Muckle, D. P. Zaleski, A. L. Steber, B. H. Pate, V. Lattanzi, S. Spezzano, M. C. McCarthy and A. J. Remijan, ApJ **755**, 153 (2012).

[29] A. Belloche, K. M. Menten, C. Comito, H. S. P. Müller, P. Schilke, J. Ott, D. Thorwirth, C. Hieret, A & A **482**, 179 (2008).

[30] J. M. Hollis, F. J. Lovas, P. R. Jewell, ApJ Lett. **540**, L107 (2000).

[31] J. E. Dickens, W. M. Irvine, M. Ohishi, M. Ikeda, S. Ishikawa, A. Nummelin, Å. Hjalmarson ApJ **489**, 753 (1997).

[32] H. E. Matthews, P Friberg, W. M. Irvine, ApJ **290**, 609 (1985).

[33] H. J. Cleaves, Monatshefte Chem. **134**, 585 (2003).

[34] C. J. Bennett, Y. Osamura, M. D. Lebar, R. I. Kaiser, ApJ 698 (2005).

[35] B. Blank, H. Fischer, Helvetica Chimica Acta **56**, 45 (1973).

[36] M. Rodler, J. Mol. Spec. **114**, 23 (1985).

[37] P. F. Bernath, *Spectra of Atoms and Molecules,* Oxford university press (1995).

[38] A. R. W. McKellar, D. R. T. Appadoo, J. Mol. Spec. **250**, 106 (2008).

[39] D-L Joo, A. J. Merer, D. J. Clouthier, J. Mol. Spec. **197**, 68 (1999).

2. Experimental and Computational Methods, and Data Analysis

I. AUSTRALIAN SYNCHROTRON

All experiments included in this thesis were performed at the Terahertz & Far-infrared (IR) beamline at the Australian Synchrotron, Victoria, Australia. Synchrotrons produce highly polarised, intense, light beams from the acceleration of electrons in a circular-like (polygonal) pattern. In brief, the electrons are generated by an electron gun and then accelerated by a linear accelerator to speeds close to the speed of light (99.9997%). The electrons are injected into a booster ring before being transferred to a storage ring consisting of magnets designed to deflect the electrons in a circular-like pattern. This change in direction of the electrons causes them to emit energy in the form of photons. Separating the "bending" magnets, are straight sections, that contain insertion devices, i.e. undulators and wigglers that cause the beam to periodically deflect between alternating magnets, with the aim to further increase the intensity of the light. The storage ring is kept under ultrahigh vacuum to prevent electrons from colliding with gases in the air, that decay the beam. The light produced at each "stage" in this storage ring is used by the individual beamlines, where it may be focussed and split into desired wavelengths for use in experimentation. The immense intensity from the THz & Far-IR beamline allows for the detection of unstable and weakly absorbing species with good S/N, within a reasonable time frame, making it ideal for measuring the rotational and ro-vibrational spectra of both "diatomic" and polyatomic species, such as those presented in this thesis [1]. A variety of optical filters, detectors and beam splitters are available at the Australian Synchrotron, outlined below, to provide ideal light coverage and intensity in the THz to mid-IR region, however, only synchrotron radiation between ~30–700 cm^{-1} was used for the studies reported in this thesis. A standard Globar source was used for the mid-IR studies.

II. FTIR SPECTROMETER

This technique is one of the most well known and commonly used forms of IR spectroscopy due to its high sensitivity, good spectral resolution, and high throughput of radiation. The core of a Fourier Transform Infrared (FTIR) spectrometer is the interferometer, which was originally designed by Michelson in 1891. An interferometer basically contains a beam splitter and two mirrors (Fig. 1). For the experiments presented in Chapter 3-7, broadband IR light is directed toward the beam splitter where half the light is transmitted through and the other half reflected. The reflected half travels towards mirror one (M_1) and the transmitted half travels to mirror two (M_2), where they are both reflected back. Whilst mirror one is fixed, mirror two can be moved closer to, or further away from, the beam splitter, causing the two beams to interfere constructively or destructively when they recombine. The recombined beam is then directed through a sample compartment, after which it is focussed onto a detector. The resulting spectrum is known as an interferogram, which is in the form of intensity as a function of the distance moved by M_2. A Fourier transformation is then used to convert the interferogram into a more useful (transmittance) spectrum of intensity as a function of wavelength (Fig. 2). This is then ratioed against a "background" (transmittance) spectrum and by taking the negative log, one creates an absorbance spectrum [2]. The THz & Far-IR facility at the Australian

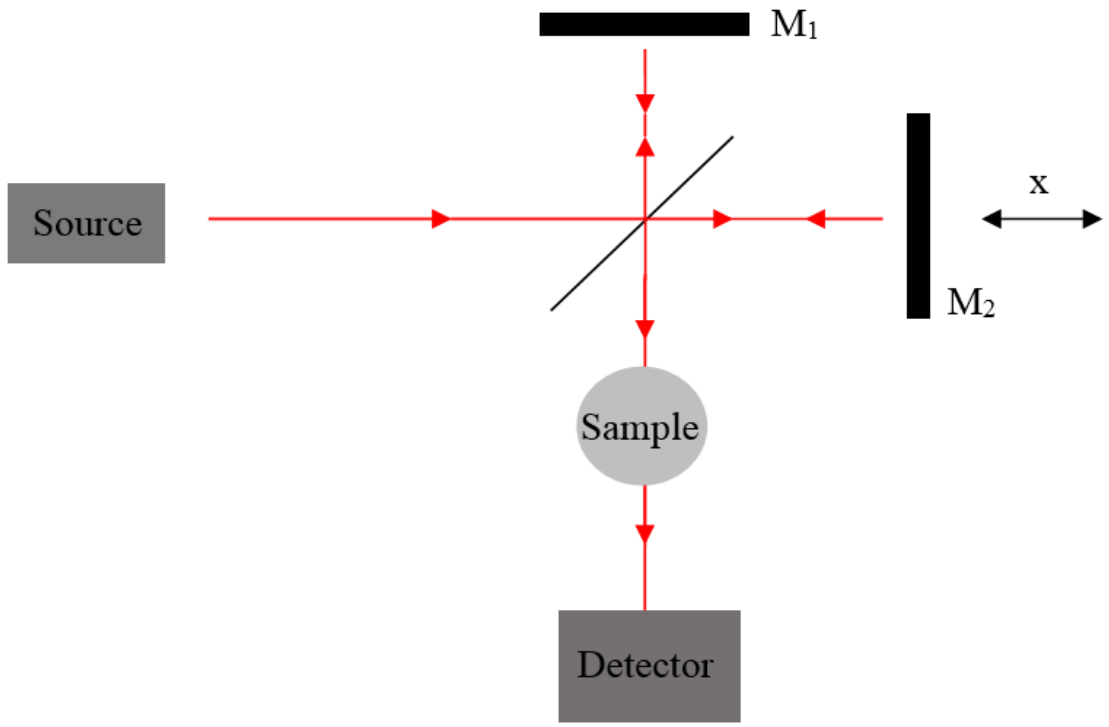

Figure 1. Simplistic representation of an interferometer.

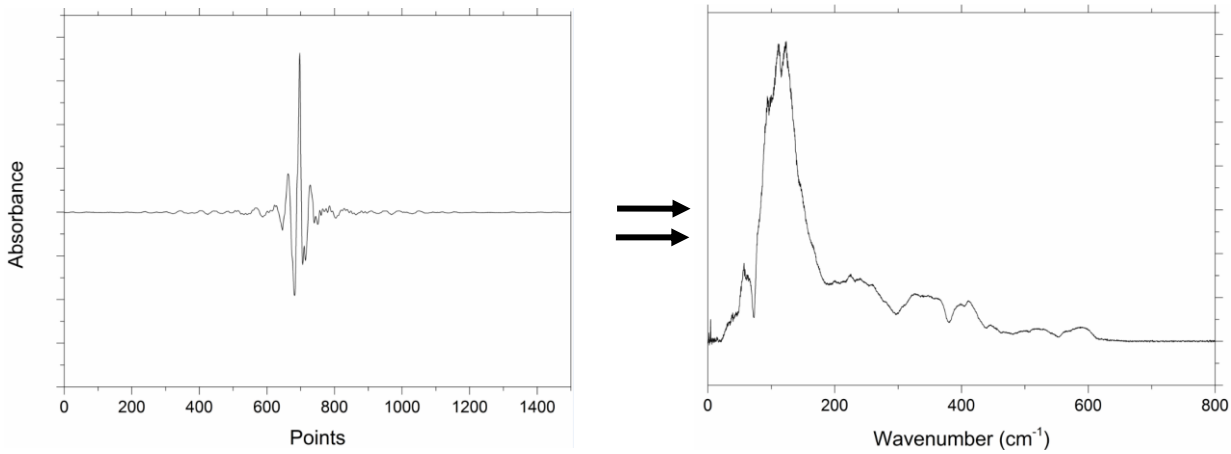

Figure 2. Interferogram (left) and its Fourier transformed transmission spectrum (right). The set up used, included a Mylar Beam splitter, polyethylene windows and Silicon bolometer detector, resulting in optimal light intensity around 150 cm^{-1}. This set up was used for the far-IR experiments on D_2–Xe and D_2–O_2, and the second set of experiments for H_2–Xe.

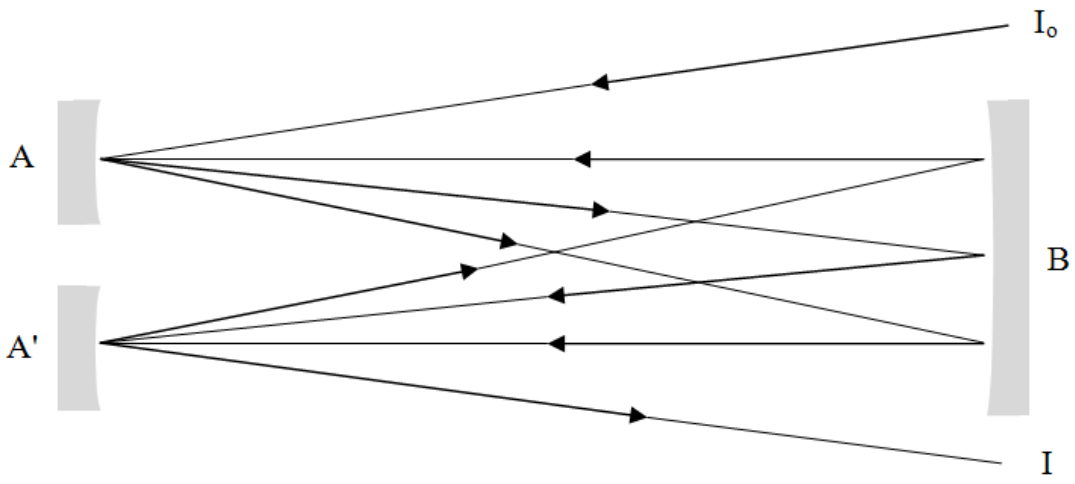

Figure 3. Simple diagram showing the path of light through a multipass cell at 8 passes.

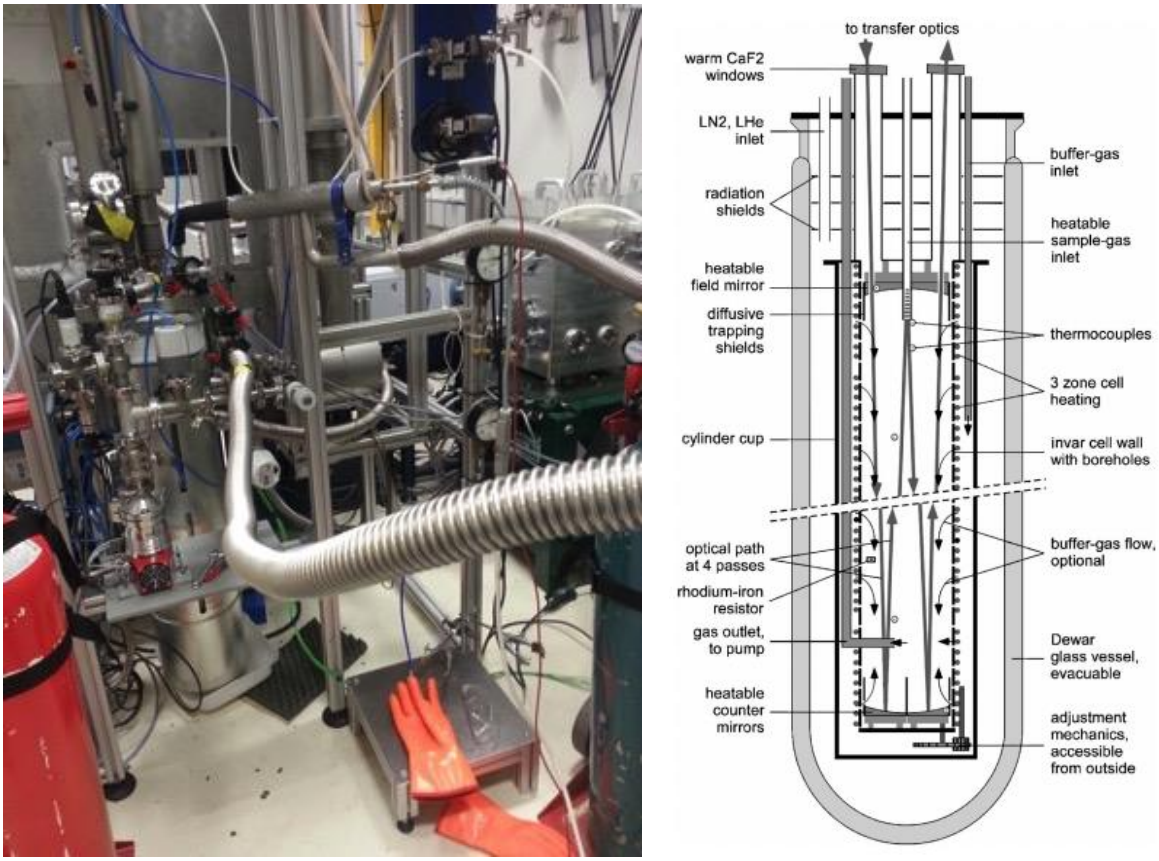

Figure 4. The Enclosive flow cooling cell at the Australian Synchrotron (left) showing the set up for H_2–O_2 experiments where the outer jacket is being filled with liquid nitrogen through the stainless steel bellows. A detailed cross section of the multiple reflection cell that can be cooled with liquid or gas nitrogen is also provided (right) reproduced with permission from Rev. Sci. Instrum. [3].

Synchrotron has a Bruker IFS 125/HR FTIR with a scanning arm that moves up to 5 m. The long M_2 pathlength results in a large optical path difference, which allows for a high maximum resolution of 0.00096 cm^{-1}.

III. MULTIPASS AND ENCLOSIVE FLOW COOLING CELLS

A multipass cell, 570 mm in length, available at the THz & Far-IR beamline at the Australian Synchrotron was used for the vinyl alcohol experiments presented in this thesis. Also available at the Australian Synchrotron is an Enclosive Flow Cooling (EFC) used for experiments involving van der Waals complexes, utilising only the multipass cell, 625 mm, and the cooling capacity of the outer jacket (Fig. 4). The use of a multipass (White) cell, described in more detail elsewhere [4], allows for the beam of IR light to pass through the sample multiple times increasing the pathlength, which by Beer's law, increases the absorbance. The cell contains three spherical, concave mirrors as shown in Figure 3. Two mirrors, A and A', are located at one end and the third, B, at the other with its centre of curvature half way between A and A'. The number of passes through the cell can be changed (in multiples of 4) by adjusting the tilt of mirrors A and A'. Although a longer pathlength resulting from more passes is ideal, the loss in light intensity must also be considered as the absorbance is proportional to the intensity of incident light.

IV. MEASUREMENT OF VAN DER WAALS COMPLEXES

All experiments involving van der Waals complexes used the multipass cell in the enclosive flow cooling (EFC) cell. The outer jacket of the cell was filled with liquid nitrogen for H_2–O_2 or cold (160 K) nitrogen gas for H_2–Xe. 200 Torr of each gas, save for oxygen at 140 Torr (which is its vapour pressure at 80 K), was introduced into the cell at 16 passes, providing a pathlength of 10 m. For the far-IR experiments the FTIR spectrometer, with an aperture of 12.5 mm and set to a resolution of 0.15 cm^{-1}, was equipped with a Mylar Beam splitter. For the first set of H_2–Xe experiments a liquid helium cooled silicon bolometer photodetector and KBr windows were used providing high light intensity around 500 cm^{-1} (Fig. 5). Due to the time required to change and reoptimise conditions, the silicon bolometer detector and polyethylene windows were used for the second set of experiments during which D_2–Xe was also investigated. This resulted in optimal light intensity around 150 cm^{-1} (Fig 2.)

The mid-IR experiments on H_2–O_2 used the available globar source (as opposed to the Synchrotron source), which passed through KBr windows and into the cell at 32 passes, resulting in a pathlength of 20 m. The FTIR spectrometer, using an aperture of 1.7 mm and a resolution of 0.3 cm^{-1}, was equipped with a KBr Beam splitter and MCT detector. This provided optimal light intensity in the desired range, around 4100 cm^{-1} to 4800 cm^{-1} (Fig.6).

Spectra presented here are composed of multiple scans over hours/days depending on S/N improvement and time constraints. As a rough guide the H_2–Xe spectrum is composed of approximately 15000 scans, D_2–Xe 50000 scans, H_2-O_2 84000 scans and D_2–O_2 100000 scans. More scans for the deuterated complexes were performed and averaged due to the difficulty in detecting these complexes, and the lower induced dipole of D_2 compared with H_2.

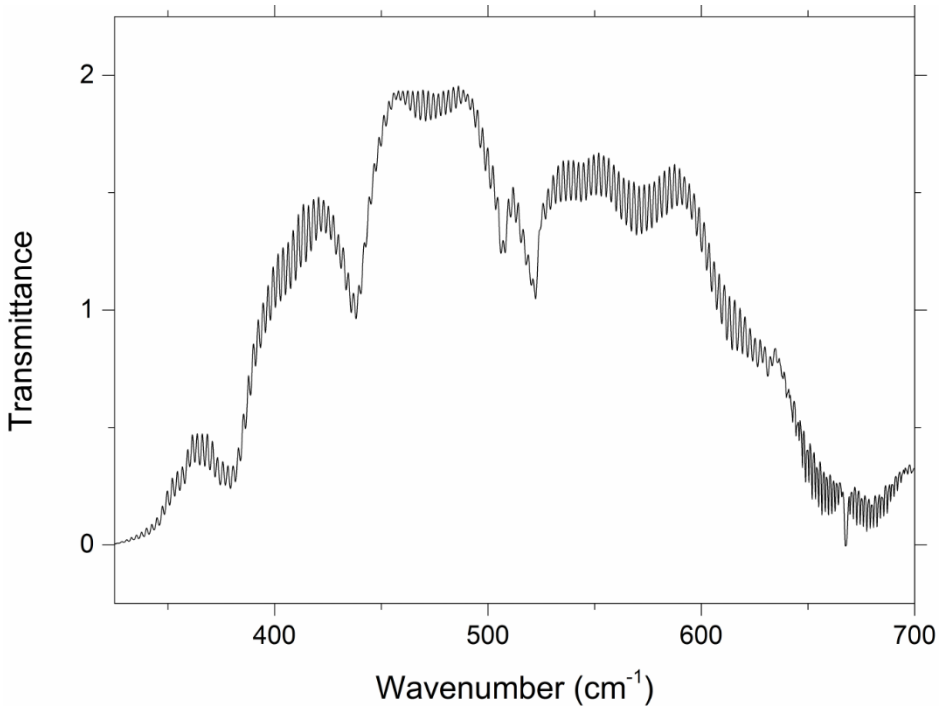

Figure 5. Synchrotron light profile for the first H_2–Xe experiment using the Si-bolo photodetector and KBr windows.

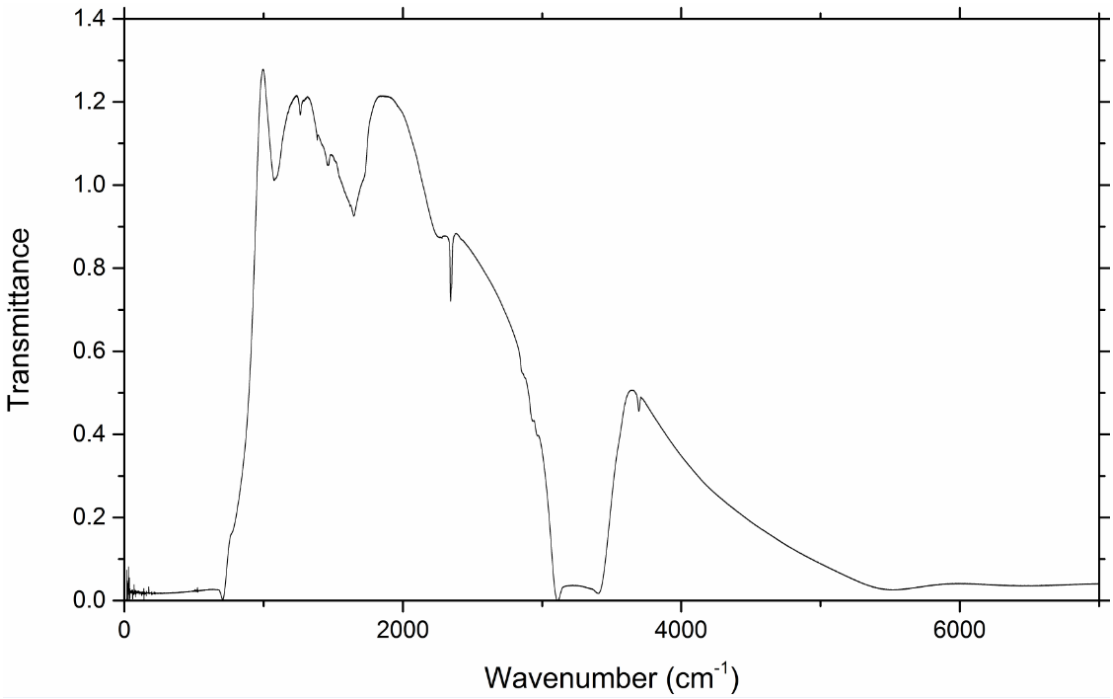

Figure 6. Light profile of the globar source directed into a vented multipass cell, used in conjunction with a KBr Beam splitter, KBr windows and an MCT detector, for the mid-IR experiments on H_2–O_2.

V. MEASUREMENT OF VINYL ALCOHOL

For the experiments involving vinyl alcohol, the precursor, 2-chloroethanol, was pyrolysed at a temperature of 950 °C through a clean 300 mm quartz tube with a diameter of 25 mm (Fig. 7 left). The products were then continuously flowed through the multipass cell, described above, at room temperature with 16 passes providing a total pathlength of 10 m (Fig. 7 right). The contents were pumped out through a nitrogen trap and a pump exhaust. Spectra of vinyl alcohol were collected at cell pressures of 0.5 Torr and 2 Torr, to provide details in both the intense band origin regions and also to provide good S/N in the weaker regions (e.g. for *anti*-vinyl). For the high pressure experiments a 50 mL round bottom flask was used, approximately 3/4 filled and was warmed with heating tape to ~50 °C. The tubing connecting the round bottom to the pyrolysis tube was also heated to ~50 °C. For the low pressure experiments a 5 mL sealable pyrex finger was used at room temperature. In both cases the room temperature sample was pumped through the system for about 5-10 minutes to remove air and any impurities with a higher vapour pressure. The spectrometer was operated at maximum resolution (0.00096 cm^{-1}), using a 6.3 mm or 10 mm circular aperture for the low and high pressure experiments, respectively. The apparatus was equipped with a Mylar Beam splitter, polyethylene windows, and liquid helium cooled silicon bolometer. This setup provided optimal light intensity below 700 cm^{-1} (see Fig. 8).

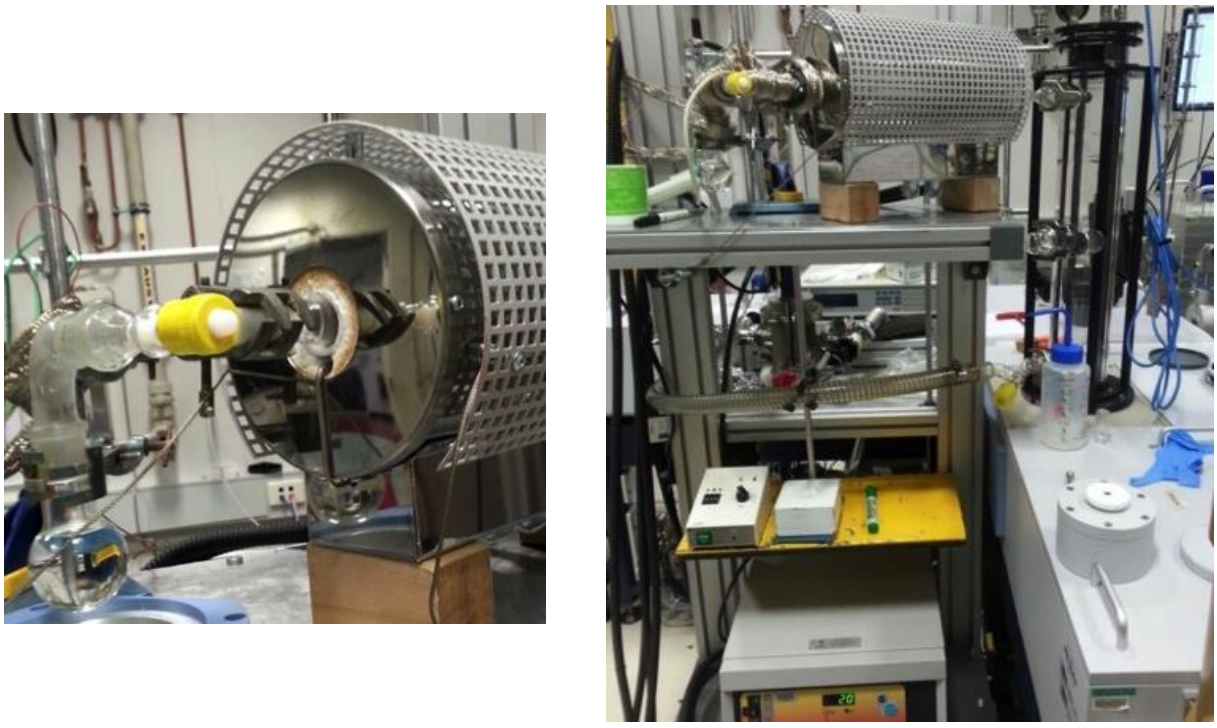

Figure 7. On the left is the set up showing the round bottom flask containing almost 50 mL of 2-chloroethanol attached to the quartz pyrolysis tube in the oven with a valve to seal off and somewhat regulate the flow (used for the high pressure vinyl alcohol experiments). On the right is the full set up for the high pressure experiments of vinyl alcohol where the pyrolysis tube is connected to the room temperature multipass cell which sits in the sample chamber past the interferometer. Note that heating tape was also wrapped around the round bottom flask containing the precursor.

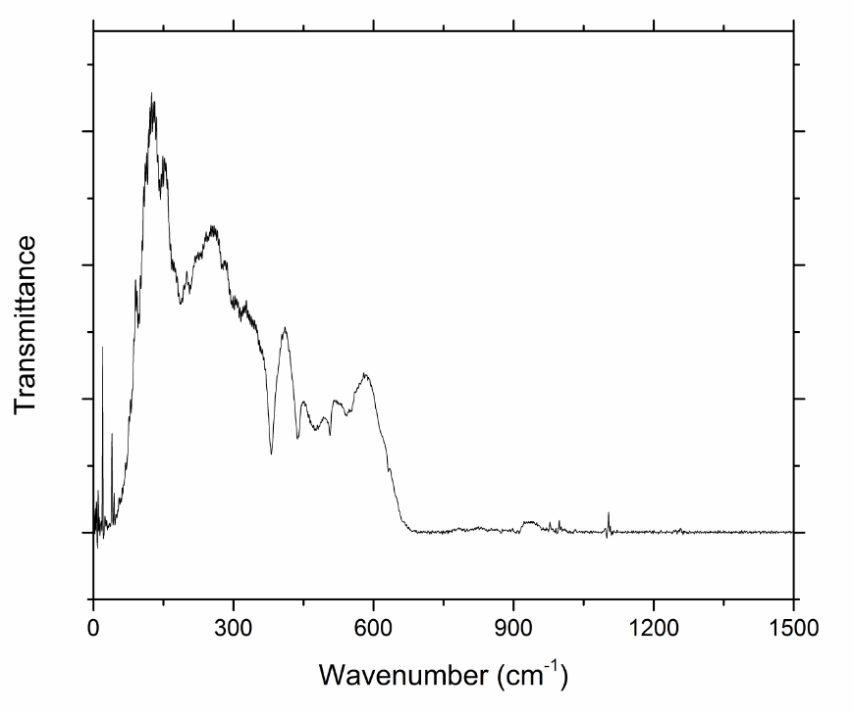

Figure 8. Synchrotron light profile for the far-IR vinyl alcohol experiments.

Monodeuterated vinyl alcohol used the same setup as the 'high pressure' vinyl alcohol experiments. The precursor, 2-chloroethanol, was successfully deuterated by mixing 25 mL of it with 3 x 10 mL D_2O. For each deuteration attempts were made to dry the mixture by using a rotary evaporator, followed by extraction of the precursor with dichloromethane, and finally mixing with $MgSO_4$. The formation of a rather strong azeotrope between water and 2-chloroethanol, however, made the water exceptionally difficult to remove.

Like for the van der Waals complexes, the vinyl alcohol spectra are composed of multiple scans run over hours/days. Approximately 8000 scans for the low pressure and 2000 scans for high pressure experiments were compiled and 7000 for monodeuterated vinyl alcohol.

VI. SPECTROSCOPIC ANALYSIS

PGOPHER [5] is a spectral fitting program that can be used to fit and simulate electronic, vibrational and rotational spectra. The program is used in this thesis to fit asymmetric top Hamiltonians to rotational structure within the ν_{15} OH torsional vibration of vinyl alcohol; this allows for the extraction of vibrational, rotational, and centrifugal distortion parameters. The simulation of vinyl alcohol began with defining the molecular properties, i.e. asymmetric top with C_s symmetry, along with the experimental conditions such as temperature and resolution. The representation used which defines the axes must also be selected. In this thesis the I^r representation was used, where the x, y and z axes are defined as *a*, *b* and *c*, respectively (see Figure 1 in Chapter 1 and Table 1 in Ref. [5]).

The next step was to simulate the fundamental band by providing ground and excited state rotational constants, band origins and the symmetry of both states, e.g. *a″* for $\nu_{15} = 1$. For *anti*-vinyl alcohol this was done using the ground state rotational and centrifugal distortion constants up to the quartic level from Rodler's microwave study [6]. The difference between the ground and excited state rotational constants from an MP2 anharmonic frequency calculation was added to the ground state constants to get a reasonable estimate of the excited state rotational constants. The ν_{15} OH torsional band is a *c*-type transition and therefore must be defined as so. From here the simulation gave a useful approximation to the experimental spectrum, which can be imported as an overlay for comparison.

The process for improving the fit from here varies for each molecule and vibration and its difficulty depends largely on the accuracy of the initial constants provided. Each simulation in this thesis was fit to a Watson's *A* reduced Hamiltonian, typically starting with rotational constants and the band origin, and gradually including higher order centrifugal distortion parameters. A detailed description of the fit and assignment of line positions from this point is provided in Chapters 5-7 for *syn*-, *anti*- and monodeuterated vinyl alcohol respectively.

VII. COMPUTATIONAL CALCULATIONS

Using the Gaussian 09 electronic structure package [7] optimisation calculations were performed in order to provide minimum energy structures of *syn* and *anti*-vinyl alcohol. *Anti*-vinyl alcohol, being a local rather than global minimum was successfully minimised by constraining the CCOH dihedral angle to 180°. The optimisations were performed starting with second order Møller-Plesset theory (MP2) and then subsequently using coupled cluster theory incorporating single, double and perturbative triple excitation contributions [CCSD(T)]; this provided a coordinate geometry closer to what is likely to be "observed" experimentally. Both MP2 and coupled cluster methods are considered post Hartree-Fock (HF) and improve upon the HF method by introducing electron correlation and many body interactions. This is essential for reliable and accurate computation of molecular properties of the molecules studied here. In both instances, a Dunning's correlation-consistent (cc) quadrupole-zeta basis set, i.e. cc-pVQZ, was used, where p = polarised, V = valence.

Anharmonic frequency calculations were subsequently performed based on the optimised geometry coordinates from which the vibrational frequencies of the molecules along with their rotational and centrifugal distortion constants were extracted. Since Gaussian 09 does not have analytic second gradients implemented in the CCSD(T) method, all anharmonic frequencies were calculated using the MP2 approach. The frequencies provided by the anharmonic frequency calculations allowed for accurate location and confident assignment of the bands observed experimentally. The rotational and centrifugal distortion constants, along with those previously reported experimentally, provided a good starting point for spectral simulations using PGOPHER [5], as mentioned above. This then enabled further refinement of these constants based on the measured spectra.

REFERENCES

[1] M. R. Stem, J. Chem. Ed. **85**, 983 (2008).

[2] W. Herres, J. Gronholz, J. Comput. Appl. Lab. **2**, 216 (1984).

[3] S. Bauerecker, M. Tarascjewski, C. Weitkamp, H. K. Cammenga, AIP **72**, 3946 (2001).

[4] J. U. White, J.O.S.A. **32**, 285 (1942).

[5] C. M. Western, J. Quant. Spectrosc. Radiat. Transfer **186**, 221 (2017).

[6] M. Rodler, J. Mol. Spec. **114**, 23 (1985).

[7] M. J. Frisch, G. W. Trucks, H. B. Schlegel, G. E. Scuseria, M. A. Robb, J. R. Cheeseman, G. Scalmani, V. Barone, B. Mennucci, G. A. Petersson, H. Nakatsuji, M. Caricato, X. Li, H. P. Hratchian, A. F. Izmaylov, J. Bloino, G. Zheng, J. L. Sonnenberg, M. Hada, M. Ehara, K. Toyota, R. Fukuda, J. Hasegawa, M. Ishida, T. Nakajima, Y. Honda, O. Kitao, H. Nakai, T. Vreven, J. A. Montgomery, Jr., J. E. Peralta, F. Ogliaro, M. Bearpark, J. J. Heyd, E. Brothers, K. N. Kudin, V. N. Staroverov, R. Kobayashi, J. Normand, K. Raghavachari, A. Rendell, J. C. Burant, S. S. Iyengar, J. Tomasi, M. Cossi, N. Rega, J. M. Millam, M. Klene, J. E. Knox, J. B. Cross, V. Bakken, C. Adamo, J. Jaramillo, R. Gomperts, R. E. Stratmann, O. Yazyev, A. J. Austin, R. Cammi, C. Pomelli, J. W. Ochterski, R. L. Martin, K. Morokuma, V. G. Zakrzewski, G. A. Voth, P. Salvador, J. J. Dannenberg, S. Dapprich, A. D. Daniels, O. Farkas, J. B. Foresman, J. V. Ortiz, J. Cioslowski, and D. J. Fox, Gaussian 09, Revision A.02, Gaussian, Inc., Wallingford CT, 2009.

Statement of Authorship

Title of Paper	Infrared Spectroscopy of the H_2/D_2–Xe and H_2/D_2–O_2 van der Waals Complexes
Publication Status	☐ Published ☐ Accepted for Publication ☐ Submitted for Publication ☑ Unpublished and Unsubmitted work written in manuscript style
Publication Details	

Principal Author

Name of Principal Author (Candidate)	Hayley A Bunn		
Contribution to the Paper	Experimental work, analysis and write up		
Overall percentage (%)	80		
Certification:	This paper reports on original research I conducted during the period of my Higher Degree by Research candidature and is not subject to any obligations or contractual agreements with a third party that would constrain its inclusion in this thesis. I am the primary author of this paper.		
Signature		Date	19/01/2017

Co-Author Contributions

By signing the Statement of Authorship, each author certifies that:

i. the candidate's stated contribution to the publication is accurate (as detailed above);

ii. permission is granted for the candidate in include the publication in the thesis; and

iii. the sum of all co-author contributions is equal to 100% less the candidate's stated contribution.

Name of Co-Author	Paul L Raston		
Contribution to the Paper	Conceptualisation of project and experiments. Support and advice on experiments and editing of drafts. 20%		
Signature		Date	18/01/17

3. Infrared Spectroscopy of the H_2/D_2–Xe and H_2/D_2–O_2 van der Waals Complexes

Hayley Bunn[1], Paul L. Raston[2]

[1]*Department of Chemistry, University of Adelaide, SA 5005, Australia*
[2]*Department of Chemistry and Biochemistry, James Madison University, Harrisonburg, Virginia 22807, USA*

Here we present the far-infrared spectra of H_2/D_2–Xe and D_2–O_2 along with the mid-infrared spectrum of H_2–O_2, recorded at the Terahertz & Far-Infrared Beamline facility at the Australian Synchrotron. For H_2–Xe, we see reasonably well resolved *N* and *T* ($\Delta l = \pm 3$, where *l* is the *end-over-end* rotational quantum number of the complex) branch peaks in the j_H = 3–1 [i.e. *S*(1)] band of molecular hydrogen (where j_H is the rotational quantum number of the hydrogen molecule), and only partially resolved analogous peaks in the j_H = 2–0 [*S*(0)] band. The D_2–Xe and D_2–O_2 spectra show the presence of *P* and *R* ($\Delta l = \pm 1$) branches yet lack any rotational fine structure; the larger reduced mass of D_2 compared to H_2 should result in a reduced rotational constant of the complex and more rotationally bound states, however, spectra were not well enough resolved to provide this information. We observed 'sharp' peaks in the mid-infrared region, corresponding to the *end-over-end* rotation of H_2–O_2, that are comparatively noisier than spectra of the same complex in the far-infrared, where the synchrotron light is brightest.

I. INTRODUCTION

Among the first van der Waals complexes to undergo rotationally resolved spectroscopic studies were those that contain molecular hydrogen and a rare gas (Rg) atom [1].The majority of work done both experimentally and theoretically has involved the H_2–Ar complex, for which the potential energy surface (PES) is the most accurately known among these species [2, 3]. Other studies have investigated H_2–Rg complexes with Rg = He [4], Ne [5], Kr [6], and Xe [1].

Spectroscopic investigations into the H_2–Xe complex are somewhat restricted due to the expense involved in obtaining Xe. However, Xe is highly polarisable in comparison with the other rare gases, and since the induced dipole moment is proportional to the polarisability in H_2–Rg complexes, H_2–Xe will have the strongest absorptions. The spectroscopy of H_2–Xe dates back to 1971 [7] where the collision induced H_2 spectra was accompanied by some rotational substructure. Defined *P* and *R* branches with unresolved transitions and broad, yet resolved, *N* and *T* branch peaks were observed, and an analysis allowed for determination of several parameters such as its rotational constant (0.463 cm^{-1}). It was noticed in that study that the H_2–Rg complexes did not strictly obey a normal rigid rotor model with an isotropic intermolecular potential, but were affected by the anisotropy in the intermolecular potential (which leads to additional splittings). The isotropic potential model provided a good overall agreement, but the additional substructure in more highly resolved spectra, required the introduction of an anisotropic potential [7]. The spectra were then further improved that same year by the use of reduced densities to decrease pressure broadening [8]. Based on these spectroscopic results, the PES of H_2–Xe was improved upon [9], accounting for the effects relating to the anisotropy in the PES [10].

Recently, spectra of H_2–Xe were published by McKellar [1], improving upon the accuracy of the line positions by reducing the line widths. He reported up to and including l = 10 (where l is the *end-over-end* rotational quantum number of the complex) bound *end-over-end* rotational states, as evidenced in spectra collected in the mid-infrared (IR) region. The spectra of D_2–Xe were also reported, which showed evidence for up to l = 17 rotationally bound states [1]. That study provided accurate mid-IR band origins along with greatly improved rotational constants (0.4713 cm^{-1} and 0.4715 cm^{-1} for B' and B'') as well as centrifugal distortion constants for H_2–Xe. Additional weak and blended lines are also noticeable in the H_2–Xe spectra resulting from both the *P* and *R* and the *N* and *T* branch transitions having multiple components. Even at such low temperatures and pressures and with a medium resolution (0.04 cm^{-1}), not all of the fine structure transitions were resolved. Severe blending was also observed in the D_2–Xe spectra. In addition to this, Xe has 8 naturally occurring isotopes meaning each detected ro-vibrational peak is made up of 8 individual lines at slightly different frequencies. Isotopic 'splitting' has not been observed to date for H_2–Xe, however it has been previously observed for other complexes, e.g. Xe–CO [11-13]. The first part of this chapter focuses on the far-IR spectra of the H_2– and D_2–Xe van der Waals complexes, with an attempt to resolve blended peaks, which could be used to assist in refining the PES of the complex.

Besides Rg species, van der Waals complexes of H_2 with another diatomic molecule such as O_2 are of interest. Previously, H_2–O_2 has been studied using low energy scattering experiments [14], and theoretical work in modelling the H_2–O_2 PES [15, 16] predicted up to 5 rotationally bound excited states. Van der Waals complexes composed of homonuclear diatomic molecules such as H_2 and O_2 are difficult to study via spectroscopic techniques as they possess small induced dipole moments (~10^{-3} D) and therefore exhibit very weak spectra. Obtaining well resolved spectra involves using long path lengths and low temperatures at moderate pressures. It wasn't until early 2015 that the first spectrum of H_2–O_2 was reported [17]; we identified 2 collisionally induced absorption bands, corresponding to *ortho* (j_H = odd) and *para* hydrogen (j_H = even), with superimposed rotational fine structure. The analysis of the fine structure, corresponding to the complexes *end-over-end* rotation, resulted in determination of rotational and centrifugal distortion constants, along with the number of bound rotational excited states (up to l = 7); this can naturally assist in the refinement of its PES.

The mid- and far-IR spectra of H_2–N_2 was reported by McKellar in 1990 where he obtained evidence for 8 bound rotationally excited states [18]. Surprisingly, the rotational constant for the heavier oxygen species compared to N_2 is larger, which results from a smaller intermolecular separation. This was explained by the difference in the dimers average "structure" (Collinear for H_2–N_2 and parallel stacked for H_2–O_2). The collinear geometry is favoured by attractive electrostatic interactions, resulting from multipole-multipole interactions alone in both complexes, however, the strong short range exchange (repulsive) interaction in H_2–O_2 overall disfavours this geometry and results in a parallel stacked geometry [17, 19-21]. Accurate spectroscopic data of the H_2–N_2 complex allowed for its probable identification in the

atmosphere of Titan [18, 22-28], and similar data for H_2–O_2 could help in refining its PES, which is important in estimating the abundance of O_2 in the ISM [17].

The second part of this chapter aims to extend the recently reported far-IR H_2–O_2 spectroscopy into the mid-IR, as well as looking at the far-IR spectrum of the deuterated equivalent, D_2–O_2, with the intent of helping refine its PES.

II. EXPERIMENTAL

The far-IR spectrum of H_2/D_2–Xe was collected at the THz & Far-IR Beamline at the Australian Synchrotron. The van der Waals complex was formed by combining 200 Torr of each species into a nitrogen gas cooled enclosive flow cooling (EFC) cell [29] held at 160 K. The synchrotron radiation was coupled to a Bruker IFS 125 HR FTIR spectrometer (equipped with a Mylar Beam splitter), followed by a White cell located inside the EFC cell (at 16 passes resulting in a pathlength of 10 m). The output radiation was then focussed onto a liquid helium cooled silicon bolometer detector. Note that the first set of H_2–Xe experiments used a liquid helium cooled silicon bolometer photodetector providing optimal light intensity around 600 cm^{-1} wherein lies the $S(1)$ band (see below), yet is restricted at lower wavenumbers (below approximately 350 cm^{-1}) wherein lies the $S(0)$ band (see below). The spectra were recorded at a resolution of 0.15 cm^{-1}.

The low temperature IR spectra of the H_2/D_2–O_2 van der Waals complexes were also collected at the THz & Far-IR Beamline at the Australian Synchrotron as previously outlined [17]. The complex was produced by combining 140 Torr of O_2 and 200 Torr of H_2/D_2 at 80 K in the liquid nitrogen cooled EFC cell that was coupled to the Bruker IFS 125 HR FTIR spectrometer. In the mid-IR H_2–O_2 experiments the FTIR spectrometer was equipped with a KBr Beam splitter and a liquid nitrogen cooled MCT detector, and the spectra were recorded at a resolution of 0.3 cm^{-1}. We used an internal globar light source directed into the EFC cell set to 32 passes, proving a pathlength of 20 m. For optimal light intensity in the far-IR for the collection of D_2–O_2 spectra, the FTIR spectrometer was equipped with a Mylar Beam splitter and a liquid helium cooled silicon bolometer detector. The spectrum of D_2–O_2 in the far-IR was recorded at a resolution of 0.15 cm^{-1}, making use of the synchrotron radiation at 16 passes.

III. FAR-IR SPECTROSCOPY OF H_2/D_2–Xe

The hydrogen molecule in H_2–Rg complexes are essentially freely rotating, which makes the rotational quantum number of H_2, j_H, a good label within the complex. As such, the ro-rotational spectra of H_2–Rg are centred around the rotational transition of molecular hydrogen at approximately 350 cm^{-1} and 600 cm^{-1} ($6B$ and $10B$, where B is the rotational constant for H_2) for *para* and *ortho* hydrogen.

The selection rules for spectra involving H_2–Rg complexes in the far-IR are a change in j_H of 2, and a change in the *end-over-end* rotational quantum number, l, of ± 1 (P and R branches) or ± 3 (N and T branches). The $S(1)$ and $S(0)$ bands for the H_2–Xe complex are presented in Figures 1 and 2 respectively, where S denotes $\Delta j_H = 2$ and the number in parentheses is the

initial value of j_H. The $S(1)$ band in Figure 1 shows well defined P and R braches as well as resolved N and T branch lines up to l = 10 (see Table 1). Figure 2 (left) shows part of the $S(0)$ band where only the T transitions are observed and the rest are obscured by limited light in this region (see Table 1 for assignments).

In Table 1, we also present a comparison of the transition frequencies to those calculated using a typical nonrigid linear rotor equation, i.e.

$$E(l)= S(X) + B[(l'(l' + 1)) – (l''(l'' + 1))] – D[(l'(l' + 1))^2 – (l''(l'' + 1))^2], \quad (1)$$

where B is the rotational constant for the complex, D is the centrifugal distortion constant for the complex, and $S(X)$ (X = 0 or 1) is the perturbed band origin of H_2. A different optical set up was used in a later experiment to resolve the lower wavenumber transitions and is shown in Figure 2 (right). This spectra, however, has much poorer S/N and only shows resolved P and R branches with no rotational fine structure.

TABLE 1. Assigned Far-IR Transitions of H_2–Xe (in cm^{-1}).

Transition	$l' \leftarrow l''$	$S(0)$	Calc[a]	$S(1)$	Calc[a]
$N(10)$	7 ←10	-	330.41	563.79	561.21
$N(9)$	6 ←9	-	332.74	565.58	563.54
$N(8)$	5 ←8	-	335.18	567.81	565.98
$N(7)$	4 ← 7	-	337.73	570.26	568.53
$N(6)$	3 ←6	-	340.35	572.87	571.15
$N(5)$	2 ←5	-	343.04	575.58	573.84
$N(4)$	1 ←4	-	345.79	578.45	576.59
$T(1)$	4 ←1	361.38	362.63	-	593.43
$T(2)$	5 ←2	364.19	365.39	596.29/595.87[b]	596.19
$T(3)$	6 ←3	366.89	368.12	599.33/598.67 [b]	598.92
$T(4)$	7 ←4	369.45	370.80	602.10/601.36 [b]	601.60
$T(5)$	8 ←5	371.97	373.42	604.64/603.83 [b]	604.22
$T(6)$	9 ←6	374.17	375.98	606.95/606.08 [b]	606.78
$T(7)$	10 ←7	375.95	378.48	608.82/608.06 [b]	609.28

[a]Using $E(l)= S(X) + B[(l'(l' + 1)) – (l''(l'' + 1))] – D[(l'(l' + 1))^2 – (l''(l'' + 1))^2]$, where, B is rotational constant for the complex, D is the centrifugal distortion constant for the complex, and $S(X)$ (X = 0 or 1) is the perturbed band origin of H_2.
[b]Less intense "split" peak.

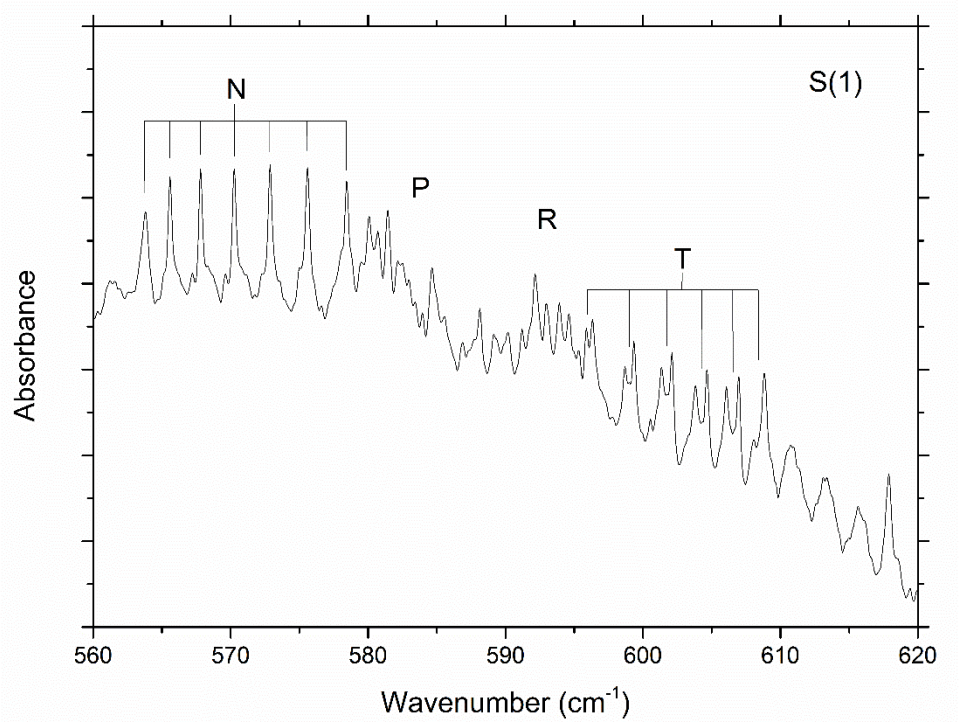

Figure 1. The far-IR spectra of the H_2–Xe *S*(1) band with resolved *N*, *P*, *R* and *T* branch transitions.

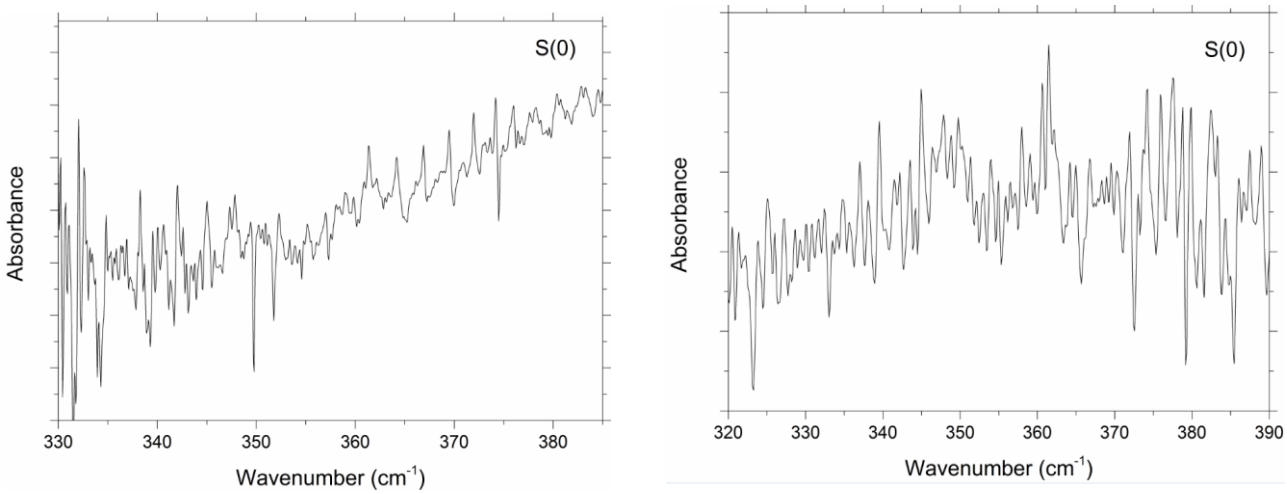

Figure 2. The far-IR spectra of the H_2–Xe *S*(0) band. The left figure shows well resolved *T* transitions from the first set of experiments. The spectrum on the right was taken during the second set of experiments, where only traces of the *P* and *R* branches are visible.

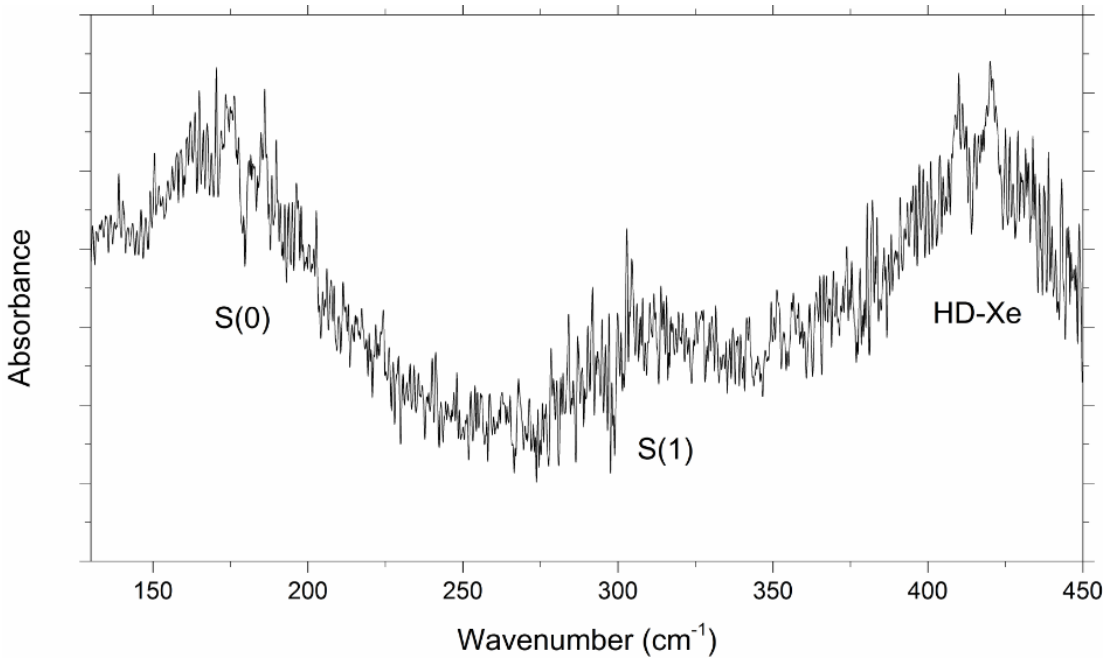

Figure 3. Far-IR spectrum of the D_2–Xe van der Waals complex at 160 K showing the *S*(0) and *S*(1) bands. The higher wavenumber feature around 415 cm^{-1} shows *P* and *R* branch characteristics and is most likely due to HD–Xe.

The experiments conducted here for the H_2–Xe van der Waals complex are based off the 2013 mid-IR study by McKellar [1]. Table 1 shows the assigned *N* and *T* transitions according to McKellar's work [1], where he assigned up to and including $l = 10$. McKellar was also able to resolve additional splitting of some peaks and indicated there were still further blended lines. Despite our efforts to resolve these blended lines, only minor splittings of some *T* transitions in the *S*(0) band were observed; these transitions are tentatively assigned and are presented in Table 1. The less detailed spectra reported here are thought to be largely due to the comparatively smaller pathlength used in this study: McKellar utilised a 3.5 m cell at 32 passes resulting in a total pathlength of 112 m, and used resolution of 0.04 cm^{-1}, and here, we used a ~0.6 m cell with 16 passes resulting in a 10 m pathlength, and we used a resolution of 0.15 cm^{-1}. The lack of splitting also relates to the higher pressures used to achieve useful S/N levels in our far-IR experiments.

The greater reduced mass results in a smaller rotational constant for both D_2 and D_2–Xe relative to H_2 and H_2–Xe. This can be seen in Figure 3, where the *end-over-end* rotation for the D_2–Xe complex is centred around the D_2 rotational transitions at 180 cm^{-1} and 300 cm^{-1} for the *S*(0) and *S*(1) bands respectively. The smaller rotational constants also result in more bound states that are closer together in energy and we would therefore expect additional sharp features in closer proximity. In both cases, however, only *P* and *R* branches are observed with no resolved rotational fine structure (Fig. 4). There is also evidence for *P* and *R* branches around 415 cm^{-1} (Fig. 5); these are likely due to the *S*(1) transition of HD–Xe, centred around the rotational transition of HD ($10B$, where *B* is the rotational constant estimated to be 45 cm^{-1} [30]).

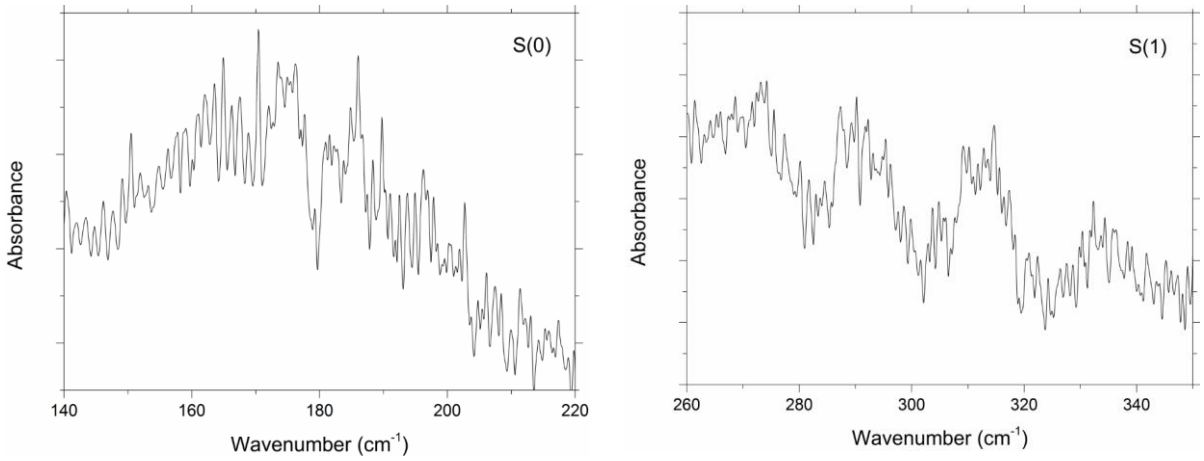

Figure 4. An expanded view of the *S*(0) (left) and *S*(1) (right) bands of D_2–Xe.

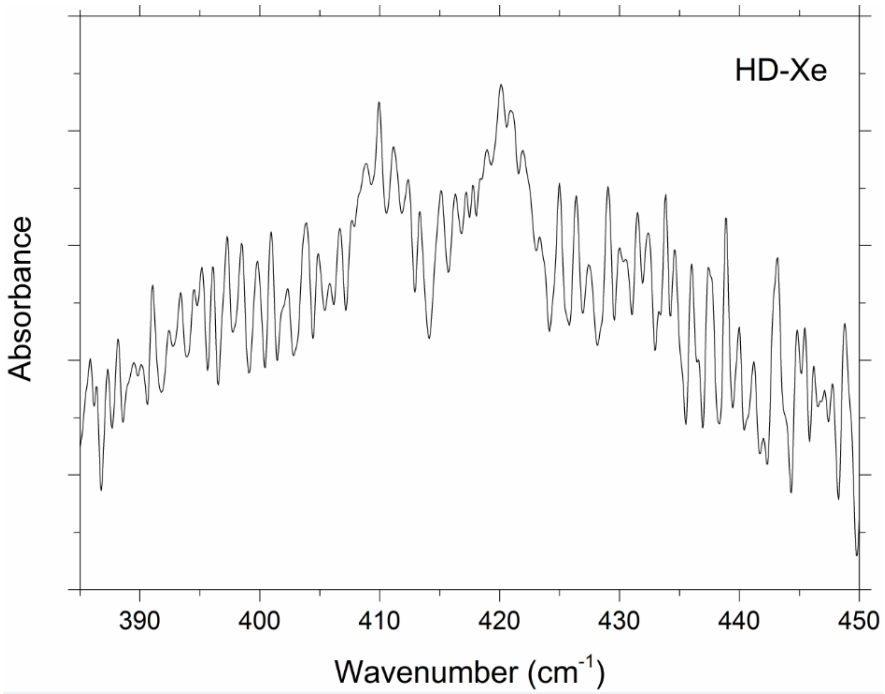

Figure 5. *P* and *R* branch features, thought to be the *S*(1) band of HD–Xe.

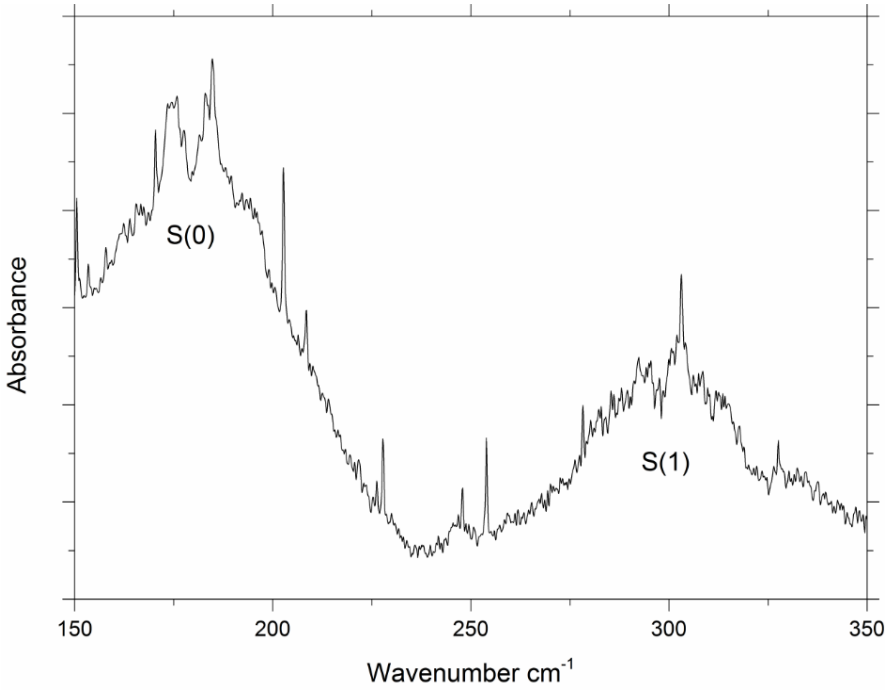

Figure 6. A far-IR survey spectra of the *S*(0) and *S*(1) bands of the D_2–O_2 van der Waals complex at 80 K. Sharp lines throughout the spectra are due to impurities.

IV. FAR-IR SPECTROSCOPY OF D_2–O_2

Just like the D_2–Xe spectra reported above, the *end-over-end* rotational transitions for D_2–O_2 are also centred around the rotational transition for molecular deuterium at about 180 cm^{-1} and 300 cm^{-1}. The selection rules for this complex are the same as for the H_2–Xe complex described above. The *S*(0) and *S*(1) transitions for D_2–O_2 are shown in Figure 6. We see broad underlying features corresponding to collision induced absorptions. As for the H_2–O_2 far-IR spectra [17] the *S*(0) and *S*(1) bands correspond to $\Delta j_{H2/D2} = 2–0$ and $\Delta j_{H2/D2} = 3–1$, which for deuterium is *ortho* and *para* respectively. However, as the more thermodynamically favourable state ($j_D = 0$) is already predominant at room temperature the decrease in temperature to 80 K has a much smaller effect on the *ortho/para* ratio than for H_2.

As mentioned above, the larger reduced mass of D_2 should result in there being more rotationally bound states that are closer together in energy. Clear *P* and *R* branches are evident in the *S*(0) and *S*(1) bands of the complex. Unfortunately, the spectrum is lacking any well resolved *N* and *T* transitions that would be most informative in this respect. The lack of resolved rotational fine structure compared with H_2–O_2 is likely due to the smaller induced dipole moment of the D_2–O_2 complex.

V. MID-IR SPECTROSCOPY OF H_2–O_2

Figure 7 shows the ro-vibrational spectra of the H_2–O_2 van der Waals complex between 4000 cm^{-1} and 5000 cm^{-1}. As for H_2–Rg complexes, the hydrogen molecule in H_2–O_2 is essentially freely rotating, and its vibrations are essentially unaffected, meaning that the ro-vibrational bands of the complex are approximately centred at the vibrational frequencies of free molecular hydrogen. The selection rules for the *end-over-end* rotational transitions for the

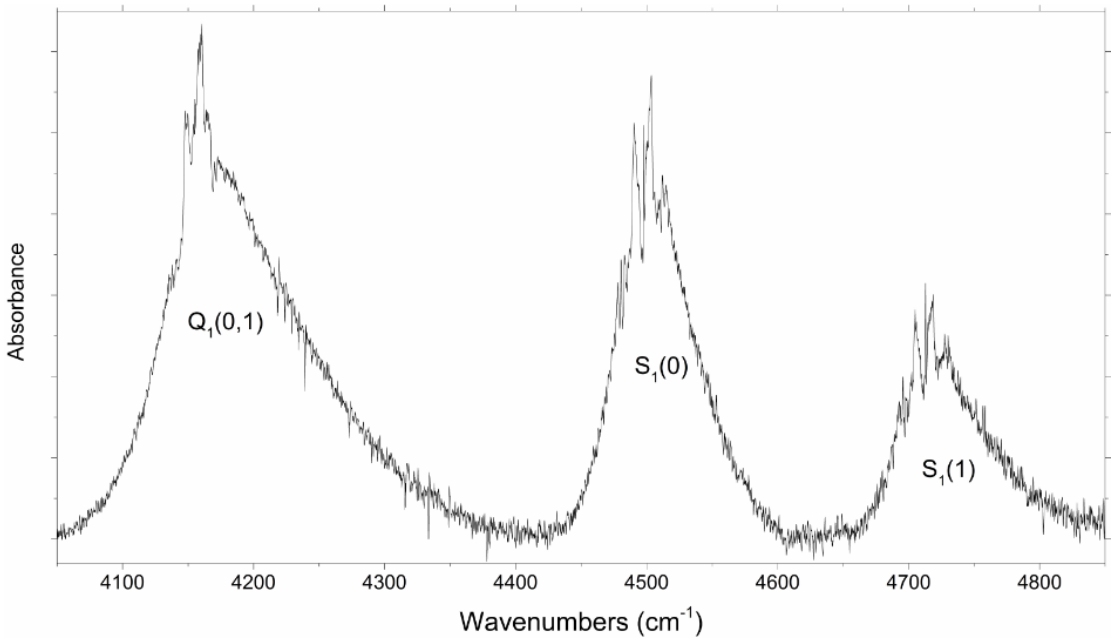

Figure 7. The mid-IR spectrum of H_2–O_2 (fine structure), accompanying the collision induced absorption band of molecular hydrogen (broad underlying structure), at 80 K.

$Q_1(1)$, $S_1(0)$, and $S_1(1)$ bands are $\Delta l = \pm 1$ (*P* and *R*) and $\Delta l = \pm 3$ (*N* and *T*), while $Q_1(0)$ is restricted to only $\Delta l = \pm 1$ transitions. The *Q* and *S* labelling indicate Δj_{H2} = 0 and 2 respectively, the subscript 1 is $\nu_{H2} = 1 \leftarrow 0$ and the number in parentheses is the initial value of j_{H2}. Again we see (Fig. 7) broad underlying features due to collision induced absorption of molecular hydrogen, along with somewhat resolved superimposed fine structure corresponding to the *end-over-end* rotational transitions of the complex. The spectra were recorded using normal hydrogen which is composed of 75% *ortho* (j_H = 1) and 25% *para* (j_H = 0). At 80 K and in presence of paramagnetic oxygen, *ortho* and *para* hydrogen should reach a thermal equilibrium relatively fast, which is what we saw in the far-IR spectrum of H_2–O_2 [17]. Here, however, we observed a drop off in the intensity as we go to higher wavenumbers, and we suspect this is an artefact which results from discrepancies in the intensity between the sample and background transmission spectra.

A close up of the $S_1(0)$ and $S_1(1)$ bands are shown in Figure 8, and the assignment of the *N* and *T* branch peaks are reported in Table 2. This assignment was assisted by the previously reported H_2–N_2 [18] and H_2–O_2 (far-IR) [17] spectra, along with calculated values, as per equation (1) (shown as vertical dashed lines in Figure 8 and also presented in Table 2). The mid-IR assignments reported here are quite tentative, and only three *N* branch peaks in the $S_1(0)$ band are well resolved. Although tentative, we do not observe any transitions beyond l = 7, which agrees with the previous far-IR study [17]. The *P* and *R* branches can also be seen for the $S_1(0)$ and $S_1(1)$ bands, but the fine structure is not well resolved. Figure 9 shows a close up of the $Q_1(0)$ and $Q_1(1)$ bands, where we see nicely resolved *P* and *R* branches. As mentioned, we do not expect *N* and *T* transitions for the $Q_1(0)$ band, however we do for $Q_1(1)$, and an attempt has been made to assign these weakly resolved peaks in Table 3.

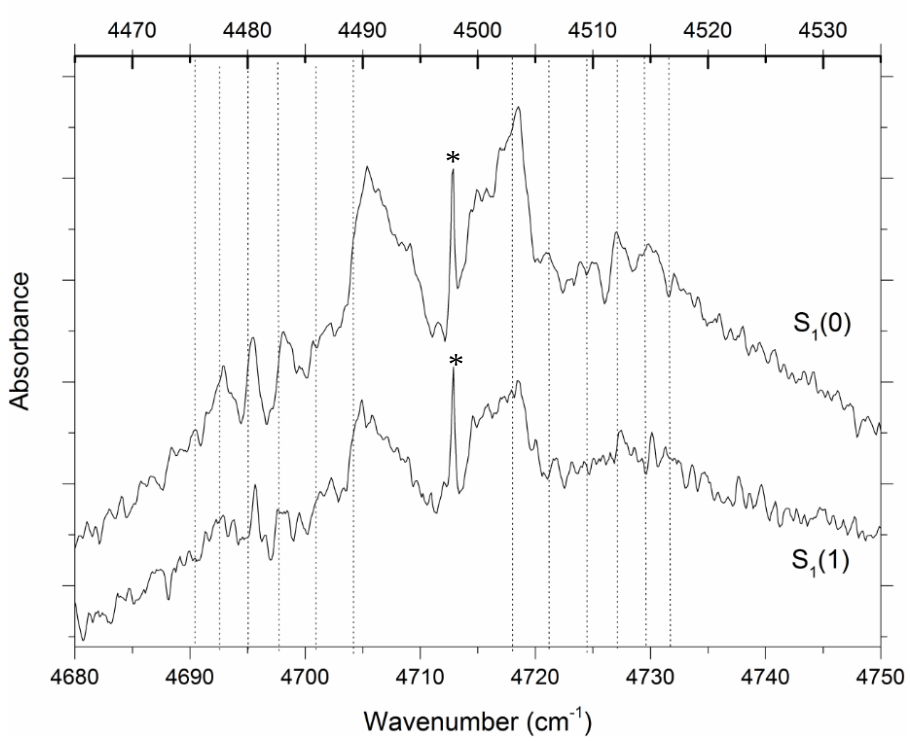

Figure 8. An expanded view of the experimental rotational fine structure in the $S_1(0)$ (top axis range) and $S_1(1)$ (bottom axis range) bands of H_2–O_2. The dashed lines correspond to *N* and *T* line positions calculated using the nonrigid linear rotor model. The sharp peaks at approximately 4498 cm^{-1} and 4713cm^{-1} (shown by the asterisks) are quadrupole transitions

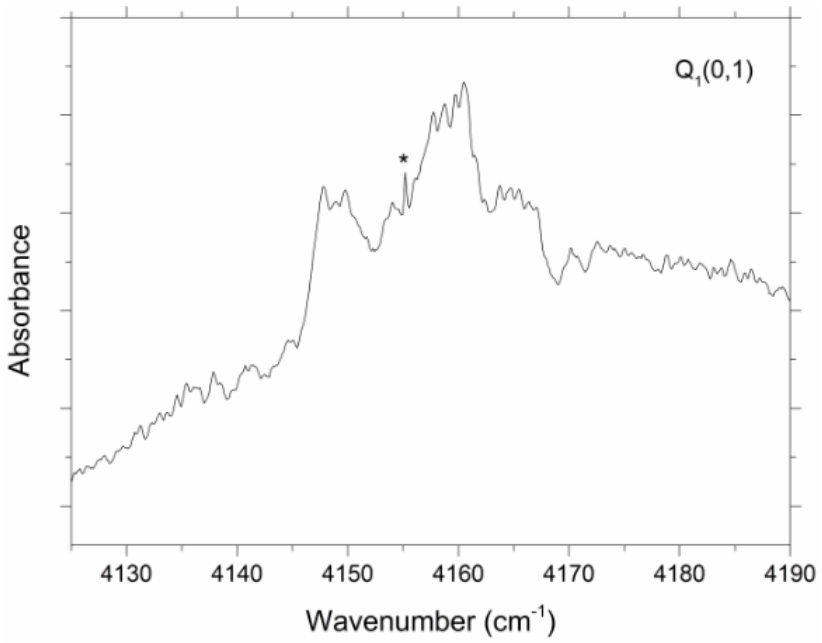

Figure 9. An expanded view of the $Q_1(0,1)$ regions in the mid-IR spectra of the H_2–O_2 van der Waals complex. The small sharp feature at approximately 4155 cm^{-1} (shown by the asterisk) is due to the quadrupole transition of H_2.

TABLE 2. Tentatively assigned mid-IR $\Delta j_H = 2$ transitions of H_2–O_2 (in cm^{-1}). Uncertainty shown in parentheses corresponds to the difference between the peak centroid and peak maximum.

Transition	$l' \leftarrow l''$	$S_1(0)$	Calc[a]	$S_1(1)$	Calc[a]
N(7)	4 ← 7	4477.90(0)	4477.50	4692.62(24)	4692.50
N(6)	3 ←6	4480.44(0)	4479.95	4695.64(0)	4694.95
N(5)	2 ←5	4483.10(43)	4482.74	4698.05(45)	4697.74
N(4)	1 ←4	4486.79(45)	4485.81	4702.00(27)	4700.81
T(1)	4 ←1	4506.06(1)	4506.19	4721.72(16)	4721.19
T(2)	5 ←2	4509.50(61)	4509.26	4723.79(6)	4724.26
T(3)	6 ←3	4512.30(21)	4512.06	4727.55(12)	4727.06
T(4)	7 ←4	4514.87(7)	4514.51	4730.15(4)	4729.51
T(5)	8 ←5	4517.10(6)	4516.54	4731.29(2)	4731.54

[a]refer to Table 1.

TABLE 3. Tentatively assigned mid-IR $\Delta j_H = 0$ Transitions of H_2–O_2 (in cm^{-1}).

Transition	$l' \leftarrow l''$	$Q_1(0)$	$Q_1(1)$
		4135.44	
		4138.00	
		4140.69	
		4144.91	
P(7)	6 ← 7		4154.08
P(6)	5 ← 6	4147.84	
P(5)	4 ← 5	4148.90	
P(4)	3 ← 4	4149.77	4156.12
P(3)	2 ← 3		4157.73
P(2)	1 ← 2		4158.73
		4151.96	
R(1)	2 ← 1	4156.12	4163.74
R(2)	3 ← 2	4157.73	4164.68
R(3)	4 ← 3	4158.73	4165.47
R(4 or 5)	6 ← 5	4159.76	4166.33
		4160.56	
		4161.48	
		4162.36	
		4163.74	
		4164.68	
		4165.47	
		4167.02	
		4170.20	
		4172.63	

VI. SUMMARY

We reported the far-IR spectra of H_2–Xe, providing assignments up to and including l = 10, which is consistent with the mid-IR work reported by McKellar [1]. Splitting was observed in parts of the spectra, however improvements are needed to further resolve the blended lines. The far-IR spectra of both D_2–Xe and D_2–O_2 were less informative and work must be extended for both of these complexes. The mid-IR spectra of H_2–O_2 has a lower S/N than the analogous spectra in the far-IR owing to the lower light intensity in the mid-IR region. Tentative assignments of the H_2–O_2 complex in the mid-IR are reported up to and including l = 7. Better rotationally defined spectra are required in all cases presented here in order to provide useful data for theoretical modelling. This is likely best achieved by using longer pathlengths, which would make higher resolutions feasible.

ACKNOWLEDGEMENTS

This research was undertaken on the THz & Far-IR Beamline at the Australian Synchrotron, Victoria, Australia. We are grateful to Dom Appadoo for stimulating discussions and expert assistance. We would also like to acknowledge Courtney Ennis, Irene Willcocks and Aidan Karayilan for their assistance in collecting the spectra and Greg Metha for helpful advice.

REERENCES

[1] A. R. W. McKellar, Can. J. Phys. **91**, 957 (2013).

[2] R. Moszynski, B. Jeziorski, A. Wormer, et al., Chem. Phys. Lett. 161 (1994).

[3] A. R. W. McKellar, J. Chem. Phys. **105**, 2628 (1996).

[4] B. W. Bakr, D. G. A. Smith, K. Patkowski, J. Chem. Phys. **139**, 144305 (2013).

[5] A. R. W. McKellar, Can. J. Phys. **87**, 411 (2009).

[6] A. R. W. McKellar, J. Chem. Phys. **122**, 084320 (2005).

[7] A. K. Kudian, H. L. Welsh, Can. J. Phys. **49**, 230 (1971).

[8] A. R. W. McKellar, H. L. Welsh, J. Chem. Phys. **55**, 595 (1971).

[9] R. J. Le Roy, J. M. Hutson, J. Chem. Phys. **86**, 837 (1987).

[10] A. R. W. McKellar, Faraday Discuss. Chem. Soc. **73**, 89 (1982).

[11] K. A. Walker, T. Ogata, W. Jäger, M. C. L. Gerry, I. Ozier, J. Chem. Phys. **106**, 7519 (1997).

[12] M. D. Brookes, A. R. W. McKellar, Mol. Phys. **97**, 127 (1999).

[13] K. A. Walker, A. R W. McKellar, J. Mol. Spec. **205**, 331 (2001).

[14] S. Chefdeville, Y. Kalugina, C. Naulin, Sci. **341**, 1094 (2013).

[15] W. M. Fawzy, J. Chem. Phys. **131**, 044318 (2009).

[16] Y. Kalugina, O. D. Alpizar, T. Stoeklin, F. Lique, Phys. Chem. Chem. Phys. **14**, 16458 (2012).

[17] H. Bunn, T. Bennett, A. Karaylian, P. L. Raston, ApJ **799**, 65 (2015).

[18] A. R. W. McKellar, J. Chem. Phys. **93**, 18 (1990).

[19] B. Bussery, P. E. S. Wormer, J. Chem. Phys. **99**, 1230 (1993).

[20] W. M. Fawzy, J. Chem. Phys. **131**, 044318 (2009).

[21] L. Gomez, B. Bussery-Honvault, T. Cauchy, M. Bartolomei, D. Cappelletti, F. Pirani, Chem. Phys. Lett. **99**, 109 (2007).

[22] B. C. R. Hanelm, M. Flaser, V. Kunde, P. Lowman, W. Maguire, J. Pearl, J. Pirraglia, R. Samuelson, D. Gautier, P. Gierasch, S. Kumar, C. Ponnamperuma, Sci. **204**, 972 (1979).

[23] D. Gautier, A. Marten, J. P. Baluteau, G. Bachet, Can. J. Phys. **61**, 1455 (1983).

[24] A. R. W. McKellar, Can. J. Phys. **62**, 760 (1984).

[25] L. Frommhold, R. Samuelson, G. Birnbaum, ApJ Lett. **283**, 79 (1984).

[26] J. Schaefer, A&A **182**, 40 (1987).

[27] A. R. W. McKellar, ApJ **326**, 75 (1988).

[28] A. Borysow, L. Frommhold, ApJ **303**, 495 (1986).

[29] S. Bauerecker, M. Tarascjewski, C. Weitkamp, H. K. Cammenga, AIP **72**, 3946 (2001).

[30] L. Ulivi, P. de Natale, M. Inguscio, ApJ **378**, 29 (1991).

Statement of Authorship

Title of Paper	Far-Infrared Synchrotron Spectroscopy and Torsional Analysis of the Important Interstellar Molecule, Vinyl Alcohol
Publication Status	☑ Published ☐ Accepted for Publication ☐ Submitted for Publication ☐ Unpublished and Unsubmitted work written in manuscript style
Publication Details	H.Bunn, R. J. Hudson, A. S. Gentleman, P. L. Raston, ACS Earth and Space Chemistry 1, 70 (2017)

Principal Author

Name of Principal Author (Candidate)	Hayley A Bunn		
Contribution to the Paper	Experimental work, analysis and write up		
Overall percentage (%)	60		
Certification:	This paper reports on original research I conducted during the period of my Higher Degree by Research candidature and is not subject to any obligations or contractual agreements with a third party that would constrain its inclusion in this thesis. I am the primary author of this paper.		
Signature		Date	14/03/2017

Co-Author Contributions

By signing the Statement of Authorship, each author certifies that:

i. the candidate's stated contribution to the publication is accurate (as detailed above);

ii. permission is granted for the candidate in include the publication in the thesis; and

iii. the sum of all co-author contributions is equal to 100% less the candidate's stated contribution.

Name of Co-Author	Paul L Raston		
Contribution to the Paper	Conceptualisation of project and experiments. Support and advice on experiments and editing of drafts (20%)		
Signature		Date	14/03/2017

Name of Co-Author	Alexander S. Gentleman		
Contribution to the Paper	Advice on calculations and editing of drafts (10%)		
Signature		Date	15/03/2017

Name of Co-Author	Rohan Hudson	
Contribution to the Paper	Assisting in experiments (10%)	
Signature		Date 23/3/17

Bunn, H., Hudson, R.J., Gentleman, A.S. & Raston, P.L. (2017). Far-Infrared Synchrotron Spectroscopy and Torsional Analysis of the Important Interstellar Molecule, Vinyl Alcohol.
ACS Earth and Space Chemistry 1(2), 70-79.

Statement of Authorship

Title of Paper	High Resolution Spectroscopy of the Coriolis Perturbed Far-Infrared Bands of *Syn*-Vinyl Alcohol
Publication Status	☐ Published ☐ Accepted for Publication ☐ Submitted for Publication ☑ Unpublished and Unsubmitted work written in manuscript style
Publication Details	To be slightly reworked before submission

Principal Author

Name of Principal Author (Candidate)	Hayley A Bunn		
Contribution to the Paper	Experimental work, analysis and write up		
Overall percentage (%)	80		
Certification:	This paper reports on original research I conducted during the period of my Higher Degree by Research candidature and is not subject to any obligations or contractual agreements with a third party that would constrain its inclusion in this thesis. I am the primary author of this paper.		
Signature		Date	19/01/2017

Co-Author Contributions

By signing the Statement of Authorship, each author certifies that:

i. the candidate's stated contribution to the publication is accurate (as detailed above);

ii. permission is granted for the candidate in include the publication in the thesis; and

iii. the sum of all co-author contributions is equal to 100% less the candidate's stated contribution.

Name of Co-Author	Paul L Raston		
Contribution to the Paper	Conceptualisation of project and experiments. Support and advice on experiments and editing of drafts. 20%		
Signature		Date	18/01/17

5. High Resolution Spectroscopy of Coriolis Perturbed Far-Infrared Bands of *Syn*-Vinyl Alcohol

Hayley Bunn[1], Paul L. Raston[2]

[1]*Department of Chemistry, University of Adelaide, SA 5005, Australia*
[2]*Department of Chemistry and Biochemistry, James Madison University, Harrisonburg, Virginia 22807, USA*

This paper reports the high resolution far-infrared spectrum of *syn*-vinyl alcohol in the OH torsional (ν_{15}) region. We analysed the intense ν_{15} fundamental band at ~407 cm^{-1} as well as its first and second hot bands at ~368 cm^{-1} and ~323 cm^{-1}, respectively. This resulted in refinement of the ground state constants, and determination of excited state rotational and centrifugal distortion constants up to the sextic level. Coriolis perturbations are evident in the ν_{15} fundamental due to interactions with the ν_{11} CCO bending fundamental, and its inclusion in the analysis greatly improves the fit. The first hot band also shows evidence of Coriolis interactions of $2\nu_{15}$ with $\nu_{13,}$ and possibly ν_{11}. The inclusion of the perturbing ν_{13} fundamental, previously reported by Joo *et al.* (1999), greatly improves the fit. Perturbations are also evident in the second hot band, however, the lack of detailed information on potential interacting states in this region, due in part to the weaker nature of this band, only allows for preliminary constants to be determined for $3\nu_{15}$.

I. INTRODUCTION

Vinyl alcohol, the simplest enol, is rather difficult to study spectroscopically due to its unstable nature and therefore low abundance, under most conditions, compared with acetaldehyde [1]. The spectroscopic observation of vinyl alcohol, however, dates back to 1973 where it was first observed by the use of Chemically Induced Dynamic Nuclear Polarisation (CIDNP) enhanced ^{1}H NMR spectroscopy [2]. Here, the group was able to increase the tautomerisation time of vinyl alcohol to acetaldehyde to about 1 second, by using non acidic solutions. Vinyl alcohol was later observed in other NMR studies with the use of both ^{1}H, ^{13}C and CIDNP [2-5]. Shortly after this, vinyl alcohol observations were reported in the gas phase by Saito (1976) [6], where he recorded the microwave spectrum of the most stable rotamer, *syn*-vinyl alcohol. The vinyl alcohol in that study was produced from the thermal dehydration of ethylene glycol. Saito reported accurate ground state (GS) rotational and higher order centrifugal distortion constants up to the sextic level for both "normal" and monodeuterated vinyl alcohol (CH_3CHOD), along with *a, b* and *c* dipole moments (0.616, 0.807 and 1.016 D respectively) from Stark measurements.

Vinyl alcohol, along with up to 10 isotopic species, were later observed in the infrared (IR) using matrix isolation techniques [7, 8]. Following this, spectroscopic studies into gas phase *syn*-vinyl alcohol were performed in the IR, where, in 1991 Koga *et al.* [9] identified 10 out of the 15 fundamental bands between 600–3600 cm^{-1}. In that study, vinyl alcohol was produced from the pyrolysis of cyclobutanol. The analysis of the ν_{13} CH_2 wagging mode at 817 cm^{-1}, recorded at a resolution of 0.016 cm^{-1}, provided rotational and centrifugal distortion constants up to the quartic level. These constants were further refined, including sextic terms, in 1999

by Joo *et al.*[10]. The group provided a high apodised resolution of 0.004 cm^{-1}, and an analysis was performed on the ν_{13} mode, including perturbations from the first overtone of ν_{15} at 776 cm^{-1}. Rotational and centrifugal distortion constants were also reported for $2\nu_{15,}$ from which the ν_{15} fundamental was predicted to lie at 388 cm^{-1} (assuming a harmonic potential).

In the preceding chapter we reported the first gas phase far-IR observation of the ν_{15} band at 407 cm^{-1}, where the difference with respect to the predicted band origin by Joo *et al.* [10] indicates a high degree of anharmonicity in the potential. The additional observation of hot bands at 368 cm^{-1} and 323 cm^{-1} further confirms this anharmonic nature of the *syn*-vinyl alcohol potential well. This was the first gas phase far-IR spectrum of vinyl alcohol, where, previously, the OH torsional band has only been investigated by matrix isolation techniques at 413 cm^{-1} [8]. The preceding chapter also reports the first IR observation of vinyl alcohol's higher energy rotamer, *anti*-vinyl alcohol, where the only other gas phase observation was reported in 1985 by Rodler, by means of microwave spectroscopy. In the same year Rodler [11] reported additional microwave transitions for *syn*-vinyl alcohol and improved assignments for some previously observed by Saito [6]. In 2015 a study investigating the $O(^1D)$ insertion reactions of methane and ethylene to form methanol and vinyl alcohol, also reported some additional transitions not observed previously by Saito or Rodler [12].

The following chapter continues on from Chapter 4 providing a detailed analysis of *syn*-vinyl alcohol's ν_{15} vibrational band, corresponding to the OH torsion with the fundamental and first two hot bands located at ~407 cm^{-1}, ~368 cm^{-1} and ~323 cm^{-1} respectively. We report refined GS and ν_{15} & $2\nu_{15}$ excited state rotational and higher order centrifugal distortion constants up to the sextic level.

II. EXPERIMENTAL

The high resolution Fourier-transform IR (FTIR) spectrum of vinyl alcohol was obtained at the THz & Far-IR Beamline of the Australian Synchrotron as detailed previously [13]. The sample was prepared by pyrolysis of 2-chloroethanol at temperatures ranging near 950 °C. The gaseous products were flowed continuously through a room temperature multiple reflection cell using a pressure of 0.5 or 2 Torr, which allowed for well resolved transitions to be observed around the intense band origin, in addition to weaker regions. The synchrotron radiation was coupled to a Bruker IFS 125 HR FTIR spectrometer equipped with a Mylar Beam splitter and polyethylene windows. The resulting beam was directed into the cell at 16 passes, resulting in a path length of 10 m. Following this, the light was detected with a liquid helium cooled silicon bolometer detector. This set up allowed for maximum light intensity in the far-IR region, particularly below 700 cm^{-1}. The spectra were recorded at maximum resolution (0.00096 cm^{-1}).

III. RESULTS AND DISCUSSION

Vinyl alcohol is an asymmetric top with 15 fundamental modes, 2 of which lie in the far-IR region. The high resolution (0.00096 cm^{-1}) spectrum of vinyl alcohol presented here was recorded between 100 and 700 cm^{-1}, where the symmetric ν_{11} and asymmetric ν_{15} bands lie;

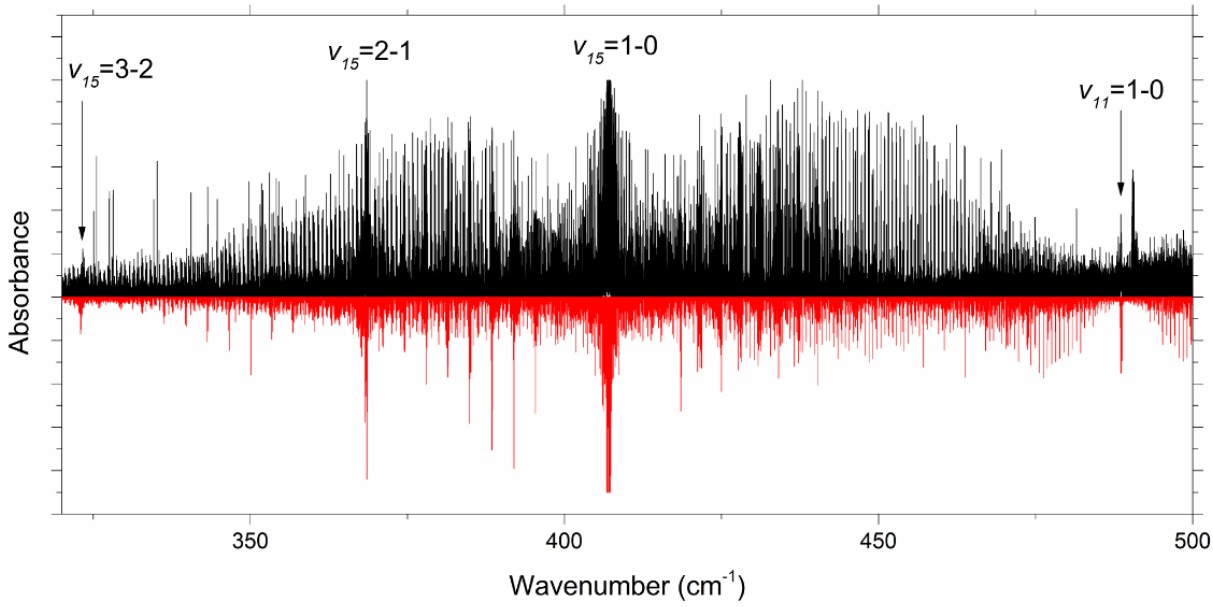

Figure 1. High resolution, 0.00096 cm^{-1}, survey spectrum in black with the fit in red showing the band origins of the ν_{15} fundamental and first two hot bands at 407 cm^{-1}, 369 cm^{-1} and 323 cm^{-1}, respectively, as well as the ν_{11} fundamental at 489 cm^{-1}.

looking at Figure 1, we see them at 488.7 cm^{-1} and 407.2 cm^{-1}, respectively. The first two hot bands of ν_{15} are also evident with band origins centered around 368.5 cm^{-1} and 323.1 cm^{-1}. The strong ν_{15} vibrational mode is best described as an OH torsion, with *c*-type character, and reveals well resolved rotational sub-structure, as shown previously [13]. The selection rules for ν_{15} are $\Delta J = 0, \pm 1$ for the *Q* and *P/R* branches, respectively, with $\Delta K_a = \pm 1(\pm 3, \pm 5, ...)$ and $\Delta K_c = 0(\pm 2, \pm 4, ...)$. The ν_{11} mode, on the other hand, is a CCO bend with mixed *a*/*b*-type character.

A high resolution analysis has been performed for the ν_{15} fundamental using the spectral fitting program, PGOPHER [14]. The only other high resolution IR analysis reported for vinyl alcohol is on the ν_{13} (CH_2 wagging) mode, which resulted in GS rotational and centrifugal distortion constants up to the sextic level [10]. These, along with scaled constants for ν_{15}, from anharmonic frequency calculations performed at the MP2/cc-pVQZ level on a CCSD(T)/cc-pVQZ optimised structure (refer to Chapter 4 [13]), were used to initially simulate the spectrum.

Lines were assigned beginning with low (unblended) *J* transitions, and slowly progressing to higher *J*. The assignments were simultaneously fit to a Watson's *A*-reduced Hamiltonian in the I^r representation, with the form,

$$\hat{H} = (A - \bar{B})\hat{J}_a^2 + \bar{B}\hat{J}^2 - \bar{B}\hat{J}_{bc}^2 - \Delta_K\hat{J}_a^4 - \Delta_{JK}\hat{J}^2\hat{J}_a^2 - \Delta_J\hat{J}^4 - \delta_K\left(\hat{J}_a^2\hat{J}_{bc}^2 + \hat{J}_{bc}^2\hat{J}_a^2\right) - 2\delta_J\hat{J}^2\hat{J}_{bc}^2 + \Phi_K\hat{J}_a^6 + \Phi_{KJ}\hat{J}^2\hat{J}_a^4 + \Phi_{JK}\hat{J}^4\hat{J}_a^2 + \Phi_J\hat{J}^4 \quad (1)$$

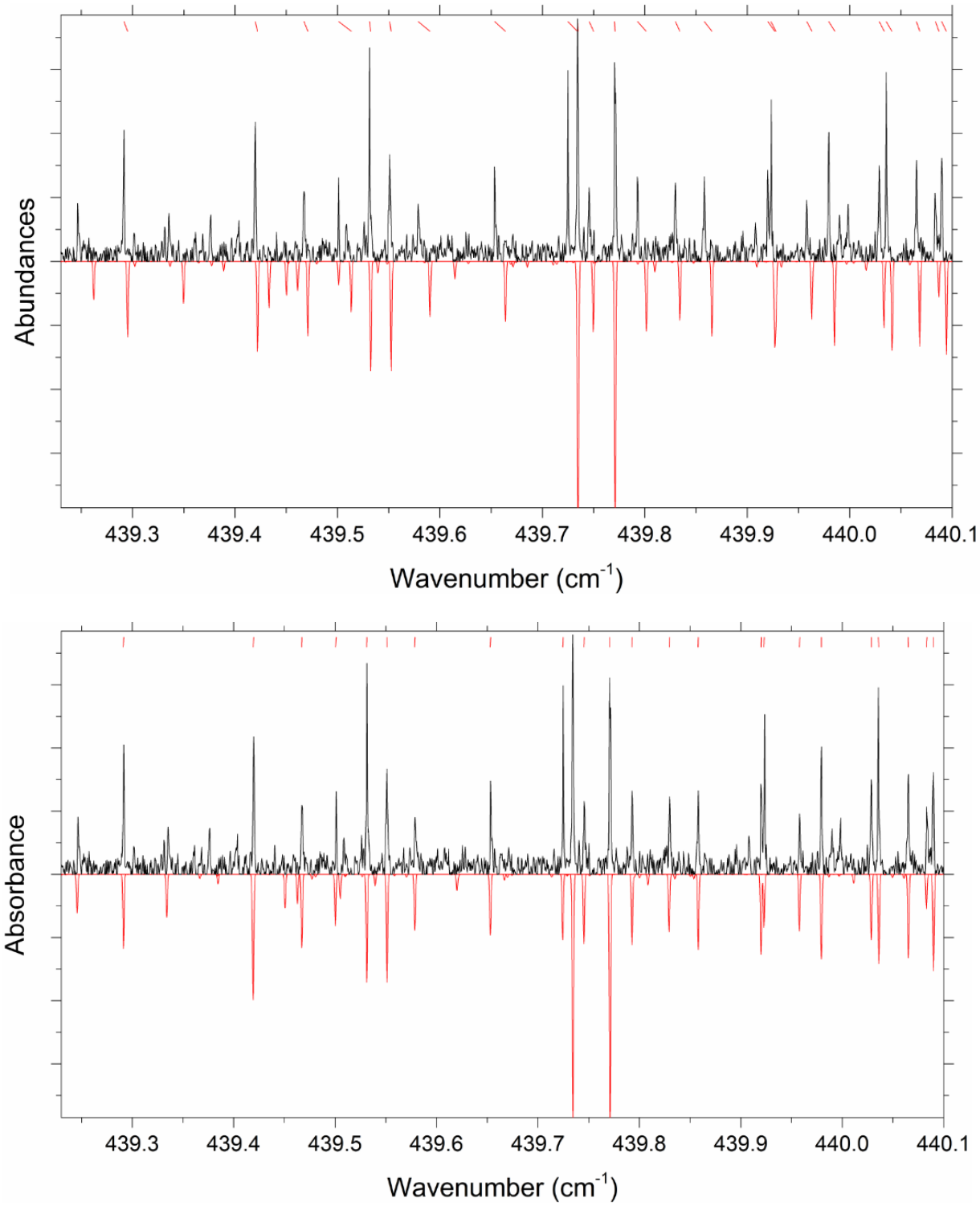

Figure 2. The fit of the simulation (red) to the high resolution experimental spectrum (black) of *syn*-vinyl alcohol's ν_{15} fundamental. In the top figure we see perturbations in the *R* branch region, at high *J* transitions. Improvement is evident (bottom) following inclusion of the ν_{11} fundamental and corresponding Coriolis constants reported in Table 1. Note that the "missing peaks" within the simulation compared to the experimental spectra are assigned to transitions resulting from the first hot band. The red ticks in the top of each figure indicate the position difference between the simulation and experimental assignments.

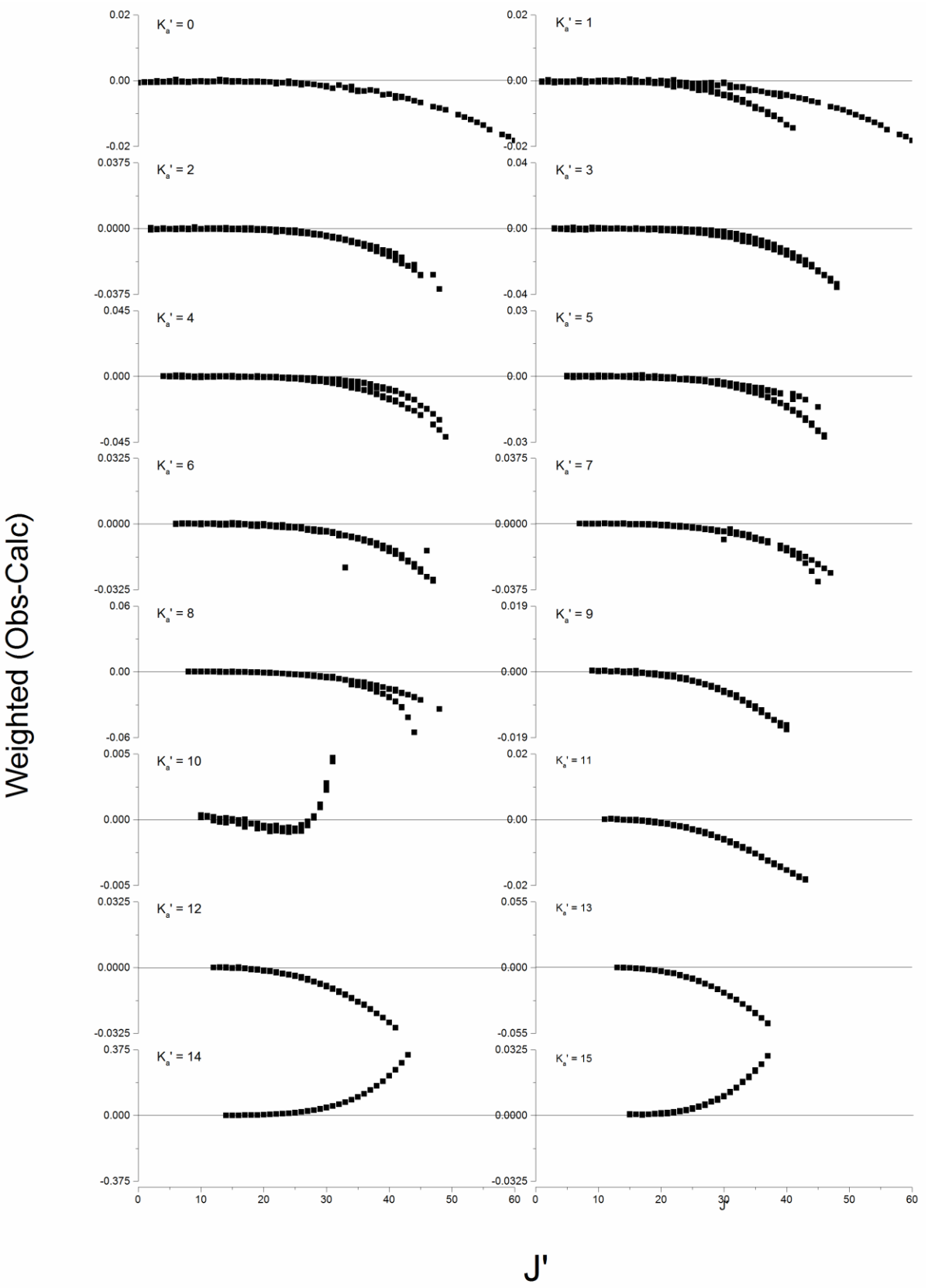

Figure 3. Residuals in the ν_{15} fundamental of *syn*-vinyl alcohol up to $K_a' = 16$. Curvature indicates perturbations caused by the nearby ν_{11} state.

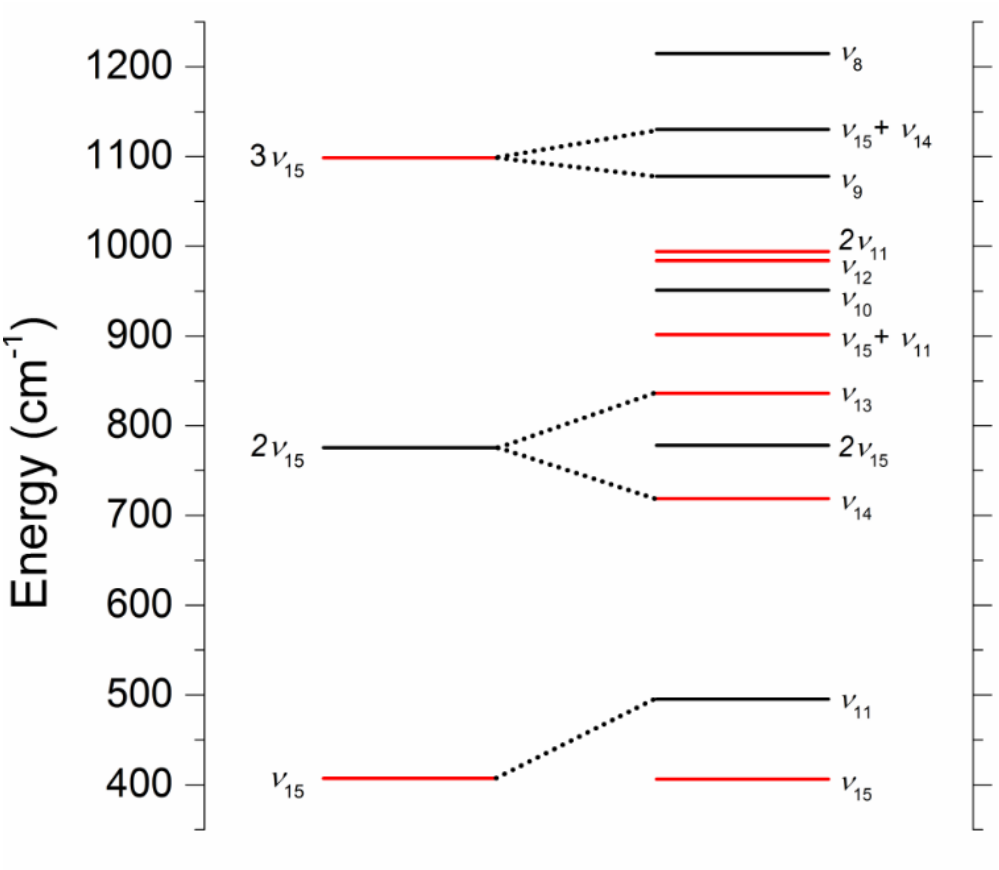

Figure 4. The energy levels for the ν_{15} OH torsional vibration and the nearby calculated states for *syn*-vinyl alcohol extracted from an anharmonic frequency calculation. The levels in red indicate asymmetric modes and those in black, symmetric. The dotted line indicates possible interactions with the condition of an energy difference of < 100 cm^{-1}.

In this equation, $\bar{B} = \frac{1}{2}(B + C)$, $\hat{J}$ is the total angular momentum with components along the *a*, *b* and *c* axes ($\hat{J}_a$,$\hat{J}_b$,$\hat{J}_c$), and $\hat{J}_{bc}^2 = \hat{J}_b^2 - \hat{J}_c^2$. The corresponding *A*, *B* and *C* rotational constants were initially refined in the ν_{15} manifold, providing a decent, rough fit to experiment. Inclusion of both quartic ($\Delta_K, \Delta_{JK}, \Delta_J, \delta_K, \delta_J$) and sextic centrifugal distortion parameters ($\Phi_K, \Phi_{KJ}, \Phi_{JK}, \Phi_J$), whilst constraining Φ_J to 0, resulted in an improved overall fit. Throughout the fit, assignments with an exceptionally large residual error were systematically removed.

Following a preliminary fit, we noticed a shift of high *J* transitions in the *R* branch, indicative of a Coriolis perturbation, as shown in Figure 2 (top). The corresponding residual error resulting from this shift in the observed and simulated transitions is presented in Figure 3, showing up to K_a' = 16 for all observed *J* values. Figure 4 plots an energy level diagram of the observed fundamental and hot bands for *syn*-vinyl alcohol along with the nearby, calculated, fundamentals, overtones and combinations bands. The energy levels connected by the dotted lines represent possible interactions between levels, with a requirement that the energy difference is less than 100 cm^{-1}. A *b*- and *c*- axis ($\Delta K_a = \pm 1, \pm 3$) Coriolis interaction is evident between the ν_{15} and ν_{11} states and was initially suspected as being responsible for the

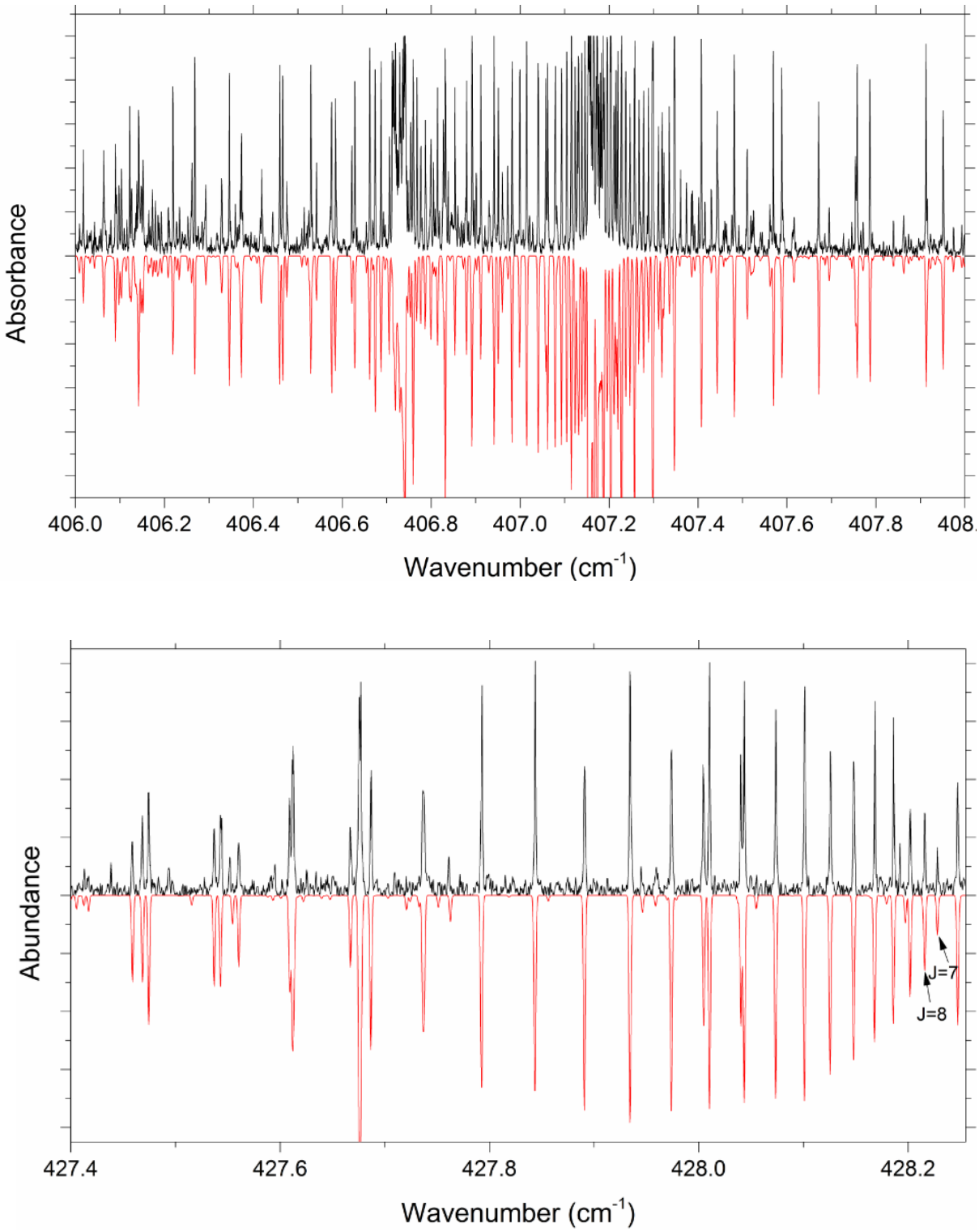

Figure 5. Final fit of the simulation (red) to the high resolution experimental spectrum (black) of the ν_{15} fundamental transitions of *syn*-vinyl alcohol. In the top figure we see a fit to the band origin region and in the bottom is the K_a = 6-7 sub-band.

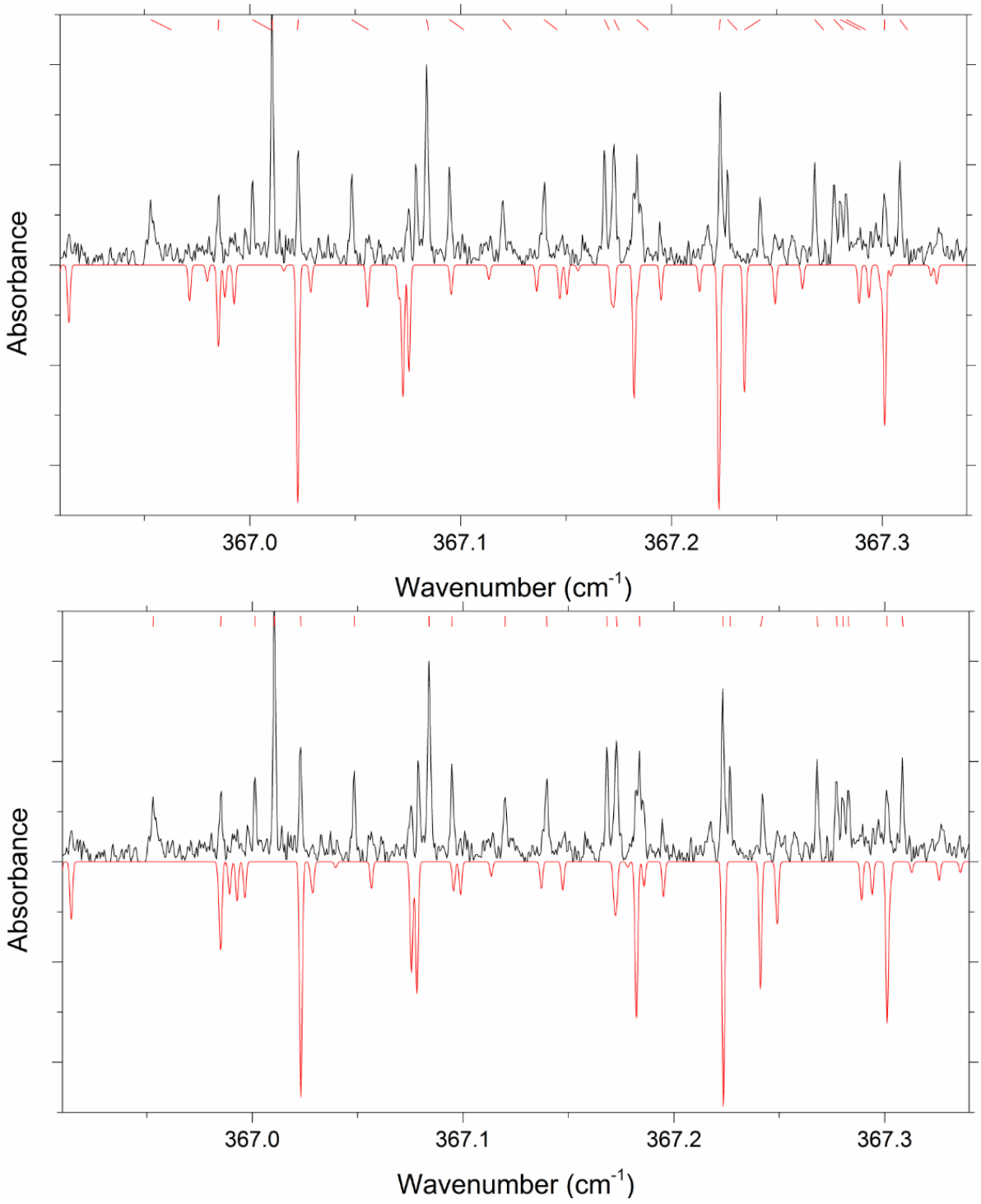

Figure 6. A fit of the simulation (red) to the high resolution experimental spectrum (black) of the *syn*-vinyl alcohol ν_{15} hot band. We see perturbations, observed via the shift between experimental and simulation, in the *R* branch region, at high *J*, in the top figure. The bottom figure shows the improvement between the experimental and simulation following the inclusion of the ν_{11} Coriolis constants reported in Table 1. Note that the "missing peaks" in the simulated spectra are assigned to transitions from the fundamental. The red ticks in the top of the figure indicate the position difference between the simulation and experimental assignments.

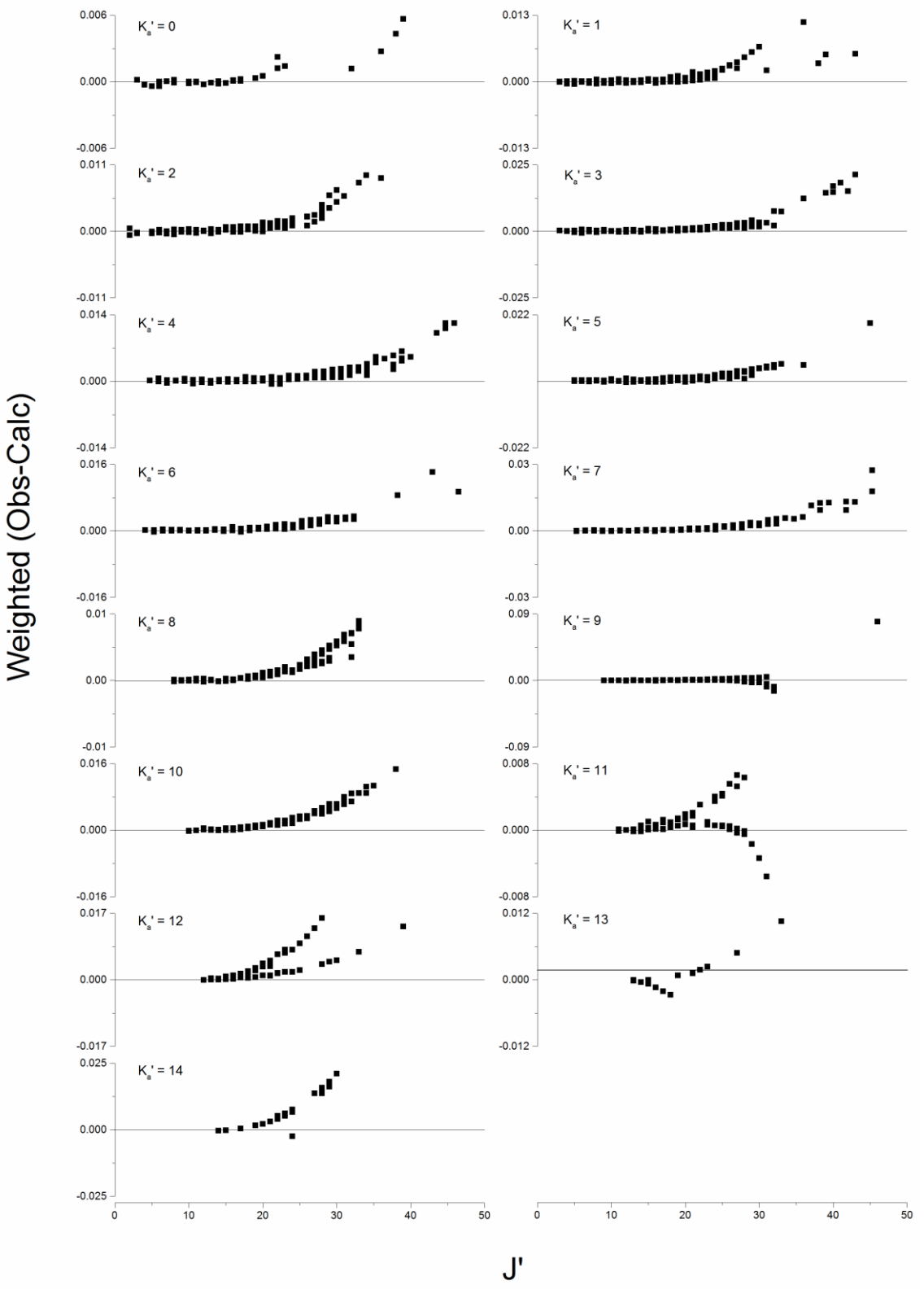

Figure 7. Shifts in rotational levels of the ν_{15} hot band of *syn*-vinyl alcohol up to $K_a' = 14$.

perturbations to the line positions shown in Figure 2. The observation of the ν_{11} fundamental band in this experiment greatly helped in initially estimating its spectroscopic constants.

We have assigned up to 211 transitions in the ν_{11} fundamental with a maximum J' of 28, K_a' of 11 and K_c' of 18. The higher order sextic distortion parameters for ν_{11} were constrained to refined GS values, and the less sensitive Bbar ($\bar{B} = \frac{1}{2}(B + C)$) and Bdelta ($\delta = (B - C)$)) terms were allowed to float during the fitting procedure. Inclusion and refinement of this ν_{11} state and the perturbation linking it with the ν_{15} manifold greatly improved the fit for the ν_{15} fundamental [Fig. 2 (bottom)]. A total of 4518 IR transitions have been included in the fit for the ν_{15} fundamental band of *syn*-vinyl alcohol, with a maximum J' of 59, K_a' of 19, and K_c' of 59. The overall residual error of 0.00027 cm^{-1} is comparable to the experimental apodised resolution (0.00048 cm^{-1}).

From the high resolution IR analysis of the ν_{13} fundamental by Joo *et al.* [10], the authors mentioned that the GS constants derived from previously reported microwave data could not reproduce the transitions observed in the IR region; and so they reported refined values. For the final fit, microwave transitions reported by Rodler [11], Saito [6] and Hays *et al.* [12] were included and given a weighting of 139, 278 or 695 times that of the IR lines, depending on the experimental resolution (20 kHz, 40 kHz, or 100 kHz, respectively). 112 microwave/millimetre wave transitions have been included in the fit with a maximum J' of 23, K_a' of 11 and K_c' of 18, and a resulting unweighted residual error of 0.00026 cm^{-1}. The accuracy of this final fit performed for the fundamental band is also evident in Figure 5, which shows a close up of the fit around the band origin and $K_a = 7 \leftarrow 6$ sub-band. Within the *Q* branch region we see overlap with both the *P* and *R* branches, seen as both separate or merged peaks. For example, in Figure 5 (bottom), we see a less intense peak located in the *Q* branch, and a less intense peak at approximately 428 cm^{-1} belonging to the *R* branch.

In addition to the fundamental, fits to the first and second hot bands were also performed. The initial simulation and assignment of the first hot band was assisted by scaled calculated constants, from anharmonic frequency calculations, and by assuming a linear trend between states. Multiple perturbations observed in Figure 4 with these higher energy states, i.e. $2\nu_{15}$ and $3\nu_{15}$, of *syn*-vinyl alcohol, makes for a much more complicated analysis. Joo *et al.* [10] showed that the ν_{13} fundamental, at 816.7 cm^{-1} was severely perturbed by a Coriolis interaction with the $2\nu_{15}$ manifold of states, and the vibrational energy of $2\nu_{15}$ was very accurately determined to be 775.685 cm^{-1}. Following the inclusion of the Coriolis perturbation parameters resulting from the interaction between $2\nu_{15}$ and ν_{13} as per ref. [10], we still see shifting of high *J* transitions in the residuals, which could be resulting from an interaction of $2\nu_{15}$ with ν_{14} [Fig 6 (top)]. This is also evident in a plot (Figure 7) of the residual error between the simulated and observed peaks for all values of *K*a', with an obvious increase in error with higher *J*. Figure 4 shows the possible interaction of $2\nu_{15}$ with ν_{14}, however, the spectra are not extensive enough at this stage to include an interaction between the two vibrational manifolds. 2101 IR lines have been assigned for the first hot band, with a

TABLE 1. The rotational, centrifugal distortion and Coriolis coupling constants of *syn*-vinyl alcohol as observed and assigned using the program PGOPHER with comparison to those calculated through an anharmonic frequency calculation at MP2/cc-VQZ on a CCSD(T)/cc-VQZ optimised structure.

Parameter	Calc. (GS)	Exp. (GS)	Calc.	Exp. (ν_{15})	Calc.	Exp. (ν_{11})
v_0 (cm^{-1})				407.162707 (15)		488.713433(82)
A (MHz)	59619	59660.7789(11)	59324	59334.687(16)	59602	59642.188(82)
B (MHz)	10506	10561.66516(22)	10447	10514.1174(27)	10530	10559.563(47)[a]
C (MHz)	8924	8965.78568(20)	8928	8971.7322(19)	8911	8960.896(23)[a]
Δ_K(kHz)	872.2	916.319 (75)	-	878.38 (14)	-	938.39(77)
Δ_{JK} (kHz)	-55.23	-61.314(19)	-	-47.165(31)	-	-71.46(18)
Δ_J (kHz)	7.567	7.7368 (10)	-	7.5326(14)	-	7.667(20)
δ_K (kHz)	28.55	29.025(10)	-	19.735(71)	-	51.5(11)
δ_J (kHz)	1.607	1.66635(15)	-	1.56099(62)	-	0.502(12)
Φ_K (Hz)	-35.12	46.53779(24)	-	49.64(32)	-	46.5[b]
Φ_{KJ} (Hz)	12.33	-4.60(12)	-	-30.72(14)	-	-4.60[b]
Φ_{JK} (Hz)	-0.9392	-0.137(19)	-	0.555(22)	-	-0.137[b]
N_{lines}	112 microwave + 4518IR				211IR	
Max. J, K_a, K_c	59, 19, 59				28, 11, 18	
σ_{rms} (MHz)	8.17					
ζ^{bc} (MHz)	-23.1627(53)					
ζ^{+3} (MHz)	0.110426(86)					

[a] $\bar{B}$ and "B_δ" were used and the values of B and C calculated from the relationship $\bar{B} = \frac{1}{2}(B + C)$ and $B_\delta = B - C$.
[b] constrained to GS values.

maximum J' of 53, K_a' of 14, and K_c' of 53. The total assigned IR transitions for the fundamental and first hot band ranging from approximately 300 cm^{-1} to 500 cm^{-1} have a total average residual error of 0.00026 cm^{-1}.

The second hot band, provides for an even more difficult analysis; in Figure 4 we see potential interactions of $3\nu_{15}$ with ν_9 as well as a nearby combination band of ν_{15} + ν_{14}. The reduced intensity of this band and numerous potential perturbations has limited the ability to assign transitions. That said, a rough fit to the band origin could be performed and is shown in Figure 8. The trend observed in the differences between the GS & ν_{15} and ν_{15} & $2\nu_{15}$ constants were used to initially predict the $3\nu_{15}$ rotational and centrifugal distortion constants, and allowed for a rather reliable assignment of transitions around the band origin.

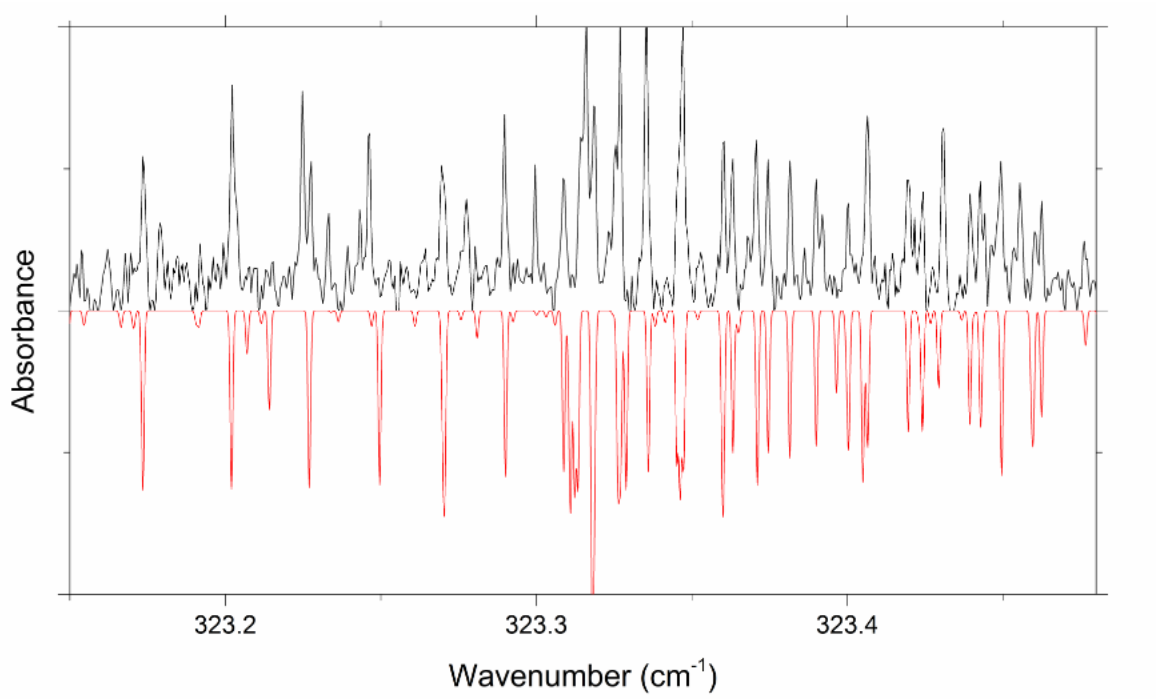

Figure 8. Fit (red) to the high resolution, 0.00096 cm^{-1}, experimental spectra (black) at the band origin for the second ν_{15} hot band of *syn*-vinyl alcohol.

Considerable improvement of this fit will benefit from the collection of spectra with better S/N, and subsequent inclusion of perturbations.

The vibrational, rotational, and centrifugal distortion constants for the GS, ν_{15} & $2\nu_{15}$ and ν_{11} state are compared with calculated values in Table 1, showing good agreement up to and including the quartic level. This is indicative of a good fit with physically meaningful constants. We note that sextic terms, however, have a larger discrepancy, and suspect this is due to an artefact of reducing the Hamiltonian [15]. It has been reported previously [15] that the *A*-reduction of the Hamiltonian has more significant effects on the sextic constants and are therefore expected to show more variation. Table 1 also presents the refined Coriolis perturbation parameters (ζ) for the interaction between the ν_{15} and ν_{11} states. Table 2 shows an accumulation of the previously reported constants for *syn*-vinyl alcohol where a significant improvement from microwave studies is observed, with a small improvement from the IR study by Joo *et al.* [10].

In Table 3 we present the resulting rotational and centrifugal distortion constants for $2\nu_{15}$. Unfortunately anharmonic frequency calculations in Gaussian 09 do not provide higher order constants above the GS, but the constants here seem reasonable (based on what we see in Table 1). Assignments for the second hot band are so far tentative and constants have not been included here for that reason. It is likely that the collection of more intense spectra in this region along with a high resolution analysis of ν_9 and possibly ν_{14} could assist in improving the fit to the second hot band. Alternatively, the use of higher level anharmonic frequency calculations, e.g. at the CCSD(T) level, may provide reasonably accurate Coriolis interaction parameters (that could be useful in the fit).

TABLE 2. Experimentally determined ground state rotational and centrifugal distortion constants of *syn*-vinyl alcohol compared to those previously reported.

Parameter	Hays *et al.* (2015)	Joo *et al.* (1999)	Rodler *et al.* (1984)	Saito (1976)	Current work
A (MHz)	59660.78243(199)	59660.7785(57)	59660.80(2)	59660.2(23)	59660.7789(11)
B (MHz)	10561.60521(49)	10561.6672(10)	10561.665(3)	10561.55(48)	10561.66516(22)
C (MHz)	8965.84204(44)	8965.78751(93)	8965.786(3)	8965.82(42)	8965.78568(20)
Δ_K(kHz)	914.853(129)	915.078(90)	917(1)	-	916.319 (75)
Δ_{JK} (kHz)	-59.876(38)	-60.914(20)	-61.6(4)	-	-61.314(19)
Δ_J (kHz)	7.49749(278)	7.7645(21)	7.71(2)	-	7.7368 (10)
δ_K (kHz)	-0.115784(67)	29.0406(93)	28.97(5)	-	29.025(10)
δ_J (kHz)	-1.665723(297)	1.66748(17)	1.664(2)	-	1.66635(15)
Φ_K (Hz)	-	43.18(19)	-	-	46.53779(24)
Φ_{KJ} (Hz)	-	-4.419(90)	-	-	-4.60(12)
Φ_{JK} (Hz)	-	0	-	-	-0.137(19)
Φ_J (Hz)	-	0.0149(14)	-	-	59660.7789(11)

TABLE 3. The rotational and centrifugal distortion constants for the first hot band of *syn*-vinyl alcohol observed and assigned using the program PGOPHER with comparison to those calculated through an anharmonic frequency calculation at MP2/cc-VQZ on a CCSD(T)/cc-VQZ optimised structure.

Parameter	Calc.	Exp. ($2\nu_{15}$)
ν_0 (cm^{-1})		775.657527 (23)
A (MHz)	59028	59076.656(39)
B (MHz)	10389	10484.1282(48)
C (MHz)	8933	8977.2103(30)
Δ_K(kHz)	-	894.93(53)
Δ_{JK} (kHz)	-	-51.359214(78)
Δ_J (kHz)	-	7.6019829(24)
δ_K (kHz)	-	12.56527(14)
δ_J (kHz)	-	1.5688054(13)
Φ_K (Hz)	-	77.4(19)
Φ_{KJ} (Hz)	-	-6.36(50)
Φ_{JK} (Hz)	-	0.392(42)
N_{lines}	2101	
Max. *J*, K_a, K_c	53,14,53	
σ_{rms} (MHz)	7.73	

V. SUMMARY

The high resolution far-IR analysis of the ν_{15} OH torsional mode of *syn*-vinyl alcohol has been performed here, from which we report refined GS constants, and excited state (ν_{15} and $2\nu_{15}$) rotational and higher order centrifugal distortion constants. In total, over 6000 microwave and IR transitions have been included in the fit, with maximum J', K_a' and K_c' values of 59, 19 and 59 respectively. A strong Coriolis interaction of ν_{15} with ν_{11} was observed perturbing both the fundamental and first hot band. Inclusion of ν_{11} and the Coriolis coupling parameters associated with this perturbation are reported following a brief analysis of the observed ν_{11} fundamental resulting in a largely improved fit. We also observe the second hot band of the ν_{15} mode with rather decent S/N, considering the low population of this level. From this we were able to perform a rough fit to the band origin. This particular band shows significant perturbations providing for an interesting and intensive analysis at a later date.

ACKNOWLEDGEMENTS

This research was undertaken on the Terahertz & Far-IR Beamline at the Australian Synchrotron, Victoria, Australia. We are grateful to Dom Appadoo for stimulating discussions and expert assistance. We would also like to acknowledge Rohan Hudson and Sophia Ackling for their assistance in collecting the spectra, as well as Alexander Gentleman for assistance in calculations, and Greg Metha for helpful advice.

REFERENCES

[1] A. Gero, J. Org. Chem. **19**, 469 (1954).

[2] B. Blank, H. Fischer, Helv. Chim. Acta **56**, 45 (1973).

[3] B. Capon, D. S. Rycroft, T. W. Watson, C. Zucco, J. Am. Chem Soc. **103**, 1761 (1981).

[4] A. Henne, H. Fischer, Angew. Chem. Int. Ed. Engl. **15**, 435 (1976).

[5] W. B. Moniz, S. A. Sojka, C. F. Poranski Jr, D. L. Birkle, J. Am. Chem Soc. **100**, 7940 (1978).

[6] S. Saito, Chem. Phys. Lett. **42**, 3 (1976).

[7] M. Hawkins, L. Andrews, J. Am. Chem. Soc. **105**, 9 (1983).

[8] M. Rodler, C. E. Blom, A. Bauder, J. Am. Chem. Soc. **106**, 4029 (1984).

[9] Y. Koga, T. Nakanaga, K-i. Sugawara, A. Watanabe, M. Sugie, H. Takeo, S. Kondo, and C. Matsumura, J. Mol. Spec. **145**, 315 (1991).

[10] D-L Joo, A. J. Merer, D. J. Clouthier, J. Mol. Spec. **197**, 68 (1999).

[11] M. Rodler, A. Bauder J. Am. Chem Soc. **106**, 4025 (1984).

[12] B. M. Hays, N. Wehres, B. A. DePrince, A. A.M. Roy, J. C. Laas, S. L. Widicus Weaver, Chem. Phys. Let. **630**, 18 (2015).

[13] H. Bunn, R. Hudson, A. Gentleman, P. L. Raston, ACS Eath Space Chem. **1**, 70 (2017).

[14] C. M. Western, J. Quant. Spectrosc. Radiat. Transfer **186**, 221 (2017).

[15] J. -F. D'Eu, J. Demaison, H. Burger, J. Mol. Spec. **218**, 12 (2003).

Statement of Authorship

Title of Paper	High Resolution Spectroscopy of *Anti*-Vinyl Alcohol
Publication Status	☐ Published ☐ Accepted for Publication ☐ Submitted for Publication ☑ Unpublished and Unsubmitted work written in manuscript style
Publication Details	To be slightly reworked before submission

Principal Author

Name of Principal Author (Candidate)	Hayley A Bunn		
Contribution to the Paper	Experimental work, analysis and write up		
Overall percentage (%)	80		
Certification:	This paper reports on original research I conducted during the period of my Higher Degree by Research candidature and is not subject to any obligations or contractual agreements with a third party that would constrain its inclusion in this thesis. I am the primary author of this paper.		
Signature		Date	19/01/2017

Co-Author Contributions

By signing the Statement of Authorship, each author certifies that:

i. the candidate's stated contribution to the publication is accurate (as detailed above);

ii. permission is granted for the candidate in include the publication in the thesis; and

iii. the sum of all co-author contributions is equal to 100% less the candidate's stated contribution.

Name of Co-Author	Paul L Raston		
Contribution to the Paper	Conceptualisation of project and experiments. Support and advice on experiments and editing of drafts. 20%		
Signature		Date	18/01/17

6. High Resolution Far-Infrared Spectroscopy of *Anti*-Vinyl Alcohol

Hayley Bunn[1], Paul L. Raston[2]

[1]*Department of Chemistry, University of Adelaide, SA 5005, Australia*
[2]*Department of Chemistry and Biochemistry, James Madison University, Harrisonburg, Virginia 22807, USA*

We report the first high resolution far-infrared spectrum of the higher energy rotamer of vinyl alcohol, *anti*-vinyl alcohol. We performed a detailed ro-vibrational analysis of the relatively unperturbed ν_{15} OH torsional fundamental at ~262 cm^{-1}, which has provided ground and excited state rotational constants and higher order centrifugal distortion constants up to the sextic level. We also analysed the corresponding first hot band of *anti*-vinyl alcohol, observed with good S/N, at ~259 cm^{-1}. The band shows indications of Coriolis perturbations resulting from a likely interaction with the ν_{11} CCO bending vibration. Inclusion of unperturbed transitions so far has provided reliable rotational and centrifugal distortion constants up to the sextic level for $2\,\nu_{15}$.

I. INTRODUCTION

The atmospheric, astrochemical, and biological relevance of vinyl alcohol has largely contributed to the motivation of research into this simple, unstable, enol. Two confirmations of vinyl alcohol exist with relation to the rotation about the OH bond, referred to as *syn*- and *anti*-vinyl alcohol, where the torsional angles (CCOH dihedral) are 0° and 180° respectively. In Chapter 4 we report a computationally constructed, smoothly evolving, torsional potential showing the double well feature of vinyl alcohol corresponding to the two rotamers. Previous studies reporting the torsional potential of vinyl alcohol also show a higher energy minima at 180° corresponding to the *anti* rotamer and a lower energy minima at 0° corresponding to *syn*. The relative difference between the two minima, however, is rather disputed and appears to depend largely on the level of theory and basis set used.

In 1981 Nobes *et al.* [1] reported a torsional potential constructed from calculations performed in 30 degree increments of the dihedral angle using multiple levels of theory and a range of Pople-type split valence basis sets up to 6-31G**. Increasing the computational level from Hartree-Fock to second and third order Møller-Plesset perturbation theory correlated with a decrease in the energy difference between the two minima of about 8 kJ/mol to 7 kJ/mol [1]. In 1985 Rodler [2] reported an 8.7 kJ/mol energy difference at the Hartree-Fock level with a 6-31G** basis set, but also a 4.5 kJ/mol energy difference between the ground states (GS) of each rotamer determined semi-empirically. We extended this by performing coupled cluster optimisations with single, double and perturbative triple excitation contributions, using a Dunning's correlation consistent quadrupole ζ basis set, in 5 degree increments. The constructed torsional potential, from unscaled calculated values, resulted with the *anti*-vinyl alcohol minima located 6.4 kJ/mol (539 cm^{-1}) higher in energy than its *syn* rotamer, with a GS energy difference of 456 cm^{-1} (5.5 kJ/mol). From this we determined a Boltzmann population of 10% *anti*- to *syn*-vinyl alcohol [3].

The more stable rotamer, *syn*-vinyl alcohol, was first studied by NMR spectroscopy, where it was difficult to discern the conformational preference of the OH group with respect to the rest of the molecule [4-7]. The detection of *syn*-vinyl alcohol was then reported by matrix isolation spectroscopy [8, 9], and by spectroscopy in the gas phase [10] with high resolution analyses providing rotational, centrifugal distortion constants [11, 12]. However, unlike *syn*-vinyl alcohol, the previous work carried out on the high energy *anti* rotamer is less extensive. In a publication by Moniz *et al.* on the CIDNP enhanced ^{13}C NMR spectra, the shift in the vinyl alcohol peaks was suggested to be a result of observing the *anti* conformer as opposed to *syn* [7]. The hydrogen coupling, however, is slightly off from that reported in 1977 [13] and therefore the finding could not be confirmed. Although it was theoretically predicted to exist for a long time, it wasn't until 1985 when the existence of *anti*-vinyl alcohol was experimentally confirmed by Rodler via microwave spectroscopy [2]. The detection of 25 *a*-/*b*-type rotational transitions resulted in the determination of rotational and quartic centrifugal distortion constants.

In 2001 Turner and Apponi reported observing 7 millimetre wave transitions of vinyl alcohol towards the dense molecular cloud Sagittarius (Sgr) B2(N), with 5 of these transitions belonging to the higher energy *anti* conformer. The *a*- and *b*-axis dipole moments for *syn*- and *anti*-vinyl alcohol are μ_a= 0.616, μ_b= 0.807 and μ_a= 0.547, μ_b= 1.702 respectively [2, 10]. The higher *b*-axis dipole moment for the *anti* rotamer suggests that *b*-type transitions should be about 4.5 times more intense than *syn* if the two rotamers are present in equal abundances [14]. Methyl formate and formic acid have also been observed towards Sgr B2(N) [15] and have a torsional potential similar to that of vinyl alcohol [16, 17] with two rotameric forms located at a global minima at 0° and a higher energy minima at 180°. While both rotamers of vinyl alcohol and methyl formate have been observed and known to exist in the ISM for many years, the high energy *cis* rotamer (analogous to *anti*-vinyl alcohol) of formic acid has only very recently been observed [18].

In Chapter 4, we report the survey spectrum of gaseous vinyl alcohol in the far-infrared (IR) for the first time, assigning bands to the ν_{10} fundamental of acetaldehyde (508 cm^{-1}) which is the more stable tautomer of vinyl alcohol, the ν_{11} CCO bend of *syn*-vinyl alcohol (489 cm^{-1}), as well as the ν_{15} OH torsion of both *syn*- (407.2 cm^{-1}) and *anti*-vinyl alcohol (261.8 cm^{-1}). Interestingly the first two hot bands for *syn*-vinyl alcohol, at 368.5 cm^{-1} and 323.3 cm^{-1}, and the first for *anti*-vinyl alcohol, at 259.4 cm^{-1}, were also apparent, indicating significant population of warmer torsional states at room temperature. This was the first gas phase observation of *anti*-vinyl alcohol in the IR. From that study, the relative intensity, under non saturating conditions, of the *anti*-vinyl alcohol fundamental is about 15% of that of the *syn*-vinyl alcohol fundamental.

The following chapter continues from the previous two chapters, and provides a detailed analysis of *anti*-vinyl alcohol's ν_{15} fundamental. We report the excited torsional state ro-vibrational constants and higher order centrifugal distortion constants up to the quartic level, in addition to further refined GS constants.

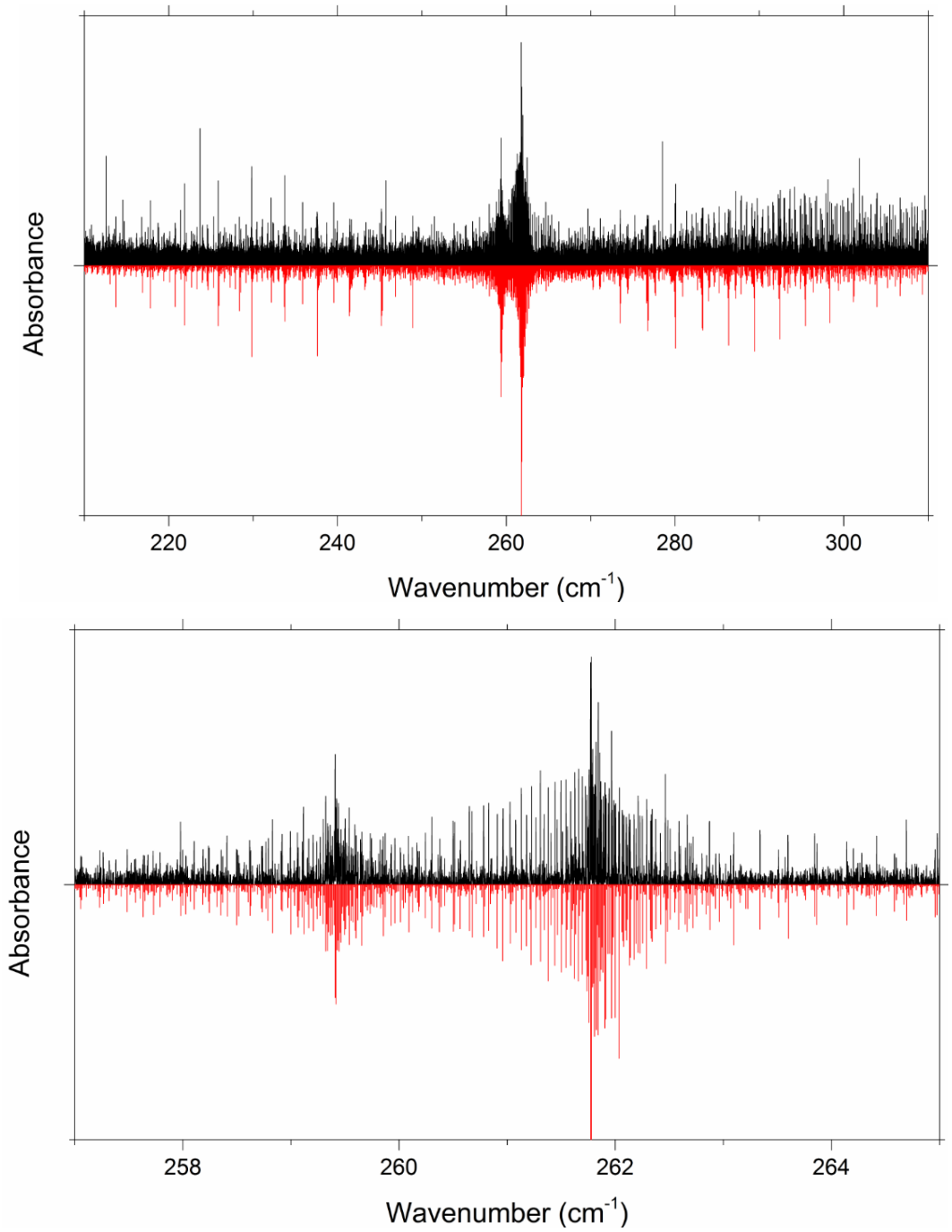

Figure 1. The high resolution, experimental (in black) and simulated (in red) spectra in the vicinity of the ν_{15} bands for *anti*-vinyl alcohol (top). An expanded view (bottom) of the band origins shows the fundamental at 261.55 cm^{-1} and the first hot band at 259.27 cm^{-1}.

II. EXPERIMENTAL

The high resolution Fourier transform IR (FTIR) spectrum of vinyl alcohol was obtained at the THz & Far-IR Beamline of the Australian Synchrotron. The spectra presented in this chapter were recorded during the same experiment as outlined in the preceding chapter. Gaseous vinyl alcohol was produced via the pyrolysis of 2-chloroethanol at 950 °C. The synchrotron

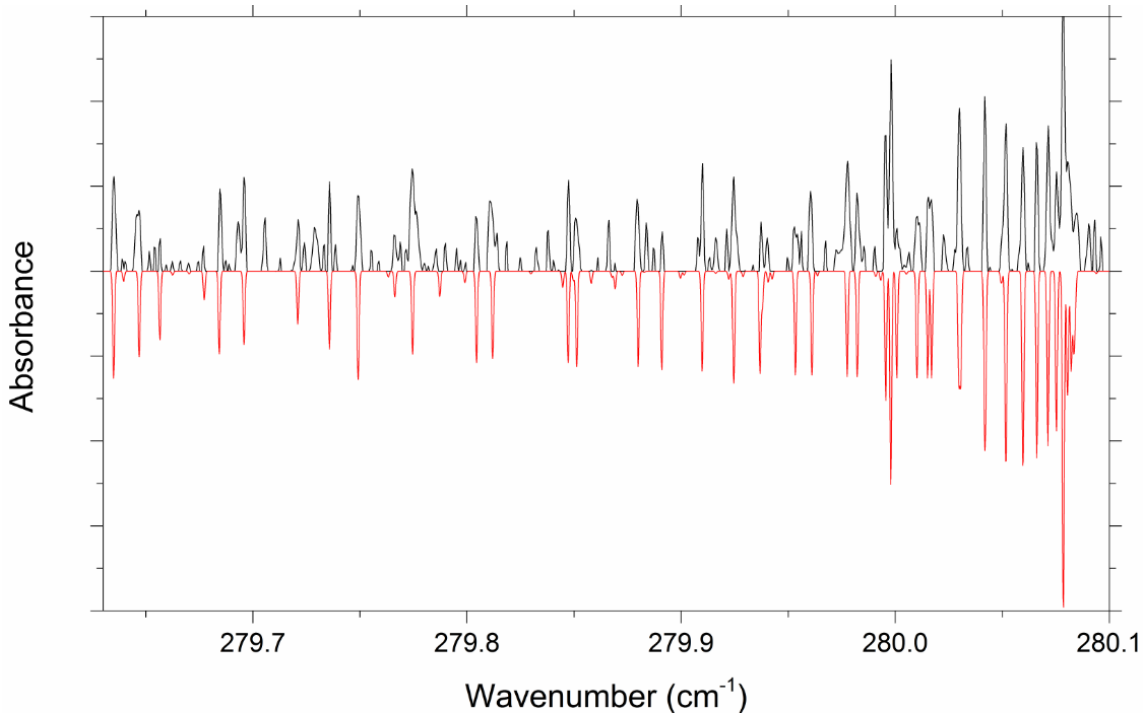

Figure 2. The high resolution experimental (top; in black) and the simulated (bottom; in red) spectra in the ν_{15} band of *anti*-vinyl alcohol in the K_a=5-6 region.

radiation, coupled to a Bruker IFS 125 HR FTIR spectrometer equipped with a Mylar Beam splitter, was directed through polyethylene windows into a multipass cell, in which the gaseous products were continuously flowed at ~2 Torr. The multipass cell was optimised for 16 passes resulting in a pathlength of 10 m. The output radiation was then directed to a liquid helium cooled silicon bolometer detector. The resulting spectrum was collected at a resolution of 0.00096 cm^{-1}. Simulations and fits to the *anti*-vinyl alcohol spectra were performed using the program PGOPHER to extract rotational and centrifugal distortion constants [19].

III. RESULTS AND DISCUSSION

The ν_{15} fundamental and first hot band of *anti*-vinyl alcohol are observed at 261.6 cm^{-1} and 259.3 cm^{-1}, respectively (Fig. 1). The GS constants reported by Rodler [2] and scaled calculated excited state constants were used to initially predict the far-IR fundamental spectrum of *anti*-vinyl alcohol. The fit, which was rather rough at this stage, was improved initially by lowering the resolution of the simulation and temporarily assigning groups of transitions within obvious K_a sub-bands. The resolution was then slowly increased whilst reassigning progressively less blended lines. From here we began assigning individual transitions beginning at low J and slowly increasing. During this process residual outliers were systematically removed and the assigned line positions were continuously fit to a Watson's *A*-reduced Hamiltonian of the I^r representation. We initially floated only ν_{15} = 1 rotational constants and constrained higher order quartic and sextic constants to GS values.

Later, these higher order constants were sequentially allowed to float, as outlined in the previous chapter on *syn*-vinyl alcohol. In order to refine the GS constants we included 25 previously

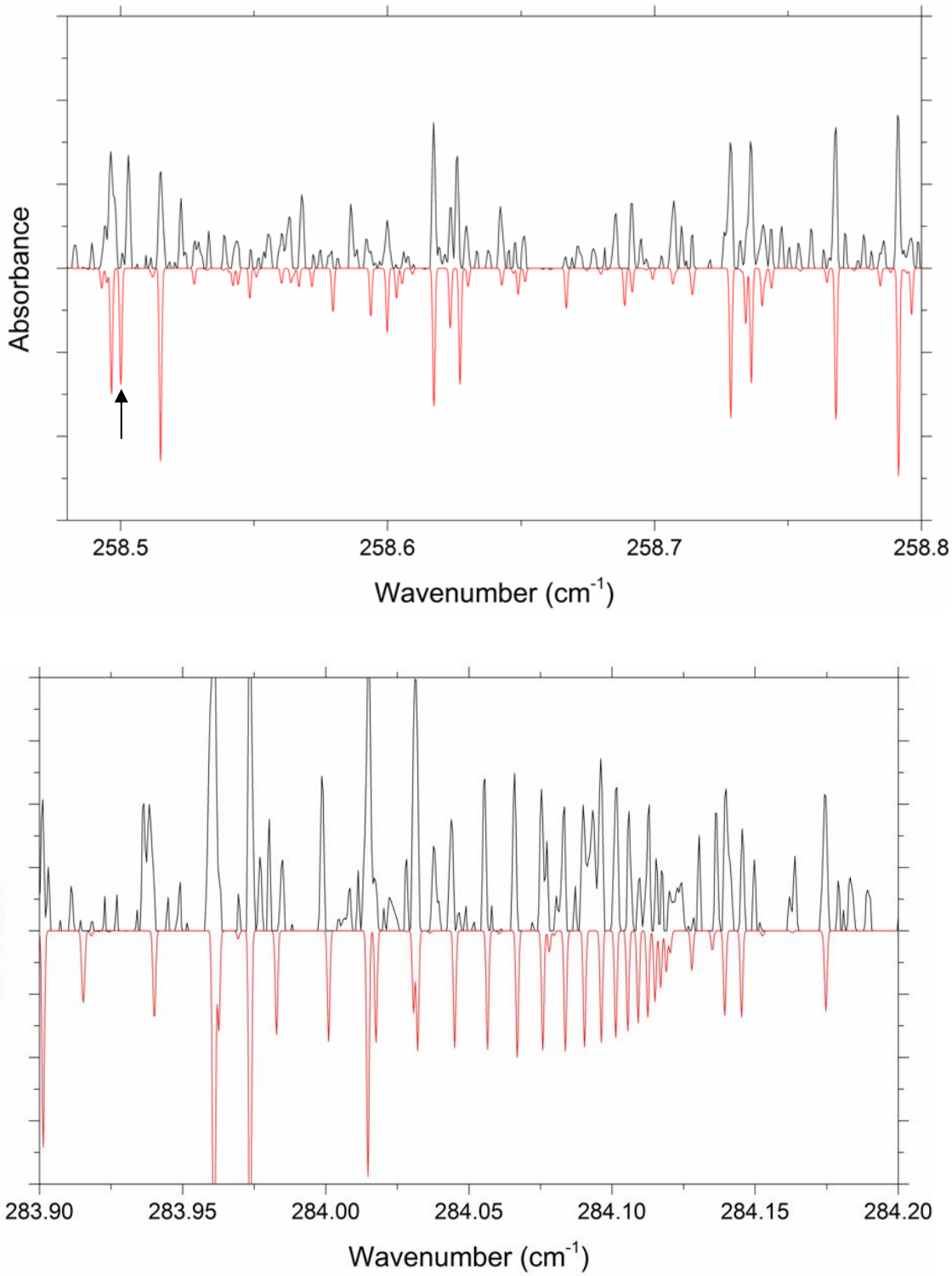

Figure 3. A fit (in red) to the hot band (ν_{15} = 2-1) for *anti*-vinyl alcohol (in black) showing "isolated" perturbations near the band origin (top), shown by the arrow, and perturbations in the K_a=7-8 region (bottom).

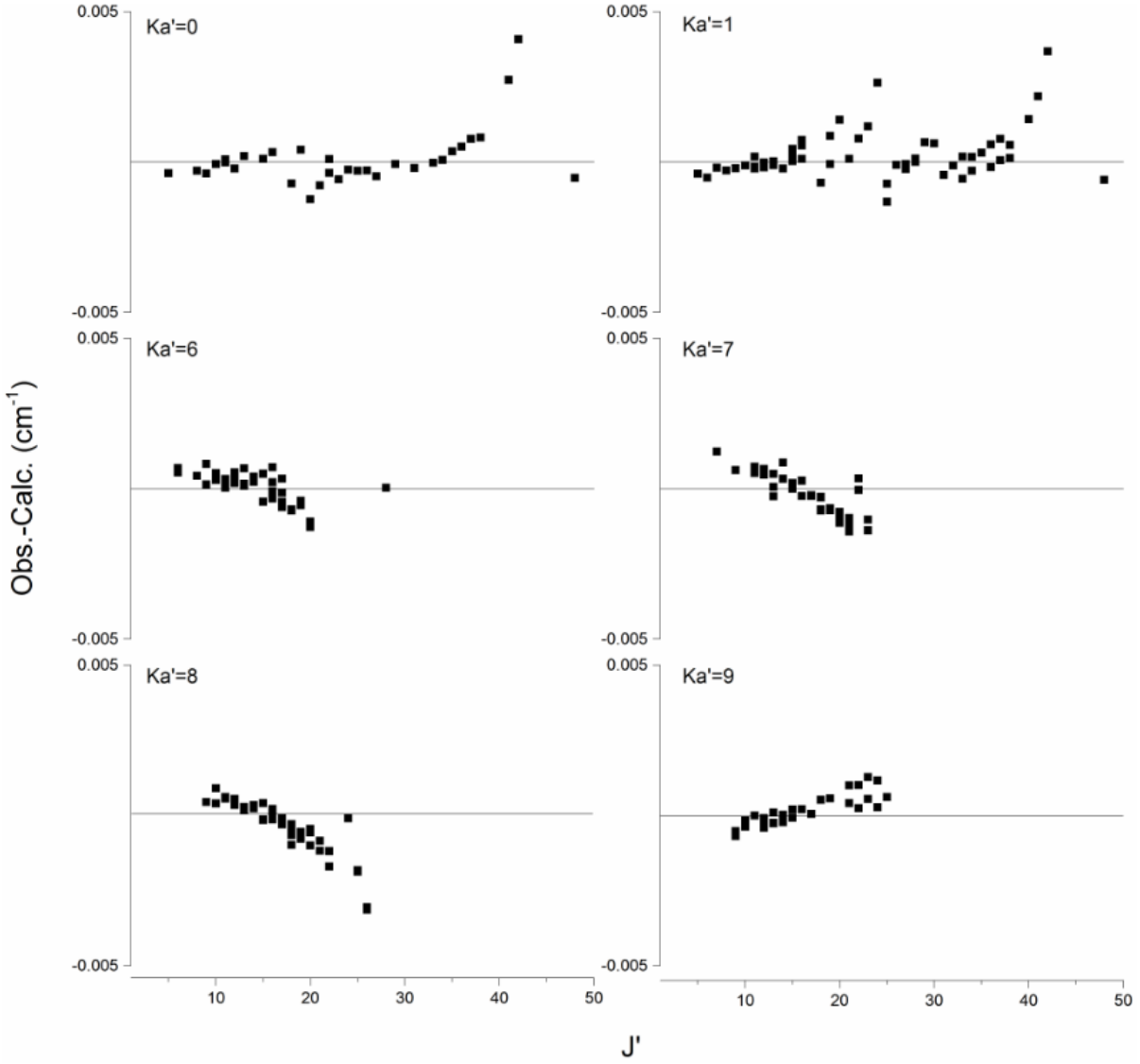

Figure 4. Residuals in the ro-vibrational levels of $2\nu_{15}$, presumably due to a *c*-type Coriolis interaction with ν_{11}.

reported microwave transitions by Rodler [2]. They were measured at a resolution of 20 MHz and were given a weighting of 0.00139 (relative to 1 for the IR lines). One microwave transition in particular (2_{11}–1_{10} reported to be at 40330.518 MHz), had an unacceptably large residual and was removed from the final analysis. Unlike for *syn*-vinyl alcohol, the ν_{15} fundamental of *anti*-vinyl alcohol is not significantly perturbed, which makes for a straight forward analysis. The fit to the fundamental can be seen in Figure 1 with a close up on the K_a = 6–5 sub-band showing an essentially perfect fit (Fig. 2).

Using a similar method as just described, a good fit to the hot band of *anti*-vinyl alcohol was achieved. However, we see evidence of perturbations, particularly at high *J*. This is most likely due to a *c*-type Coriolis interaction of ν_{15} = 2 with the nearby ν_{11} = 1 state (CCO bend) at 489 cm^{-1}. Figure 3 (bottom) shows the fit performed to the hot band, where perturbations are

TABLE 1. The observed rotational and centrifugal distortion constants of *anti*-vinyl alcohol, compared to anharmonic frequency calculations.

Parameter	Calc. (GS)	Exp. (GS)	Calc.	Exp. (ν_{15} = 1)	Calc.	Exp. (ν_{15}= 2)
v_0 (cm^{-1})				261.5511(18)		259.2716(49)
A (MHz)	62801	62868.0904(57)	61951	62079.167(27)	61102	61458.022(90)
B (MHz)	10399	10455.80723(92)	10385	10438.3831(32)	10371	10422.340(11)
C (MHz)	8922	8963.25746(87)	8944	8980.2677(22)	8967	8990.6723(57)
Δ_K(kHz)	1059	1123.99(22)	-	1076.64(41)	-	821.0(16)
Δ_{JK} (kHz)	-50.53	-58.326(23)	-	-57.247(39)	-	-66.79(18)
Δ_J (kHz)	7.063	7.29829(98)	-	7.3406(17)	-	7.2443(61)
δ_K (kHz)	30.50	31.115(13)	-	27.12(11)	-	7.63(47)
δ_J (kHz)	1.424	1.49548(20)	-	1.48609(80)	-	1.4478(33)
Φ_K (Hz)	-50.03	54.1(13)	-	47.3(17)	-	-228.2(87)
Φ_{KJ} (Hz)	-1.073	-5.81(27)	-	-5.32(28)	-	15.9(15)
N_{lines}	26 MW + 2401 IR				663 IR	
Max. J', K_a', K_c'	59,14,59				48,12,48	
σ_{rms} (MHz)	7.984				13.14	

noticeable particularly in the K_a = 7–8 region at higher J. The corresponding residual plot, Figure 4, confirms these perturbations for K_a = 7. A few "isolated" perturbations are further observed, e.g. at 258.5 cm^{-1} shown in the top of Figure 3 for K_a = 1–2. Figure 4 also shows perturbations in the K_a = 0,1,6,7, and 9 levels, where they are most prominent for K_a = 0 and 1. Note that the perturbations we observe are rather weak, resulting in poor 'S/N' in the residuals shown in Figure 4. This is due to the relatively large energy difference between the interacting bands.

We have assigned a total of 2401 IR lines to the ν_{15} = 1–0 band and another 662 to the ν_{15} = 2–1 band, with a maximum J' value of 59, K_a' of 14 and K_c' of 59. The assigned IR transitions, ranging from around 200–300 cm^{-1}, have an average (unweighted) error of 0.00044 cm^{-1}, or 0.000266 excluding ν_{15} = 2–1. Both are lower than the apodised experimental resolution of 0.00048 cm^{-1}. The resulting constants for the ground and first excited states are presented in Table 1 along with comparison to constants derived from anharmonic frequency calculations performed at MP2/cc-pVQZ on a CCSD(T)/cc-pVQZ optimised structure. The smooth evolution of the constants and comparison to constants derived from anharmonic frequency calculations indicates a good fit was achieved with physically meaningful values. Some discrepancy, however, is noticed for the sextic constants. It has been previously noted by D'Eu *et al.* [20] that sextic constants (and δ_K) are particularly susceptible to the *A*-reduction of the Hamiltonian, which may explain the discrepancy. Further comparison of the newly refined GS constants, to those previously reported by Rodler, show only a very minimal variation up to the quartic level.

Table 1 also reports the rotational and centrifugal distortion constants resulting from a fit to relatively unperturbed transitions in the ν_{15} = 2–1 band. These show reasonable values up to and including the quartic constants (excluding δ_K) compared with the experimental values for the ground and excited state. However, we see an even larger discrepancy in the sextic constants. These discrepancies and the overall poorer quality, from what we would expect, in these values could be associated with the non-inclusion of Coriolis interaction parameters within the fit. We aim to include these at a later date, following the completion of rather intensive CCSD(T) anharmonic frequency calculations. These will provide for a better initial estimate of the Coriolis parameters than what we have currently from MP2 calculations.

V. SUMMARY

Here we have presented the first high resolution spectrum of *anti*-vinyl alcohol along with a detailed analysis of the ν_{15} fundamental. Rotational and higher order centrifugal distortion constants are reported up to the sextic level for the GS, improving upon those previously reported by Rodler in 1985 from microwave spectroscopy [2]. Constants up to the sextic level for ν_{15} = 1 state have also been provided. As reported in a preceding paper [3], the first hot band of the *anti* rotamer was observed with good S/N and resolution, and we have performed a fit to unperturbed transitions resulting in accurate constants up to the sextic level. Ongoing work that includes the contribution of Coriolis perturbations in the analysis are planned to be presented at a later date.

ACKNOWLEDGEMENTS

This research was undertaken on the THz & Far-IR Beamline at the Australian Synchrotron, Victoria, Australia. We are grateful to Dom Appadoo for stimulating discussions and expert assistance. We would also like to acknowledge Rohan Hudson and Sophia Ackling for their assistance in collecting the spectra, as well as Alexander Gentleman for assistance in calculations, and Greg Metha for helpful advice.

REFERENCES

[1] R. H. Nobes, L. Radom, N. L. Allinger, J. Mol. Spec. **85**, 185 (1981).

[2] M. Rodler, J. Mol. Spec. **114**, 23 (1985).

[3] H. Bunn, R. Hudson, A. Gentleman, P. L. Raston , ACS Eath Space Chem. **1**, 70 (2017).

[4] B. Capon, D. S. Rycroft, T. W. Watson, C. Zucco, J. Am. Chem Soc. **103**, 1761 (1981).

[5] A. Henne, H. Fischer, Angew. Chem. Int. Ed. Engl. **15**, 435 (1976).

[6] B. Blank, H. Fischer, Helv. Chim. Acta **56**, 45 (1973).

[7] W. B. Moniz, S. A. Sojka, C. F. Poranski Jr, D. L. Birkle, J. Am. Chem Soc. **100**, 7940 (1978).

[8] M. Hawkins, L. Andrews, J. Am. Chem. Soc. **105**, 9 (1983).

[9] M. Rodler, C. E. Blom, A. Bauder, J. Am. Chem. Soc. **106**, 4029 (1984).

[10] S. Saito, Chem. Phys. Lett. **42**, 3 (1976).

[11] Y. Koga, T. Nakanaga, K.-i. Sugawara, A. Watanabe, M. Sugie, H. Takeo, S. Kondo, and C. Matsumura, J. Mol. Spec. **145**, 315 (1991).

[12] D-L Joo, A. J. Merer, D. J. Clouthier, J. Mol. Spec. **197**, 68 (1999).

[13] K. Yoshinda, Chem. Phys. **21**, 317 (1976).

[14] B. E. Turner, A. J. Apponi, , ApJ **561**, 207 (2001).

[15] J. L. Neil, M. T. Muckle, D. P. Zaleski, A. L. Steber, B. H. Pate, V. Lattanzi, S. Spezzano, M. C. McCarthy and A. J. Remijan, ApJ **755**, 153 (2012).

[16] M. L. Senent, M. Villa, F. J. Meléndez, R. Dominguez-Gómez, ApJ **627**, 567 (2005).

[17] M. Pettersson, E. M. S. Maçôas, L. Khriachtchev, R. Fausto, M. Räsänen, J. Am. Chem. Soc. **125**, 4058 (2003).

[18] S. Cuadrado, J. R. Goicoechea, O. Roncero, A. Aguado, B. Tercero, J. Cernicharo, A&A **596**, 1 (2016).

[19] C. M. Western, J. Quant. Spectrosc. Radiat. Transfer **186**, 221 (2017).

[20] J-F. D'Eu, J. Demaison, H. Burger, J. Mol. Spec. **218**, 12 (2003).

Statement of Authorship

Title of Paper	Far-Infrared Spectroscopy of Monodeuterated Vinyl Alcohol
Publication Status	☐ Published ☐ Accepted for Publication ☐ Submitted for Publication ☑ Unpublished and Unsubmitted work written in manuscript style
Publication Details	Possibly submitted at a later date upon collection of less hindered spectra

Principal Author

Name of Principal Author (Candidate)	Hayley A Bunn		
Contribution to the Paper	Experimental work, analysis and write up		
Overall percentage (%)	80		
Certification:	This paper reports on original research I conducted during the period of my Higher Degree by Research candidature and is not subject to any obligations or contractual agreements with a third party that would constrain its inclusion in this thesis. I am the primary author of this paper.		
Signature		Date	19/01/2017

Co-Author Contributions

By signing the Statement of Authorship, each author certifies that:

i. the candidate's stated contribution to the publication is accurate (as detailed above);

ii. permission is granted for the candidate in include the publication in the thesis; and

iii. the sum of all co-author contributions is equal to 100% less the candidate's stated contribution.

Name of Co-Author	Paul L Raston		
Contribution to the Paper	Conceptualisation of project and experiments. Support and advice on experiments and editing of drafts. 20%		
Signature		Date	18/01/17

7. Far-Infrared Spectroscopy of Monodeuterated Vinyl Alcohol

Hayley Bunn[1], Paul L. Raston[2]

[1]*Department of Chemistry, University of Adelaide, SA 5005, Australia*
[2]*Department of Chemistry and Biochemistry, James Madison University, Harrisonburg, Virginia 22807, USA*

The far-infrared spectrum of monodeuterated vinyl alcohol, CH_2CHOD, has been recorded between 100 and 600 cm^{-1}, wherein lies the low frequency OD torsional bands. The fundamental and first two hot bands of the *syn* rotamer, and the fundamental and first hot band of the higher energy *anti* rotamer were assigned with the help of quantum chemical calculations. We have performed a high resolution analysis of the fundamental and first hot band of *syn*-vinyl alcohol, which resulted in the determination of rotational and higher order centrifugal distortion constants in the ground and excited states up to the sextic level. The *anti*-vinyl alcohol bands are largely obscured by water lines introduced from the process of deuteration.

I. INTRODUCTION

Deuterium enrichment in complex molecules (i.e. molecules with ≥ 6 atoms) is suggested to largely occur from reactions with H_2D^+ on interstellar dust grains. It is then thought that these complex molecules, now containing deuterium, are desorbed from the grain into the gas phase following an increase in temperature during, e.g. protostar formation [1-5]. It has been proposed that H_2D^+ is often formed from the reaction between HD and H_3^+, which is exothermic, hence it occurs optimally in low temperature regions of interstellar space. As the temperature in the interstellar medium (ISM) increases, the reaction constant for the exothermic production of H_2D^+ decreases and eventually the reverse (endothermic) reaction is favoured [7-10]. The depletion of H_2D^+ consequently impedes the deuterium enrichment of these complex molecules. Alternatively, it has been theoretically shown that the enrichment process is possible in the presence of hydrocarbons such as CH_2D^+ and C_2HD^+, which form at higher temperatures (up to 70 K) [10]. Considering the complexity of the chemistry that occurs in molecular clouds (such as Orion), it is not surprising that there is some discrepancy between the theoretically predicted and observed abundance of deuterated species in the hot core/compact ridge regions of, e.g. Orion. This could in part be due to not considering the deuteration of species from H_2D^+ reactions at low temperatures in existing models, occurring before the heating of the hot core [10]. All in all, detection of complex deuterated species in hot core regions allows us to comprehend the likely chemical composition of molecular clouds, and how these regions have evolved.

Vinyl alcohol has been identified in the ISM towards Sagittarius (Sgr) B2(N) as detailed in Ref. [11]. To date, there have not been any reported sightings of isotopically labelled vinyl alcohol in the ISM, the most abundant of which are expected to be mono-^{13}C vinyl alcohol, followed by the monodeuterated vinyl alcohols (e.g. CH_2CHOD) [12-14]. During a microwave study reported in 1976 on *syn*-vinyl alcohol (the more stable of the two rotamers), Saito [15] observed monodeuterated vinyl alcohol and reported ground state (GS) rotational constants (*A*, *B* and *C*). In 1984, Rodler and Bauder [16] also reported the microwave spectra of *syn*-vinyl alcohol along

with 9 minor isotopologues, including CH_2CHOD, and provided refined rotational constants (as well as higher order centrifugal distortion constants; up to the quartic level). Following this, Rodler [17] reported the microwave spectrum of the higher energy rotamer (*anti*-vinyl alcohol) and its OD equivalent, and determined rotational and centrifugal distortion constants (up to the quartic level). Finally, the spectroscopic coverage of isotopically substituted *syn*-vinyl alcohol was extended into the infrared (IR) region using matrix isolation techniques, where the authors assigned all but the CH stretching vibrational bands [18].

As mentioned above, vinyl alcohol has been observed in the ISM, yet no observation of any minor isotopologues have been reported, although previously reported spectroscopic constants should be sufficient to allow for accurate predictions of cold transitions. On the other hand, methanol and the monodeuterated form, CH_3OD, have been extensively observed (particularly towards Orion) e.g. we see observations as far back as 1970 [19]. In 1979, Gottlieb *et al.* [20] reported that they observed CH_3OD towards Sgr B2, however, it was not detected in a later, sensitive, survey of Sgr B2 (reported in 1986) [21]. In 1988, Mauersberger *et al.* reported observing CH_3OD in Orion-KL, reporting 13 transitions between 80 and 160 GHz [22]. In that study they also suggested the presence of a potentially less abundant monodeuterated form, CH_2DOH. The group attempted to detect this species but due to the lack of spectroscopic data, were unsuccessful [22]. In 1993 the group reported successfully detecting this species towards Orion-KL with assistance of further unpublished spectroscopic data [23]. It has since been observed towards Sgr B2(N), along with a possible detection of CH_3OD [4]. Recently, there have also been detections of doubly deuterated [24] and triply deuterated methanol [25].

We previously reported (Chapter 4) [6] the far-IR gas phase spectra of both *syn* and *anti*-vinyl alcohol, including the first observation of the *anti* rotamer in the IR. We constructed a semi-empirical torsional potential, which suggests an *anti* abundance of 11%, that is consistent with the observed relative intensities of *syn*- and *anti*-vinyl alcohol from the acquired room temperature spectra. Following this, we reported the high resolution analyses of both the *syn* and *anti*-vinyl alcohol OH torsional fundamental (ν_{15}) and hot band(s), that provided ro-vibrational and higher order centrifugal distortion constants. We now expand on this by reporting the spectrum of monodeuterated vinyl alcohol in the far-IR, that contains both *syn*- and *anti*-vinyl alcohol bands (as well as some of their hot bands), and we determine the vibrational, rotational, and centrifugal distortion constants for the *syn* rotamer.

II. EXPERIMENTAL

The high resolution spectrum of CH_2CHOD was recorded using the THz & Far-IR Beamline at the Australian Synchrotron, as outlined in a recent study on CH_2CHOH (Chapter 4 [6]). Briefly, monodeuterated vinyl alcohol was produced by pyrolyzing monodeuterated 2-chloroethanol at 950 °C. The products were continuously flowed through a room temperature multipass cell with 16 passes, providing a total pathlength of 10 m. The optical elements in this experiment are identical to that used previously for the higher pressure (2 Torr) vinyl alcohol experiments

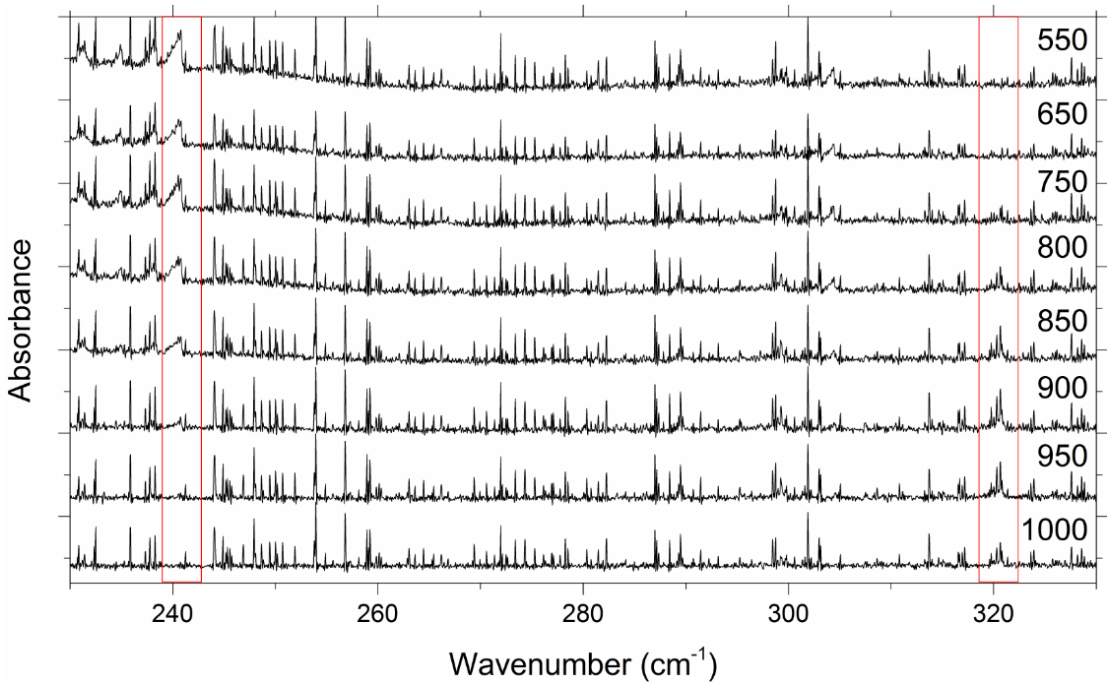

Figure 1. Low resolution (0.1 cm^{-1}) far-IR spectra showing the decrease in the monodeuterated precursor around 240 cm^{-1}, and concomitant increase in monodeuterated vinyl alcohol around 320.6 cm^{-1}, with increasing pyrolysis temperature.

(Mylar beam splitter and polyethylene windows), which also utilized the liquid helium cooled silicon bolometer detector. The monodeuterated 2-chloroethanol was prepared by hydrogen exchange (25 mL of 2-chloroethanol with 3 x 10 mL of D_2O), followed by extraction with an equivalent amount dichloromethane (x2) and a final drying over $MgSO_4$. We note that MgO would have been a more appropriate drying agent, which could have avoided spectral contamination by water lines (see below).

III. CALCULATIONS

All calculations utilised the Gaussian 09 electronic structure package, as previously described in Chapter 4 [6]. Anharmonic frequency calculations of monodeuterated *syn*- and *anti*-vinyl alcohol were performed, based on a coupled cluster optimised structure incorporating single, double and perturbative triple excitation contributions, CCSD(T). A lower level second order Møller-Plesset (MP2) was used for the anharmonic calculations due to Gaussian 09 restrictions, in addition to time constraints in performing CCSD(T) harmonic calculations. For ease of comparison, the reported harmonic frequencies are extracted from the MP2 'anharmonic' calculations.

IV. RESULTS/DISCUSSION

The successful production of monodeuterated 2-chloroethanol is evident from the shift in the ν_{20} torsional band of the most stable rotamer of 2-chloroethanol (Gg') [26]; this shift is from approximately 345 cm^{-1} to 240 cm^{-1}, as expected from $\bar{\nu}_D \approx \bar{\nu}_H \times \sqrt{m_H/m_D}$ = 244 cm^{-1}. As shown in Figure 1, we observed a marked gradual decrease in the deuterated 2-chloroethanol precursor peak as we increased the pyrolysis temperature from 800 to 950 °C. Along with the

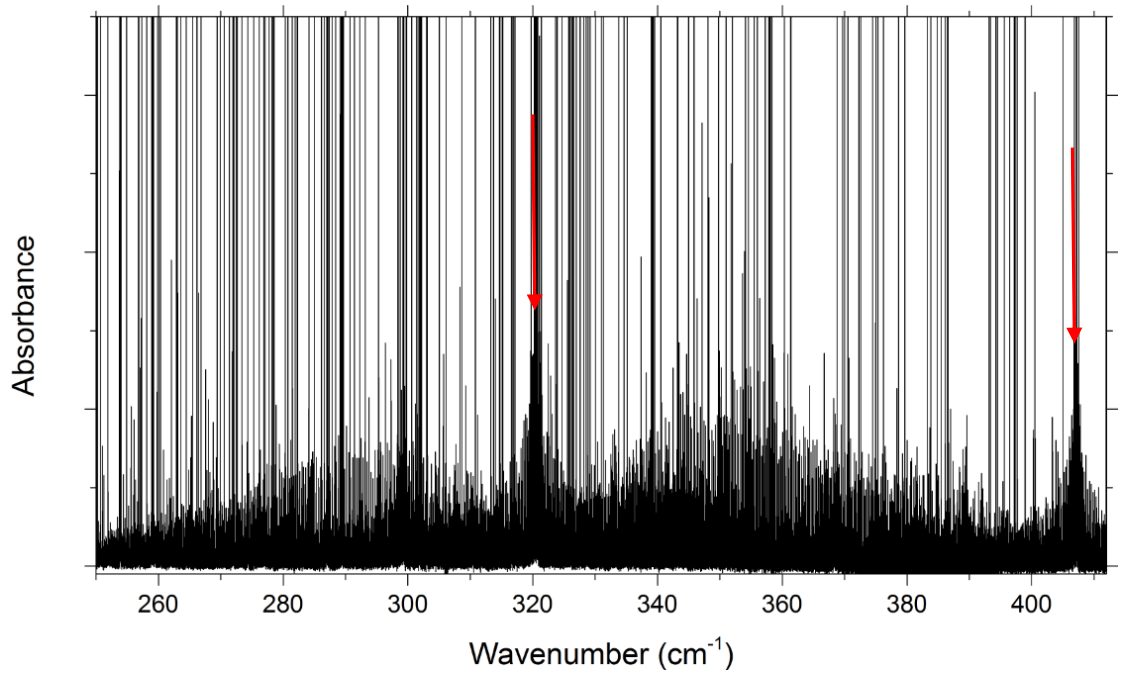

Figure 2. The high resolution (0.00096 cm^{-1}) spectrum of monodeuterated *syn*-vinyl alcohol (320.6 cm^{-1}) with comparison to non deuterated (407.2 cm^{-1}) *syn*-vinyl alcohol.

reduction of the precursor signal we saw an increase in a feature around 320 cm^{-1}, which we assign to the *a*" *c*-type OD torsional mode (ν_{15}) of monodeuterated *syn*-vinyl alcohol. This is much higher than what is expected from the above relation ($\bar{\nu}_D \approx 288$ cm^{-1}), which indicates the potential is rather anharmonic in the *syn* well. There is very good agreement, however, with the anharmonic Gaussian value (325 cm^{-1}).

In addition to the fundamental of monodeuterated vinyl alcohol, we observed the non-deuterated *syn*-vinyl alcohol fundamental at 407.2 cm^{-1}, as previously reported in Chapters 4 and 5 [6, 27]. From the relative intensities of these fundamentals (Fig. 2), we estimate that the deuterated and non-deuterated vinyl alcohol species are present in a similar abundance (indicating 50% deuteration). In a study of vinyl mercaptan (the sulphur analogue of vinyl alcohol, the precursor, ethanedithiol, was treated with D_2O in the same manner as presented here showing a 90% exchange of thiol hydrogen's [28]. The lower conversion of 2-

TABLE 1. Observed ν_{15} vibrational frequencies (cm^{-1}) of monodeuterated *syn*- and *anti*-vinyl alcohol in the far-IR, with comparison to theoretical frequencies.

Rotamer	$\nu' - \nu''$	Observed	Harmonic[a]	Anharmonic[a]	Potential function
Syn	1 – 0	320.62	344.95	325.33	318.80
	2 – 1	299.21	344.95	305.76	297.90
	3 – 2	276.3	344.95	-	274.07
Anti	1 – 0	200.6	194.83	192.48	197.66
	2 – 1	196.3	194.83	193.44	195.93

[a]Computationally determined frequencies from the Gaussian calculations.

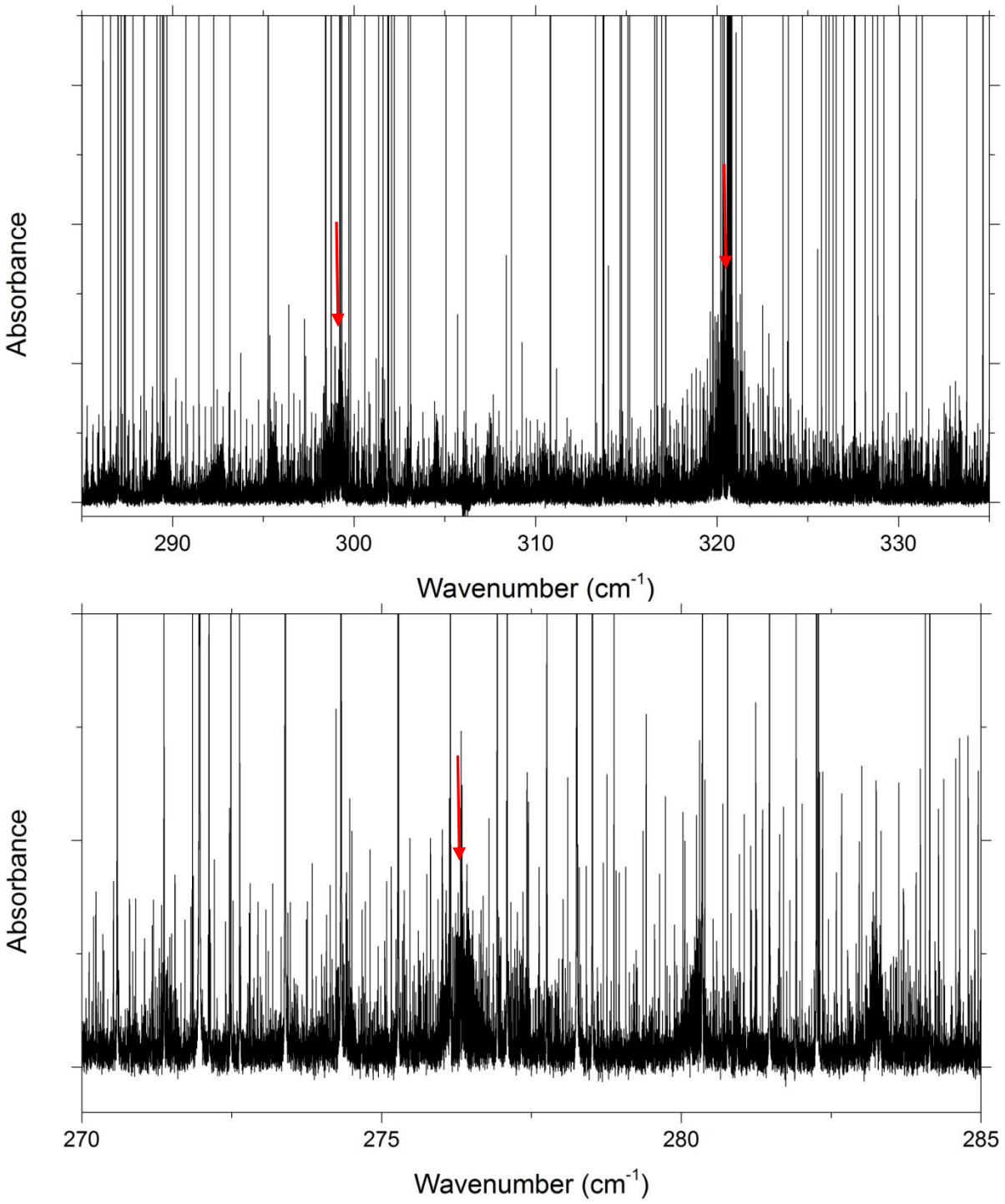

Figure 3. High resolution far-IR spectra of monodeuterated *syn*-vinyl alcohol showing an expanded view of the fundamental band origin at 320.6 cm^{-1}, first hot band near 299.2 cm^{-1} (top) and second hot band near 276.3 cm^{-1} (bottom) (indicated by the red arrows).

chloroethanol to the deuterated form, could be attributed to air exposure during the longer time frame wherein we attempted to dry. Unfortunately, 2-chloroethanol and water (H_2O/D_2O) form a strong azeotrope making the two solutions exceptionally difficult to separate, hence we see contaminating lines due to the residual water in both *syn*- and *anti*-vinyl alcohol spectra.

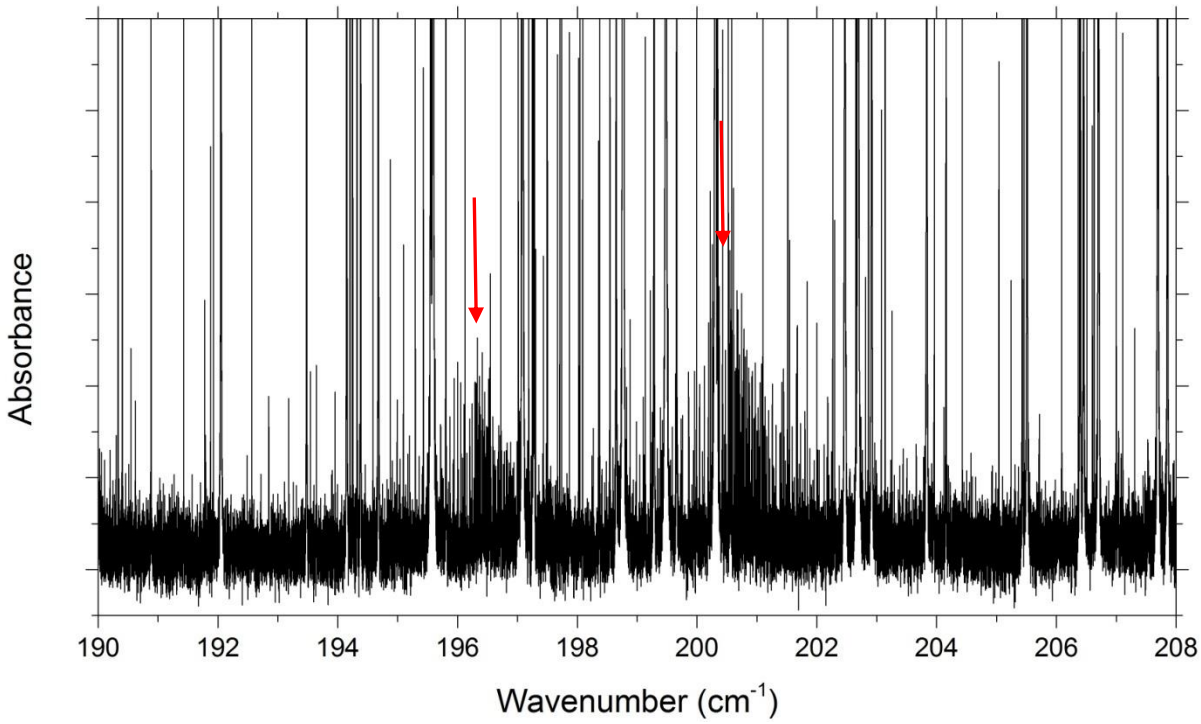

Figure 4. Far-IR spectra of monodeuterated *anti*-vinyl alcohol near 200 cm^{-1}, with the presence of a hot band near 196 cm^{-1} (indicated by red arrows).

The high resolution (0.00096 cm^{-1}) spectrum of monodeuterated *syn*-vinyl alcohol is presented in Figure 3. Here, we see the band origin of the ν_{15} fundamental which is characterised by a strong central Q branch peak (at 320.62 cm^{-1}), in addition to its first and second torsional hot bands (centred around 299.21 cm^{-1} and 276.3 cm^{-1}, respectively). The ν_{15} fundamental of *anti*-vinyl alcohol, can be seen in Figure 4 located around 200 cm^{-1}, with its first hot band around 196 cm^{-1}. Based on comparison to anharmonic frequency calculations (Table 1), the bands of *syn*- and *anti*-vinyl alcohol, along with their 1st hot bands, were easily assigned (assignment of the 2nd hot band for the *syn* rotamer relied on the 'potential function'; see following). Good agreement is evident for both rotamers, however, for *anti*-vinyl alcohol, the fundamental and hot band predictions are flipped relative to what is observed.

Figure 5 shows the Born-Oppenheimer torsional potential of vinyl alcohol [6], along with the vibrational energy levels for CH_2CHOD. Table 1 reports the corresponding energy level differences, showing better agreement compared to anharmonic frequency calculations with the observed band origins. In comparison to the normal isotopologue, the heavier deuterium atom in monodeuterated vinyl alcohol results in a much closer spacing of the energy levels, which is not surprising considering the H/D atom on the hydroxyl group is principally what vibrates. A higher relative population of the excited vibrational states in comparison to normal vinyl alcohol is expected, however, we still observe only the first hot band (ν = 2–1) for *anti* and the first two for *syn* (ν = 2–1 and ν = 3–2). This is likely due to the reduced S/N resulting from incomplete deuteration and water contamination in the spectrum. Unfortunately, the *anti*-vinyl alcohol spectral region is the most contaminated (Fig. 4), making it difficult to perform a

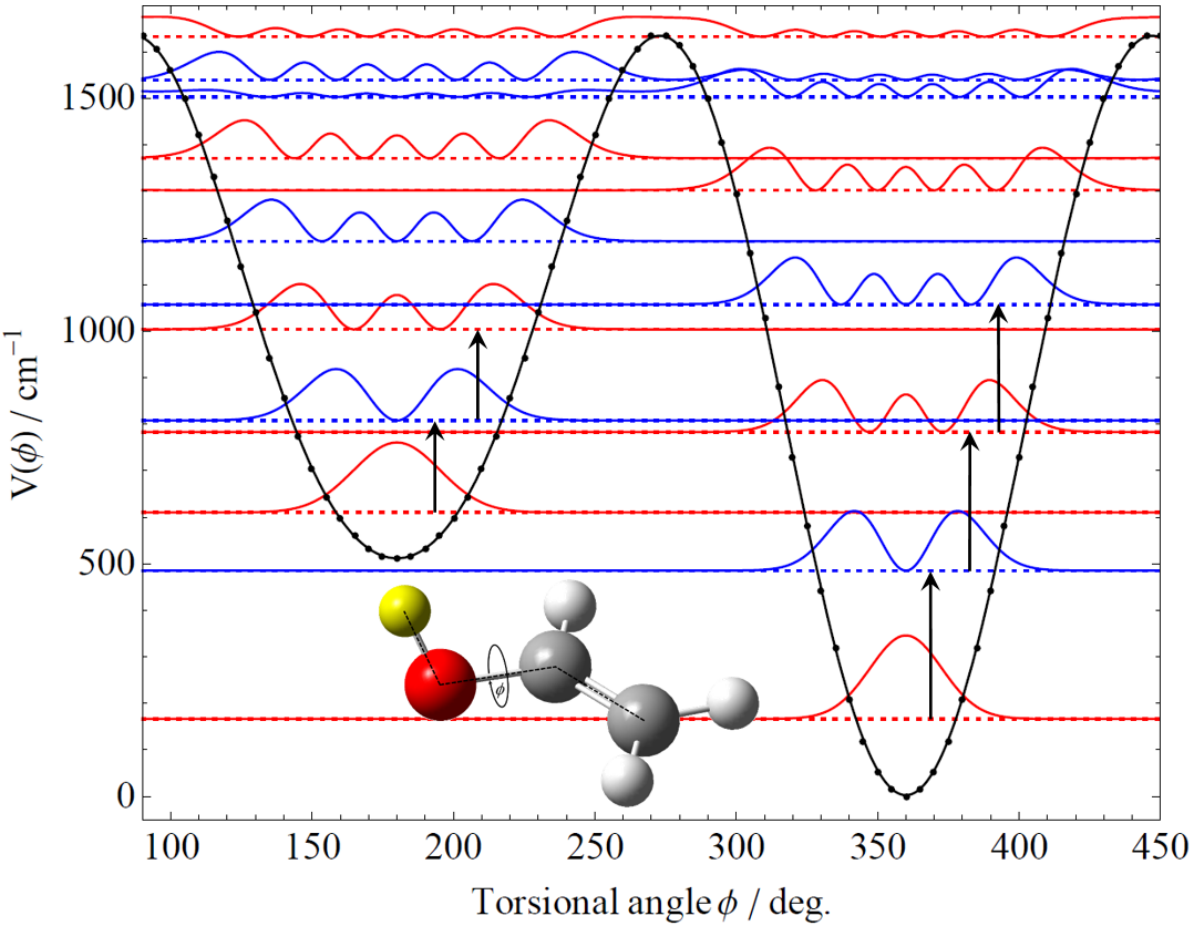

Figure 5. The OH torsional potential calculated in 5° increments (black dots) fitted to a Fourier expansion (black curve); see Chapter 4 [6] for details. Black arrows indicate the observed vibrational transitions.

detailed analysis. The *syn*-vinyl alcohol region, on the other hand, is somewhat less contaminated, allowing for a high resolution analysis to be performed.

An initial simulation (using PGOPHER [29]) of the spectrum in the OD torsional fundamental of monodeuterated *syn*-vinyl alcohol was performed using the GS rotational and centrifugal distortion constants from Rodlers 1984 microwave study [16], and predicted first excited state (ν_{15} = 1) constants (extracted from scaled [30] calculated values, up to the quartic level). Isolated transitions that were well aligned between the experimental and simulated spectra were initially assigned, later moving onto low K_a (= ±1) sub-band regions, progressively assigning transitions with increasing K_a and J.

Refinement of the spectroscopic parameters was accomplished by fitting the line positions to a Watson's *A*-reduced Hamiltonian in the I^r representation. Initially, only the excited state rotational constants (*A*, *B*, and *C*) and band origin were allowed to float, with the quartic distortion constants ($\Delta_K, \Delta_{JK}, \Delta_J, \delta_K, \delta_J$) fixed to their GS values. Initially, we provided higher weighting to the most confident assignments, and throughout the fitting process we systematically removed assignments with large residual errors. After substantially improving

the fit, the quartic distortion constants were allowed to float, starting with the largest and gradually moving onto the smallest. We found that refinement of GS constants from their initial microwave values was eventually necessary, and that was assisted by inclusion of the previously reported microwave transitions [15, 16]. Inclusion of the first two sextic terms Φ_K and Φ_{KJ}, in both ground and excited states, were noticed to considerably improve the fit, (as monitored by the average residual error). Inclusion of Φ_{JK} and Φ_J showed minimal improvement and were constrained to 0. The final rotational Hamiltonian is of the form,

$$\hat{\mathrm{H}} = (A - \bar{B})\hat{J}_a^2 + \bar{B}\hat{J}^2 - \bar{B}\hat{J}_{bc}^2 - \Delta_{\mathrm{K}}\hat{J}_a^4 - \Delta_{\mathrm{JK}}\hat{J}^2\hat{J}_a^2 - \Delta_{\mathrm{J}}\hat{J}^4 - \delta_{\mathrm{K}}\left(\hat{J}_a^2\hat{J}_{bc}^2 + \hat{J}_{bc}^2\hat{J}_a^2\right) - 2\delta_J\hat{J}^2\hat{J}_{bc}^2 + \Phi_K\hat{J}_a^6 + \Phi_{KJ}\hat{J}^2\hat{J}_a^4, \quad (1)$$

where $\bar{B} = \frac{1}{2}(B + C)$, and $\hat{J}_{bc}^2 = \hat{J}_b^2 - \hat{J}_c^2$. The total angular momentum operator, $\hat{J}$, has components along the *a*, *b*, and *c* axes, $\hat{J}_a, \hat{J}_b, \hat{J}_c$.

In Chapter 5, the high resolution analysis of *syn*-vinyl alcohol, we observed a Coriolis interaction between $\nu_{15} = 1$ at 407 cm^{-1} and $\nu_{11} = 1$ at 488 cm^{-1}, which resulted in small but significant shifts to the line positions. The ν_{11} manifold is rather unaffected by deuteration and is predicted (from CCSD(T) calculations) to appear 27 cm^{-1} away (i.e. at 468 cm^{-1}) from normal vinyl alcohol (495 cm^{-1}). This is much less than the shift in the $\nu_{15} = 1$ manifold in going from

TABLE 2. Experimental and theoretical vibrational, rotational, and higher order centrifugal distortion constants for monodeuterated *syn*-vinyl alcohol.

Parameter	Calc. (GS)	Exp.(GS)	Calc.(ν_{15})	Exp.(ν_{15})	Calc.($2\nu_{15}$)	Exp.($2\nu_{15}$)
ν_0 (cm^{-1})				320.6180494(87)		618.832763(12)
A (MHz)	52554	52585.5405(26)	52340	52424.5307(91)	52127	52281.563(13)
B (MHz)	10266	10320.50297(46)	10212	10265.2410(39)	10158	10216.6181(39)
C (MHz)	8581	8621.18840(42)	8588	8628.7209(11)	8595	8635.8775(19)
Δ_K(kHz)	599.8	607.848 (47)	-	599.994 (73)	-	596.16(12)
Δ_{JK} (kHz)	-48.43	-49.2991069 (59)	-	-44.296(11)	-	-42.1186(71)
Δ_J (kHz)	7.646	7.80075794 (32)	-	7.613969(53)	-	7.544269(84)
δ_K (kHz)	26.11	27.868159 (12)	-	17.975(31)	-	13.997(54)
δ_J (kHz)	1.735	1.78411510(86)	-	1.67839 (30)	-	1.62796(52)
Φ_K (Hz)	-5.201	20.01 (16)	-	20.67(18)	-	20.98(29)
Φ_{KJ} (Hz)	-0.3743	-1.585(45)	-	-2.275(58)	-	0
N_{lines}		3870 IR + 59 MW				2271 IR
Max. *J*, K_a, K_c		61, 20, 61				56, 18, 53
σ_{rms} (MHz)		5.544				6.024

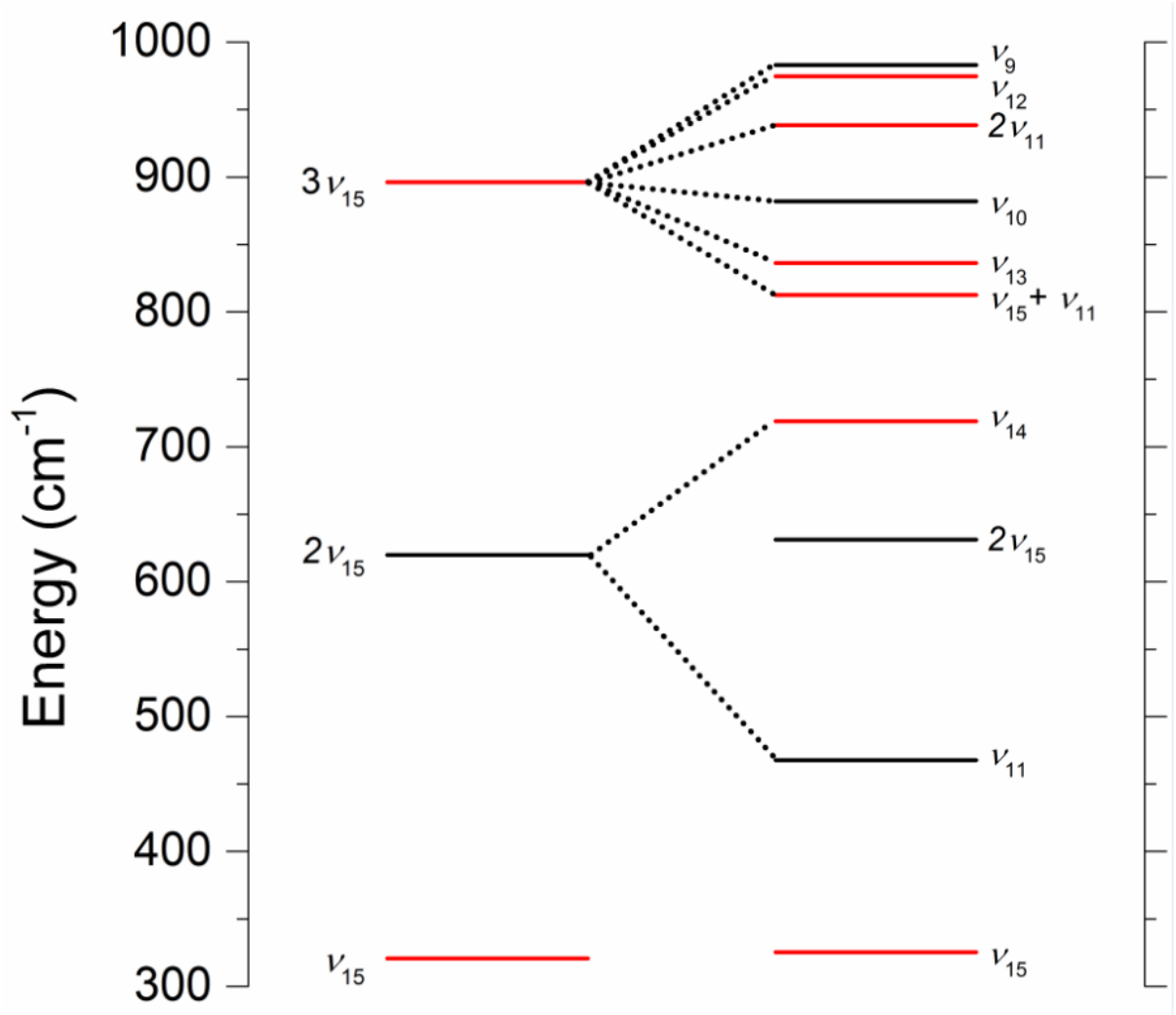

Figure 6. The observed energy levels for the ν_{15} OH torsional vibration and the nearby calculated states for *syn*-vinyl alcohol extracted from an anharmonic frequency calculation at MP2/cc-VQZ, on a CCSD(T)/cc-VQZ optimised structure. The levels in red indicate asymmetric bands and those in black, symmetric. The dotted line indicates possible interactions with an energy difference of < 100 cm^{-1}, as well as the weak interaction with ν_{11}.

normal *syn*-vinyl alcohol to monodeuterated *syn*-vinyl alcohol (from 407 to 320 cm^{-1}). This reduces the strength of the previously observed Coriolis interaction [27] to the point where it is essentially negligible, see Figure 6. The lack of obvious perturbations in the fundamental, and availability of the previously reported microwave transition frequencies allowed for a rather smooth fitting process.

A total of 3870 IR transitions have been assigned and included in the fit for this ν_{15} fundamental with a maximum J' of 61, K_a' of 20, and K_c' of 61. 59 microwave transitions have also been included from previous reports [15, 16], with a maximum J' of 22, K_a' of 5 and K_c' of 21. They were given a weighting of 139 or 695 times that of the IR transitions, depending on the estimated accuracy in the microwave studies (20 or 100 kHz [15, 16]). Table 2 summarises the

resulting ground and excited rotational and centrifugal distortion constants, including quartic and first two sextic terms.

We see good agreement between the experimental constants with those derived from anharmonic frequency calculations, indicating physically meaningful values. There is, however, a discrepancy in the sextic terms, Φ_K and Φ_{KJ}, where we observed similar values with opposite signs. It has been previously noted that sextic constants are largely affected by the reduction of the Hamiltonian [31] commonly leading to slight discrepancies and inconsistencies with the sign, when compared with experimental values. The quality of the final fundamental fit is apparent in Figure 7, which shows the intense band origin and K_a = 5–6 sub-band. The overall (unweighted) residual error was 0.00018 cm^{-1}, which is less than half of the apodised experimental resolution (0.00048 cm^{-1}).

A fit was also performed for the first hot band of monodeuterated *syn*-vinyl alcohol which can be seen in Figure 8. Like the fundamental, the first hot band is rather free of perturbations. The resulting rotational and centrifugal distortion constants are presented in Table 2, also showing good agreement with calculated values. Unfortunately, however, the anharmonic frequency calculations performed here do not provide higher order constants for any level above the GS, hence only comparison to rotational constants and band origins can be made. Due to the low intensity of the second hot band in addition to its interference by water lines, this band has not been included in the fit. Future efforts will focus on obtaining a clean high resolution spectrum, free of water, for monodeuterated vinyl alcohol. This will further improve the current *syn*-vinyl alcohol fit, and allow for a high resolution analysis for the *anti* rotamer to be performed.

It is interesting to speculate on the possibility of detecting CH_2CHOD in the ISM, using observational data of CH_3OH, CH_3OD, and CH_2CHOH. Based on column densities determined from observations toward Sgr B2, the ratio of CH_3OD/CH_3OH has been reported to be 0.007 [4]. The column density of *syn*- and *anti*-vinyl alcohol was reported, from the microwave detection of vinyl alcohol towards Sgr B2(N), to be 2 x 10^{14} cm^{-2} and 2.4 x 10^{13} cm^{-2} respectively [11]. Assuming the same ratio as methanol for CH_2CHOD/CH_2CHOH (0.007), and a total vinyl alcohol column density of 2.24 x 10^{14} cm^{-2} we can predict the monodeuterated vinyl alcohol abundance to be about 1.6 x 10^{12} cm^{-2}, which gives a *syn* and *anti* column density of 1.4 x 10^{12} cm^{-2} and 1.7 x 10^{11} cm^{-2} respectively (assuming the same relative abundance of the rotamers). These values are considerably lower than the detected column densities of most interstellar molecules, e.g. in a survey of deuterated complex organic molecules in Sgr B2(N), using the Atacama Large Millimetre/ sub millimetre Array (ALMA), the lowest observed column density is 3 x 10^{14} cm^{-2} [4]. There are, however, reported detection of molecules with lower column densities (but with larger dipole moments). For example Bacmann *et al.* reported the identification of D_2CO at a column density of 5.8 x 10^{11} cm^{-1}, using the IRAM 30 m telescope [32]. D_2CO has a dipole moment (*a* axis only) of 2.3464 D which is significantly larger than that for vinyl alcohol (non-deuterated), with *a* and *b* dipole moments of 0.616 D and 0.807 D for *syn* and 0.547 D and 1.702 D for *anti*. As the intensity of a transition is proportional

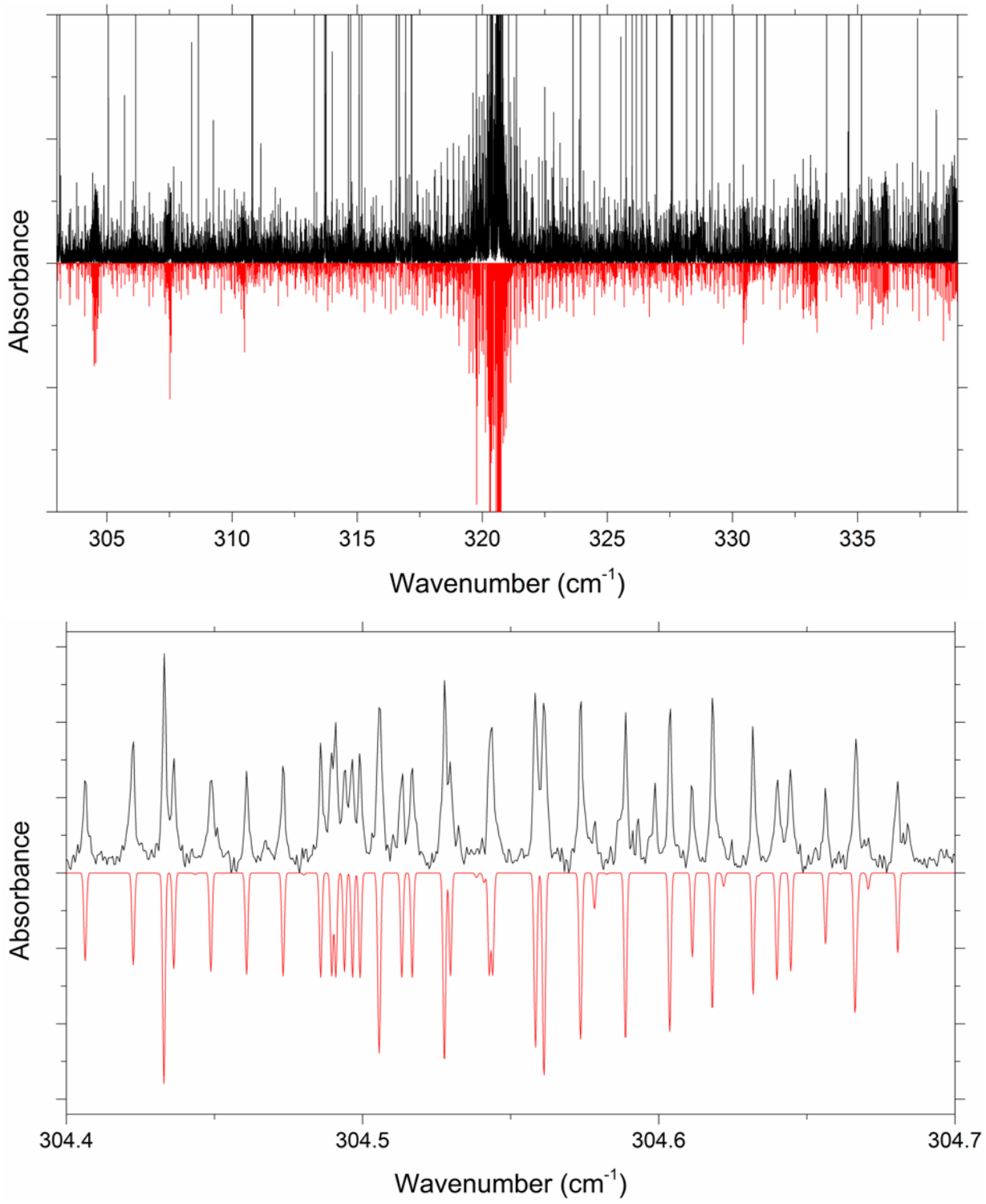

Figure 7. A fit (in red) to the measured (black) torsional fundamental spectrum of monodeuterated *syn*-vinyl alcohol at high resolution, in the vicinity of the band origin (top) and the K_a = 5–6 sub-band (bottom).

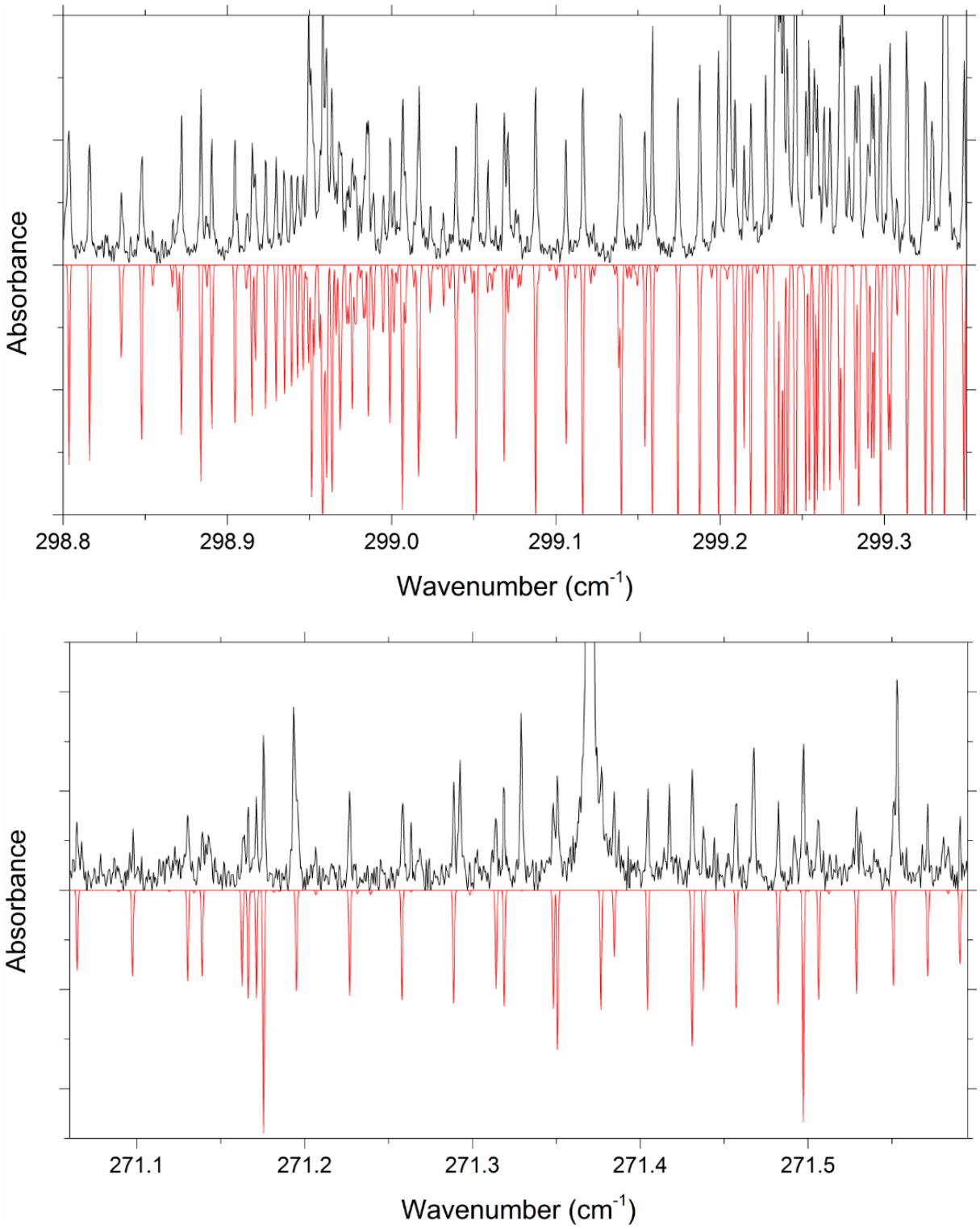

Figure 8. A fit (red) to the torsional hot band of monodeuterated *syn*-vinyl alcohol. The band origin region is shown (top) in addition to the K_a= 9–10 sub-band (bottom).

to the square of the dipole moment, the likeliness of observing monodeuterated vinyl alcohol in the ISM is rather slim. The best case scenario considering only the column density and the square of the dipole moment shows that an *a*-type transition of *syn*-vinyl alcohol is 1.9 times less likely to be observed than formaldehyde (3.5 for *b*-type transition, 6.5 for *b*-type transition of *anti*-vinyl alcohol and 63 for an *a*-type *anti*-vinyl alcohol transition). In addition to this the partition function of vinyl alcohol is larger, resulting from 3 extra atoms, therefore reducing the transition intensity further with respect to formaldehyde. However, if successful, the detection (and determination of relative abundance) of monodeuterated vinyl alcohol could allow for a better understanding of how vinyl alcohol forms in the ISM.

V. SUMMARY

Here we reported the far-IR spectrum and analysis for monodeuterated vinyl alcohol (CH_2CHOD). We observed the ν_{15} OD torsional fundamental and its first two hot bands for *syn*-vinyl alcohol (at 320.6cm^{-1}, 299.2 cm^{-1} and 276.3 cm^{-1} respectively), along with the fundamental and first hot band of *anti*-vinyl alcohol (at 200.6 cm^{-1} and 196.3 cm^{-1}). The band centres agree very well with the previously reported semi-empirical PES, with a RMS deviation between experimental and theoretical torsional energies of 1.9 cm^{-1}. A high resolution analysis of the *syn*-vinyl alcohol fundamental and first hot band has been performed, resulting in vibrational, rotational and centrifugal distortion constants (including quartic and the first two sextic terms) for $\nu_{15} = 0$, 1, and 2. The "higher temperature" experimental results, such as those presented here, should be of assistance in detecting DVA in warmer environments, since our ground and excited state rotational constants should allow for accurate predictions to be made up to several hundred Kelvin.

ACKNOWLEDGEMENTS

This research was undertaken on the THz & Far-IR Beamline and the Australian Synchrotron, Victoria, Australia. We are grateful to Dom Appadoo for assistance. We would also like to acknowledge Rohan Hudson and Junda Li for their assistance in collecting the spectra, as well as Greg Metha for advice. This research used high-performance computing services provided by eRSA.

REFERENCES

[1] C. M. Walmsley, W. Hermsen, C. Henkel, R. Mauersberger, T. L. Wilson, ApJ **172**, 311 (1987).

[2] B. E. Turner, ApJ **362**, 29 (1990).

[3] T. Jacq, C. M. Walmsley, C. Henkel, A. Baudry, R. Mauersberger, P. R. Jewell, A&A **228**, 447 (1990).

[4] A. Belloche, H. S. P. Müller, R. T. Garrod and K. M. Menten, A&A **587**, 91 (2016).

[5] C. Ceccarelli, P. Caselli, D. Bockelée-Morvan, O. Mousis, S. Pizzarello, F. Robert, D. Semenov, in *Protostars and Planets VI*, University of Arizona press, (2014).

[6] H. Bunn, R. Hudson, A. Gentleman, P. L. Raston, ACS Eath Space Chem. **1**, 70 (2017).

[7] N. G. Adams, D. Smith, ApJ **248**, 373 (1981).

[8] E. Herbst, A&A **111**, 76 (1982).

[9] D. Smith, G. Adams, E. Alge, ApJ **263**, 123 (1982).

[10] T. J. Millar, A. Bennett, E. Herbst, ApJ **340**, 906 (1989).

[11] B. E. Turner, A. J. Apponi, ApJ **561**, 207 (2001).

[12] C. Savage, A. J. Apponi, Z. M Ziurys, ApJ **578**, 211 (2002).

[13] T. Jacq, A. Baudry, C. M. Walmsley, P. Caselli, A&A **347**, 957 (1999).

[14] T. L. Wison, R. T Rood, Annu. Rev. Astron. Astrophys. **32**, 191 (1994).

[15] S. Saito, Chem. Phys. Lett. **42**, 3 (1976).

[16] M. Rodler, A. Bauder J. Am. Chem Soc. **106**, 4025 (1984).

[17] M. Rodler, J. Mol. Spec. **114**, 23 (1985).

[18] M. Rodler, C. E. Blom, A. Bauder, J. Am. Chem. Soc. **106**, 4029 (1984).

[19] J. A. Ball, C. A. Gottlieb, A. E. Lilley, H. E. Radford, ApJ Lett. **16**, 9 (1970).

[20] C. A. Gottlieb, J. A. Ball, E. W. Gottlieb, D. F. Dickinson, ApJ **227**, 422 (1979).

[21] S. E. Cummins, R. A. Linke, P. Thaddeus, ApJ **60**, 819 (1986).

[22] R. Mauersberger, C. Henkel, T. Jacq, C. M. Walmsley, A&A **194**, L1 (1988).

[23] T. Jacq, C. M. Walmsley, R. Mauersberger, T. Anderson, E. Herbst, F. C. De Lucia, A&A **271**, 276 (1993).

[24] B. Parise, C. Ceccarelli, A. G. G. M. Tielens, E. Herbst, B. Leflock, E. Caux, A. Castets, I. Mukhopadhyay, L. Pagani, L. Loinard, A&A **393**, 49 (2002).

[25] A. C. B. Parise, E. Herbst, E. Caux, C. Ceccarelli, I. Mukhopadhyay, A. G. G. M. Tielens, A&A **416**, 159 (2004).

[26] J. R. Durig, L. Zhou, T. K. Gounev, P. Klaeboe, G. A. Guirgis, L-F. Wang, J. Mol. Struct. **385**, 7 (1996).

[27] H. Bunn, P. L. Raston, to be submitted to Mol. Phys. (2017).

[28] M. Tanimoto, V. Almond, S. W. Charles, J. N. Macdonald, N. L. Owen, J. Mol. Spec. **78**, 95 (1979).

[29] C. M. Western, J. Quant. Spectrosc. Radiat. Transfer **186**, 221 (2017).

[30] V. Barone, J. Chem. Phys. **122**, 014108 (2005).

[31] J. -F. D'Eu, J. Demaison, H. Burger, J. Mol. Spec. **218**, 12 (2003).

[32] A. Baccman, B. Lefloch, C. Ceccarelli, J. Steinacker, A. Castets, L. Loinard, ApJ **585**, 55 (2003).

8. Summary and Outlook

I. VAN DER WAALS COMPLEXES

Following previously published research on the far-infrared (IR) spectroscopy of the H_2–O_2 van der Waals complex [1], Chapter 3 presented spectra in the far-IR for D_2–O_2 and mid-IR for H_2–O_2 . Resulting from the lower light intensity in the mid-IR region only a preliminary assignment of H_2–O_2 could be made, with no evidence observed for rotationally bound states above $l = 7$. The D_2–O_2 spectra was also presented in Chapter 3 showing *P* and *R* branch features but minimal fine structure. It has been previously noted that there is an enhanced difficulty in collecting spectra of complexes containing D_2, compared with H_2 [2]. The Far-IR spectra of H_2–Xe presented in Chapter 3 showed resolved *N* and *T* branch transitions, however, they are not as detailed as those previously reported in the mid-IR region [3]. This is likely due to the shorter pathlengths utilised in the present work; 10–20 m as opposed to >100 m. Although the spectra here are not of comparable quality to previous work [1, 3], it is noted that the induced dipole moments in these complexes, particularly for H_2–O_2 is extremely small (10^{-3} D), and detecting the spectra at all, is satisfying.

Possible future work involves the use of longer pathlengths to record high quality spectra that may allow an analysis to determine rotational constants for the H_2/D_2–O_2 van der Waals complexes and provide data to assist in improving the potential energy surface. Using longer pathlengths would also assist in measuring higher quality spectra for H_2/D_2–Xe, which is required to resolve the analogous blended peaks reported previously by McKellar in the mid-IR. The multipass cell (as detailed in Chapter 2) is about 600 mm long and can comfortably achieve 16 and sometimes 32 passes without significant loss of light intensity. Comparing this with the cell used in McKellar's work, which is e.g. 5.5 m in the H_2–N_2 study [4], used at 28 passes, it is evident that in order to increase pathlengths and achieve more highly resolved spectra, a longer multipass cell is required. Expanding on this, the H_2–Ne complex is of particular interest due to the minimal comprehensive spectra (in comparison with the other H_2–Rg van der Waals complexes) of this complex. This is a result of its small polarisability and therefore small number of bound rotational states. Hence, high quality spectra, likely achieved by using longer pathlengths, of the H_2–Ne complex, particularly in the far-IR, are desirable and could be a focus for future experiments.

II. VINYL ALCOHOL

Chapter 4 presents the first observation of vinyl alcohol in the far-IR spectrum showing the OH torsional motion (ν_{15}) for both *syn* and *anti* rotamers, and the CCO bending motion (ν_{11}) for the *syn* rotamer. A smoothly evolving torsional potential, constructed from CCSD(T)/cc-pVQZ optimisations in 5 degree increments about the CCOH dihedral angle, shows a 5.1 kJ/mol (scaled) energy difference between the *syn* and *anti* ground states located at 0° and 180°, respectively. The relative abundance of *anti* compared with *syn* was determined to be 11% from calculations using the Boltzmann equation and is comparable to the approximate 15% abundance determined from the relative intensity of the ν_{15} bands. High resolution

analysis was performed for both the *syn* and *anti* fundamental bands, shown in Chapters 5 and 6, respectively, as well as the first two hot bands for the *syn* rotamer and first hot band for the *anti* rotamer. The nearby CCOH bend, ν_{11} is found to cause perturbations in the fundamental band of *syn*-vinyl alcohol, resulting from a Coriolis interaction between ν_{15} and ν_{11}. A preliminary fit was performed on the ν_{11} band, observed around 488 cm^{-1}, assisted by constants extracted from anharmonic frequency calculations at the MP2 level on a CCSD(T) optimised structure. The constants from this band were then used in a fit that included the Coriolis interaction with ν_{15}. This resulted in accurate ground state and ν_{15} rotational and centrifugal distortion constants, that were reported up to the sextic level. Further Coriolis interactions affecting the first and second hot bands are evident. Introduction of the previously reported Coriolis parameters from an interaction between $2\nu_{15}$ and ν_{13} allowed for the determination of rotational and centrifugal distortion constants up to the sextic level for $2\nu_{15}$. Only a preliminary fit was performed for the second hot band due to additional interactions of $3\nu_{15}$ with nearby bands, and its weaker intensity, which resulted from a lower population in the initial state. For the *anti*-vinyl alcohol fundamental, presented in Chapter 6, no perturbations were observed and hence accurate ν_{15} rotational and centrifugal distortion constants were provided up to the sextic level with reduced effort. However, the hot band shows perturbations, again with ν_{11}. Constants for the $2\nu_{15}$ level are provided from inclusion of only unperturbed transitions.

Chapters 4–6 on vinyl alcohol will provide the basis for three publications. Chapter 4 has recently been accepted to ACS Earth and Space Chemsitry and Chapter 5, pending some minor updates in the fit, will be submitted to Molecular Physics. Chapter 6, on the high resolution analysis of *anti*-vinyl alcohol, requires some additional work before submitting for publication, likely to Molecular Astrophysics. As mentioned above, only a fit to unperturbed transitions has been performed for the *anti*-vinyl alcohol hot band. In order to improve the fit and refine the $2\nu_{15}$ rotational and centrifugal distortion constants, perturbations must be included. This will occur following the completion of CCSD(T) anharmonic frequency calculations that will allow for a more accurate initial estimate of the Coriolis parameters. These calculations are being performed by a third party (at James Madison University, Virginia, USA), due to time restrictions.

The far-IR spectrum of monodeuteratred vinyl alcohol, CH_2CHOD, in the ν_{15} region was also collected (Chapter 7). Both *syn* and *anti* rotamers were observed as well as hot band(s), however, due to problems encountered during the drying of the precursor (monodeuterated 2-chloroethanol), severe spectral contamination by water is evident. This contamination largely obscured the rotational details of the *anti* bands, therefore only a high resolution analysis was performed for the *syn* rotamer. A good fit is provided for the fundamental, which is free of perturbations, as well as a fit to the first hot band, including only unperturbed assignments. This provided rotational and centrifugal distortion constants up to the sextic level for the ground state as well as ν_{15} and $2\nu_{15}$. Besides the inclusion of perturbations, the monodeuterated fit can be improved upon following the collection of clean spectra. This can only occur from the elimination of the D_2O used to deuterate the 2-chloroethanol precursor.

The azeotrope between water and 2-chloroethanol is so strong that the best way to improve the spectra would be to dry the precursor using magnesium oxide instead of magnesium sulphate, which was used and is somewhat incompatible with 2-chloroethanol.

The vinyl alcohol research presented in Chapters 4–7 is important both astronomically and atmospherically. From the investigation performed here on vinyl alcohol, highly accurate ro-vibrational constants have been determined that are important, along with band origins, for detection of vinyl alcohol in the atmosphere and for further interstellar observations e.g. on CH_2CHOD.

Following the observation of the ν_{15} and ν_{11} bands in this work, 12 out of the 15 vibrational modes have now been reported for gas phase vinyl alcohol. The weakly absorbing CH_2 asymmetric stretching mode was tentatively reported in 1999 but has not been observed since in gas or matrix investigations [5]. Confirmation of this detection is a notable focus for future work along with the detection of the final two weak vibrational modes owing to the CH_2 symmetric stretch and the lone CH stretch. Attempts to detect these bands have already begun with the use of helium nanodroplet techniques [6], where observation of the OH stretching band may show evidence of *anti*-vinyl alcohol.

Also of note is that as part of the vinyl alcohol experiments, the spectra of 2-chloroethanol was measured in order to determine the optimal temperature and pressure for the decomposition of vinyl alcohol. The spectra of 2-chloroethanol were of good quality at high resolution showing well resolved rotational fine structure. The spectra has been analysed and will be published soon, but has not been included in this thesis.

REFERENCES

[1] H. Bunn, T. Bennett, A. Karaylian, P. L. Raston, ApJ **799**, 65 (2015).

[2] A. R. W. McKellar, H. L. Welsh, J. Chem. Phys. **55**, 595 (1971).

[3] A. R. W. McKellar, Can. J. Phys. **91**, 957 (2013).

[4] A. R. W. McKellar, J. Chem. Phys. **93**, 18 (1990).

[5] D-L Joo, A. J. Merer, D. J. Clouthier, J. Mol. Spec. **197**, 68 (1999).

[6] S. Yang, A. M. Ellis, Chem. Soc. Rev. **42**, 472 (2013).